Master's thesis

NTNU
Norwegian University of Science and Technology
Faculty of Natural Sciences
Department of Physics

Øyvind Muldal Taraldsen

Quantum Quenches in Non-centrosymmetric Superconductors

Master's thesis in Physics
Supervisor: Prof. Jacob Linder
December 2021

NTNU
Norwegian University of
Science and Technology

Øyvind Muldal Taraldsen

Quantum Quenches in Non-centrosymmetric Superconductors

Master's thesis in Physics
Supervisor: Prof. Jacob Linder
December 2021

Norwegian University of Science and Technology
Faculty of Natural Sciences
Department of Physics

NTNU
Norwegian University of
Science and Technology

Abstract

In this thesis we study a model for the short-time dynamics of the superconductivity in a particular class of materials, namely the non-centrosymmetric superconductors with spin-orbit coupling breaking the inversion symmetry. This was motivated by recent theoretical studies of the short-time dynamics of s-wave and d-wave superconductors, advances in experimental techniques and renewed research interest in several non-centrosymmetric compounds. This was in turn motivated by improvement in measurements, particularly in the fields of cold atoms and spectroscopy, which has allowed for much more detailed experimental study of systems that are not in equilibrium. The model used is derived by extending an existing Green's function technique to the non-centrosymmetric case with spin-orbit coupling. We calculate several numerical results showing the time-dynamics of the superconducting gap, compare them to the previously known results for centrosymmetric superconductors and attempt to explain the unique features seen. The main result is a possibility for short-time enhancement of the triplet component of the gap after fast changes in the spin-orbit interaction.

Sammendrag

I denne oppgaven undersøker vi dynamikken kort tid etter at et system har blitt forstyrret i en modell for ikke-sentrosymmetriske superledere. Spesifikt ser vi på ikke-sentrosymmetriske materialer der spinn-banekobling er det som bryter inversjonssymmetrien. Dette var motivert av studier i nyere tid som har tatt for seg tilsvarende dynamikk for s-bølge og d-bølge superledere, samt fremskritt i eksperimentelle teknikker og fornyet interesse i ikke-sentrosymmetriske materialer. Dette var igjen motivert av at forbedringer i måleteknikker og utstyr, spesielt innen kalde atomer og spektroskopi, har tillatt mer detaljerte eksperimentelle studier av systemer ute av likevekt. Modellen som brukes i oppgaven er utledet ved å utvide en tidligere brukt Green's funksjon teknikk til det ikke-sentrosymmetriske tilfellet med spinn-banekobling. Flere numeriske resultater som viser tidsdynamikken til det superledende gapet beregnes. De sammenlignes med tidligere kjente resultater og vi prøver å forklare hvorfor vi ser forskjellene som kommer frem. Hovedresultatet i oppgaven er en mulighet for forsterking av triplet komponenten i gapet kort tid etter en plutselig endring i styrken på spinn-bane interaksjonen.

Preface

This master thesis represents the completion of a two year Master of Science in Physics programme at the Norwegian University of Science and Technology (NTNU) and the end of five years of physics studies. After attending courses taught by Prof. Jacob Linder during my studies I was inspired by his persistence and endless curiosity. This lead me to ask him to be my supervisor. I am grateful for the opportunity i got to write this thesis with him as a supervisor at the Center for Quantum Spintronics. His insights and support has been invaluable during an unusually difficult year. I want to thank my fellow students and friends for their support and the numerous great discussions about both physics and life in general during these years of study. Finally I want to thank my family for unconditional love and support through this year.

Øyvind Muldal Taraldsen

Øyvind Muldal Taraldsen
Trondheim, Norway
December 2021

CONTENTS

CHAPTER 1

INTRODUCTION

1.1 History and Motivation

Since the discovery of superconductivity by Kamerlingh Onnes in 1911, understanding the phenomena has been the subject of intense research. The fundamental underlying physics and the huge potential for applications has been and continues to entice researchers to this day.

The first major theoretical breakthrough in explaining what happens on a microscopic level inside solid matter in a superconducting state came with the Bardeen-Cooper-Schrieffer (BCS) theory of superconductivity. This provided the first working microscopic explanation in 1957. While the BCS theory was and is very successful at explaining many properties of some superconductors like the critical temperature, the isotope effect and the critical magnetic field it was not the end of the story. Materials that did not conform to the original BCS theory was discovered: heavy fermion compounds, the famous high temperature cuprate compounds and many more. Superconductivity turned out to be a rich and complicated phenomena, to both joy and frustration of many physicists.

In more recent years the introduction of improved experimental techniques in the form of angle resolved photoemission spectroscopy (ARPES) and the extension to time resolved ARPES has given access to a wealth of measurements that where previously unavailable. In particular these allow for the probing of time dynamics and nonequilibrium properties in addition to the equilibrium properties.

In this thesis we will be dealing with the dynamical properties of a subset of superconductors that are the non-centrosymmetric superconductors. In particular we are dealing with what happens after quantum quenches, meaning that the system in question evolves in time under a different Hamiltonian than the one it was prepared in initially. In simple terms the system the system is suddenly perturbed by some external influence, for instance a laser or a strong electric field. This is motivated by the general goal of expanding the knowledge of how properties of superconductors can potentially be controlled. More specifically to the non-centrosymmmetric materials it is motivated by the possibility these have for hosting mixed parity states with both singlet and triplet components and the potential for controlling this ratio. It also allows comparison with earlier results for single band s-wave and d-wave superconductors and the centrosymmetric two-band superconductors previously examined.

1.2 Structure of Thesis

In chapter 2 we present a brief summary of theoretical prerequisites, while chapter 3 serves to set up and derive equations for the system we will be considering in the rest of the thesis. The main calculations are presented in chapter 4 and chapter 5. Main results are then presented in chapter 7.

Chapter 2 serves as a quick reminder of some of the most relevant parts of quantum many-particle mechanics with special emphasis on the Green's function methods. In chapter 3 the model we will use is built up, starting from a non-interacting system and then introducing the symmetry-breaking terms and interaction terms that are needed to model the desired properties. Some emphasis is given to the connection to real physical systems and to justify the choice of interactions. Chapter 4 is focused on calculations and derivations, known methods are re-derived for the model and the equations needed to model the time-dynamics are set up. The chapter finishes up with a section on the numerical methods used.

The spectral function and in particular the approximate calculation of this out of equilibrium is the focus of chapter 5. In chapter 6 the known results for a single band superconductor with full inversions symmetry and a quench in the interaction strength is presented. This chapter serves as a reference for comparing the results with those found the next chapter and as a test of the numerical method used. Results using the full model without inversion symmetry are finally presented and discussed in 7.

CHAPTER 2

QUANTUM MANY-PARTICLE SYSTEMS

Many-body quantum mechanical problems for interacting systems are notoriously hard to solve. They tend to remain hard even after major approximations are made. While the Schrödinger equation is normally the starting point for quantum mechanical problems a direct application turns out to be quite cumbersome. This is partly because the wave function will depend on N variables (if we ignore spin) for an N-particle system. Evaluating even a single wave function for large N tends to be very computationally intensive even for fairly simple systems.

2.1 Second Quantization

It turns out that this part of the problem can be circumvented by going to the formalism we will be using in this thesis, the so called "second quantization" (also called the "occupation number") representation where we no longer need to reference the total number of particles in the system. It even allows us to treat systems without a fixed number of particles. The subject is much too large for any complete and rigorous introduction to be given here, and we will only review some key elements. For a complete introduction the reader is instead refereed to any of the excellent textbooks on the matter [1–4].

2.1.1 Many particle states

Many-particle states are built up by constructing a basis consisting of products of single particle states. If x is a set of quantum numbers that uniquely specifies a single-particle state, then we can denote a single particle state in a Hilbert space by the vector $|\psi(x)\rangle$. The quantity x can contain both for instance spatial coordinates $\mathbf{r}$ and any discrete variables such as spin projection σ. This notation generalizes to many-particle systems where we can write a many particle state as $|\psi\rangle = |\psi(x_1, x_2, ..., x_N)\rangle$. We can use the fact that in quantum mechanics we are dealing with indistinguishable particles to describe the wave functions without referring to the individual particles. The many body wave functions of bosons are identical under exchange of particles, while wave functions for fermions pick up an overall minus sign upon exchange of two particles. This is not physically significant as long as the exchanged particles have different coordinates as

$$|\psi(x_1, x_2, ...x_i, x_j, ..., x_N)|^2 = |\psi(x_1, x_2, ...x_j, x_i, ..., x_N)|^2. \tag{2.1}$$

For fermions the Pauli exclusion principle shows up if two particles have identical states $x_i = x_j$ as picking up a minus sign by particle exchange would then mean that the whole wave function is identically zero.

This can be used to instead construct states based on how many particles occupy each single particle state

$$|\psi\rangle = |n_{\lambda_1}, n_{\lambda_2}, n_{\lambda_3}, ...\rangle \tag{2.2}$$

where n_{λ_i} is the number of particles in the state specified by the quantum numbers λ_i. For bosons n_{λ_i} can be any non-negative integer. For fermions the Pauli exclusion principle manifests in n_{λ_i} only taking the values 0 and 1. In this formalism states are constructed from an empty (vacuum) state by creation operators, for fermions(bosons) these are commonly denoted as $c^\dagger_\lambda(b^\dagger_\lambda)$, where the action of this operator on an a state is to increase the occupancy by one. We also have destruction operators denoted c_λ which reduces the occupancy by one. For fermions we can only have an occupancy of 0 or 1 and so acting twice with any $c^\dagger_\lambda$ or c_λ destroys the state. Using these operators it is possible to construct any state we want and to change states in any way we want. It can be shown that these operators must obey certain commutation relations at equal times to have the required properties, we will come back the situation when the operators are acting at unequal times. For fermions we must have

anticommutation which we denote by curly brackets

$$\{c_{\lambda_1}, c^\dagger_{\lambda_2}\} \equiv c_{\lambda_1} c^\dagger_{\lambda_2} + c^\dagger_{\lambda_2} c_{\lambda_1} = \delta_{\lambda_1 \lambda_2} \tag{2.3a}$$

$$\{c_{\lambda_1}, c_{\lambda_2}\} = \{c^\dagger_{\lambda_1}, c^\dagger_{\lambda_2}\} = 0 \tag{2.3b}$$

while for bosons we have commutation relations denoted by square brackets

$$[b_{\lambda_1}, b^\dagger_{\lambda_2}] \equiv b_{\lambda_1} b^\dagger_{\lambda_2} - b^\dagger_{\lambda_2} b_{\lambda_1} = \delta_{\lambda_1 \lambda_2} \tag{2.4a}$$

$$[b_{\lambda_1}, b_{\lambda_2}] = [b^\dagger_{\lambda_1}, b^\dagger_{\lambda_2}] = 0. \tag{2.4b}$$

2.1.2 Operators

We commonly describe operators as "one particle operators", "two particle operators" etc. This refers to the operator representing quantities of the following form

$$U = \sum_{i=1}^{N} U_i(\mathbf{r}_i, \mathbf{p}_i) \tag{2.5}$$

where U_i depends on the position $\mathbf{r}_i$ and momentum $\mathbf{p}_i$ of one particle, while two particle operators depend on two particles and etc. In second quantization we can represent any such operators by combination of creation and annihilation operators. A single particle operator takes the form

$$T_{\text{total}} = \sum_{\lambda_1 \lambda_2} T_{\lambda_1 \lambda_2} c^\dagger_{\lambda_1} c_{\lambda_2}, \tag{2.6}$$

An example of how such operators are found in second quantized form can be found in appendix A. In a similar way, two particle operator looks like

$$V_{\text{total}} = \sum_{\lambda_1 \lambda_2 \lambda_3 \lambda_4} V_{\lambda_1 \lambda_2 \lambda_3 \lambda_4} c^\dagger_{\lambda_1} c^\dagger_{\lambda_2} c_{\lambda_4} c_{\lambda_3} \tag{2.7}$$

where the matrix elements are found in a similar way as for the single particle case.

Note that in principle we can have operators acting on any number of particles and include three-, four-, five-,... body interactions, but these are ignored to a good approximation in many condensed matter systems and we restrict ourselves to two-body interactions in this thesis.

2.2 Green's Functions

Green's functions are mathematically often defined as impulse response functions, e.g. as the solutions to equations on the form

$$LG(\mathbf{r},\mathbf{r}';t,t') = \delta(\mathbf{r}-\mathbf{r}')\delta(t-t') \tag{2.8}$$

where L is some linear differential operator [1]. If the Green's function of a differential equation is known, then by linearity the solution for any source term can be obtained by integrating (performing a summation) over the relevant coordinates. In physical systems we are often interested in how systems described by differential equations respond to perturbations to link theoretical calculations and experimental data.

For single-particle quantum mechanics we insert the Schrödinger operator in equation (2.8) and get

$$\left[i\partial_t - H_0(\mathbf{r}) - V(\mathbf{r})\right] G(\mathbf{r},\mathbf{r}';t,t') = \delta(\mathbf{r}-\mathbf{r}')\delta(t-t'). \tag{2.9}$$

By insertion, one can verify that the single particle Green's function can be written as

$$G(\mathbf{r},\mathbf{r}';t,t') = -i\theta(t-t') \left\langle \mathbf{r} \right| e^{-iH(t-t')} \left| \mathbf{r}' \right\rangle, \tag{2.10}$$

explaining why it is also often called a propagator (also called a correlation function)[1].

In many-body quantum mechanics the objects we call Green's function often do not strictly follow the above definition as solutions to a linear differential equation. However, it turns out that we can think of them in similar ways [2]. We define the single-particle fermionic Green's function for a general many-body system as

$$G(\lambda_1,t_1;\lambda_2,t_2) \equiv -i\langle \mathcal{T}[c_{\lambda_1}(t_1)c^\dagger_{\lambda_2}(t_2)]\rangle \tag{2.11}$$

where $\mathcal{T}$ is the time-ordering operator and λ_i are any set of quantum numbers that uniquely specifies a single-particle state. The physical interpretation is that this describes the probability amplitude of a fermion in state λ_2 being found at time t_2 if it was created in state λ_1 at time t_1.

[1] This is strictly speaking the retarded propagator.

[2] They are also related to solutions of differential equations, for more details see [1]

We also define the "retarded" and "advanced" Green's functions for later use

$$G^R(\lambda_1, t_1; \lambda_2, t_2) \equiv -i\theta(t_1 - t_2)\langle\{c_{\lambda_1}(t_1), c^\dagger_{\lambda_2}(t_2)\}\rangle \tag{2.12}$$
$$G^A(\lambda_1, t_1; \lambda_2, t_2) \equiv i\theta(t_2 - t_1)\langle\{c_{\lambda_1}(t_1), c^\dagger_{\lambda_2}(t_2)\}\rangle, \tag{2.13}$$

and the "lesser" and "greater" Green's functions

$$G^>(\lambda_1, t_1; \lambda_2, t_2) \equiv -i\,\langle c_{\lambda_1}(t_1)c^\dagger_{\lambda_2}(t_2)\rangle \tag{2.14}$$
$$G^<(\lambda_1, t_1; \lambda_2, t_2) \equiv i\,\langle c^\dagger_{\lambda_2}(t_2)c_{\lambda_1}(t_1)\rangle\,, \tag{2.15}$$

meaning that

$$G^R(\lambda_1, t_1; \lambda_2, t_2) = \theta(t_1 - t_2)(G^>(\lambda_1, t_1; \lambda_2, t_2) - G^<(\lambda_1, t_1; \lambda_2, t_2)) \tag{2.16}$$
$$G^A(\lambda_1, t_1; \lambda_2, t_2) = -\theta(t_2 - t_1)(G^>(\lambda_1, t_1; \lambda_2, t_2) - G^<(\lambda_1, t_1; \lambda_2, t_2)). \tag{2.17}$$

The Green's functions provide us with an important link between theory and experiment through the spectral function [5]

$$A(\mathbf{k}, \omega) = -\frac{1}{\pi}\,\mathrm{Im}\,G^R(\mathbf{k}, \omega), \tag{2.18}$$

which can further be related to the lesser Green's function in what is known as the fluctuation-dissipation theorem [1] for the fermionic single-particle Green's functions

$$A(\mathbf{k}, \omega) \propto \mathrm{Im}\,G^<(\mathbf{k}, \omega)n(\omega) \tag{2.19}$$

where $n(\omega)$ is the Fermi-Dirac distribution.

The spectral function is in turn related to the signal measured in angle-resolved photoemission spectroscopy (ARPES) which is the subject of the next section [3].

[3] Some authors use a prefactor -2 instead of $-1/\pi$.

2.3 ARPES

The ARPES technique is an experimental method that can directly probe the momentum dependent electronic band structure in a solid. This makes it an very powerful tool for studying condensed matter systems. It is based on the photoelectric effect where an electron in a solid can absorb a photon and get enough energy to escape the material. This is described by $E_{kin} = h\nu - \phi$ where E_{kin} is the maximum kinetic energy of the escaping electron, ν is the frequency of the photon, h is Planck's constant and ϕ is the work function of the solid that is a measure of the potential barrier at the surface.

While simple enough in principle, the photoemission process in solids is complicated and difficult to calculate, in most cases a number of approximations must be made to interpret the measurements. One common way to do this is the so-called three step model where the pohotoemission process is divided into three distinct steps: (i) optical excitation of the electron in the bulk, (ii) the excited electron traveling to the surface, (iii) the electron escaping from the surface of the solid. The intensity of escaped electrons is then given by the product of the probability for the optical transition, the probability of the electrons scattering during the travel to the surface and the transition probability for penetrating the surface barrier. Finally an approximation is made where the relaxation of the system during the photoemission process is neglected, called a "sudden approximation." In other words one assumes that the electron is removed at a single instant and that the effective potential of the system changes instantaneously. We note that while this makes for a convenient approximation, quantum mechanically photoemission should be described by a single step, not with several independent ones.

This leads to a convenient form of the ARPES intensity at equilibrium for a 2D single-band system [5]

$$I(\mathbf{k}, \omega) \propto A(\mathbf{k}, \omega). \tag{2.20}$$

However, out of equilibrium there are several other factors to take into account. In general the Green's functions are no longer dependent on the time difference alone, but on two independent times. A theory taking this into account has been developed [6] and the expression for the intensity in time-resolved ARPES is given by

$$I(\omega, t_0) = \mathrm{Im} \int \mathrm{d}t \, \mathrm{d}t' \, \rho(t, t', t_0) e^{i\omega(t-t')} G^{<}_{\mathbf{k}(t,t')}(t, t'), \tag{2.21}$$

where $\rho(t, t', t_0)$ describes a probe pulse of finite width. This reduces to the equilibrium expression in equation (2.20) if the probe-function can be taken

as $\rho(t, t', t_0) = 1$, denoting a continuous beam, and if the Green's function depends only on the time difference $t - t'$.

2.4 Equation of motion theory

In this thesis we are looking at the time-dependence of physical quantities, we will approach this theoretically by finding sets of differential equations for the time-dependence of the Green's functions that we can solve with some appropriate numerical scheme.

We first look at the time-derivative of a Green's function, for instance the momentum-space Green's function with respect to the first time-argument

$$\begin{aligned} i\partial_{t_1} G^R(\mathbf{k}, t_1; \mathbf{k}', t_2) &= i(-i)\partial_{t_1}\theta(t_1 - t_2)\langle\{c_{\mathbf{k}\sigma}(t_1), c^\dagger_{\mathbf{k}'\sigma}(t_2)\}\rangle + \\ &\quad + i(-i)\theta(t_1 - t_2)\langle\{\partial_{t_1} c_{\mathbf{k}\sigma}(t_1), c^\dagger_{\mathbf{k}'\sigma}(t_2)\} \\ &= \delta(t_1 - t_2)\delta(\mathbf{k} - \mathbf{k}') + \theta(t_1 - t_2)\langle\{\partial_{t_1} c_{\mathbf{k}\sigma}(t_1), c^\dagger_{\mathbf{k}'\sigma}(t_2)\} \end{aligned} \tag{2.22}$$

where we used the anti-commutation relation for fermionic operators at equal times. To evaluate this expression we need the time-derivative of the annihilation operator. We can get this from Heisenberg's equation of motion [4] which given a Hamiltonian and an operator will give us a differential equation for the time evolution of any such operator

$$\partial_{t_1} c_{\mathbf{k}\sigma}(t_1) = i[H, c_{\mathbf{k}\sigma}](t_1). \tag{2.23}$$

As a quick example, in the case of non-interacting particles this takes a particularly simple form

$$\begin{aligned} \partial_t c_{\mathbf{k}\sigma}(t) &= i[H_0, c_{\mathbf{k}\sigma}](t) \\ &= i\left(\sum_{\mathbf{k}',\sigma'} \varepsilon_{\mathbf{k}'} c^\dagger_{\mathbf{k}',\sigma'} c_{\mathbf{k}',\sigma'} c_{\mathbf{k}\sigma} - c_{\mathbf{k}\sigma} \sum_{\mathbf{k}',\sigma'} \varepsilon_{\mathbf{k}'} c^\dagger_{\mathbf{k}',\sigma'} c_{\mathbf{k}',\sigma'}\right)(t) \\ &= -i\varepsilon_{\mathbf{k}} c_{\mathbf{k}\sigma} \\ \implies c_{\mathbf{k}\sigma}(t) &= e^{-i\varepsilon_{\mathbf{k}} t} c_{\mathbf{k}\sigma}. \end{aligned} \tag{2.24}$$

In general we will be using Heisenberg's equations of motion on operators and products of operators to derive the time-dependence of the quantities we want to look at.

2.5 Superconductivity

In this section we will review some of the basic theory and some properties of superconductors. We will focus on the BCS-type theory of superconductivity as this is the most widely successful theory and it will be the basis for building the models used thesis. For a complete introduction we refer to textbooks on many-body condensed matter physics [1–3] and more specialized texts dealing with superconductivity [7].

2.5.1 Cooper pairing

One of the key ingredients in microscopic theories of superconductivity is the idea of electrons forming pairs, so called Cooper pairs. With some notable exceptions this happens through some sort of attractive interaction[4]. The problem originally examined by Cooper was the instability of the ground state of an inert Fermi-sea with to the formation of bound states when two electrons are added on top which have an arbitrarily small attraction between them acting within a thin shell of the Fermi-surface. Figure 2.1 illustrates the thin shell around the Fermi surface. Cooper found that adding these electrons gave rise to a two-particle state with energy less than twice the Fermi energy, appearing to violate the Pauli principle. However the bound state should not be viewed as a two individual electrons, but rather as a single entity which is not a fermion with a binding energy $2\varepsilon_F - E = \Delta$, where ε_F is the Fermi-energy and E is the two-particle energy of the Cooper pair. This energy can be approximated as

$$\Delta = 2\hbar\omega_0 e^{-V^{-1}N^{-1}(\varepsilon_F)}, \tag{2.25}$$

where ω_0 is the thickness of the shell around the Fermi-surface V is the attractive interaction and $N(\varepsilon_F)$ is the density of states near the Fermi-surface with the assumption that the product $VN(\varepsilon_F)$ is very small. This gives rise to an essential singularity in Δ as $VN(\varepsilon_F) \to 0$, this tells us that the result above could not be found by doing perturbation theory.

In practice this allows the electrons to shed some of the limitations of the Pauli principle. Note that we did not state that Cooper pairs are bosons, they do not obey bosonic commutation relations nor boson statistics[5]. While the problem had a quite startling solution it also appeared quite artificial in that electrons repel each other via the Coulomb interaction and no attractive

[4] See for instance the Kohn-Luttinger mechanism where a weak repulsive interaction gives rise to unconventional superconductivity [8].

[5] They are sometimes refereed to as composite bosons.

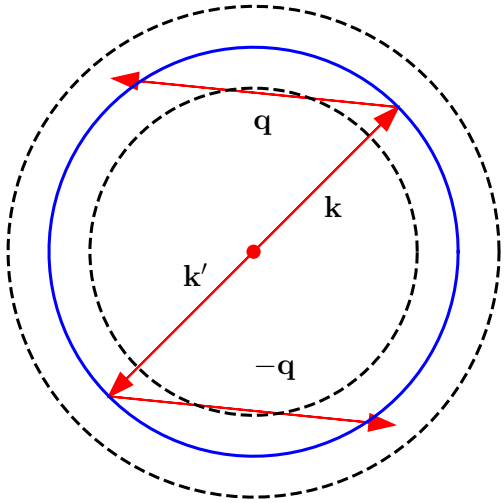

Figure 2.1: Two particles scattering within a thin shell of the Fermi surface. Note that the initial and final states both stay within the thin shell when they are initially on opposite sides of the Fermi surface and that one of the particles would scatter out of this shell there was a large deviation from this initial condition.

interaction was known. Such an interaction was however discovered, it was shown that an interaction mediated by phonons (lattice vibrations) could give rise to a net attraction. This attraction is explained by electrons attracting the ions in a crystal-lattice and leaving behind a trail of net-positive charge as illustrated in figure 2.2. As long as the temperature is low enough to not dissociate the pairs, this temperature will be on the order $\Delta \sim k_B T_0$ where k_B is Boltzmans constant and T_0 is a temperature.

We note that the phonon mediated scenario is a special case, the phenomena of Cooper pairing more generally refers to electrons forming pairs due to some attractive interaction in **k**-space [7].

2.5.2 BCS-theory

The BCS theory is in essence the many-body version of the Cooper-problem. Starting out with a many-body Hamiltonian with an effectively attractive electron-electron interaction

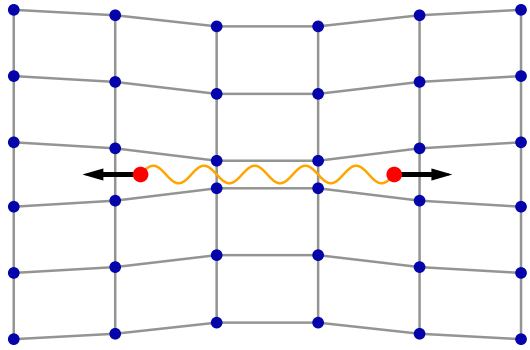

Figure 2.2: Real-space cartoon illustration of a Cooper pair with phonon-mediated superconductivity. The electrons (red) distort the lattice by attracting positive ions (blue) away from their equilibrium positions. The (relative to electrons) heavy ions have a large inertia and are slow to move, this means that the local distortion of the lattice is present after the electrons have passed. Electrons moving along the same line feel this distortion the strongest while the distortion is less significant for electrons moving perpendicular to the distortion. Moving in opposite directions minimizes the effect of the Coulomb repulsion between the electrons.

$$\mathcal{H} = \sum_{\mathbf{k},\sigma} (\varepsilon_{\mathbf{k}} - \mu) c^{\dagger}_{\mathbf{k}\sigma} c_{\mathbf{k}\sigma} + \sum_{\mathbf{k},\mathbf{k}',\mathbf{q},\sigma,\sigma'} V_{\text{eff}} c^{\dagger}_{\mathbf{k}+\mathbf{q}\sigma} c^{\dagger}_{\mathbf{k}'-\mathbf{q}\sigma'} c_{\mathbf{k}'\sigma'} c_{\mathbf{k}\sigma}, \tag{2.26}$$

where $\varepsilon_{\mathbf{k}}$ is the kinetic energy, μ is the chemical potential and V_{eff} is some effective interaction that includes both the repulsive Coulomb interaction and the attractive electron-phonon interaction. A few large simplifications can now be made, because the effective attractive interaction is only valid for a thin shell around the Fermi-surface we can ignore states that are scattered out of this shell. The scattering events that are most likely to lie within the shell are those with $\mathbf{k} = -\mathbf{k}'$. The interaction is considered approximately instantaneous and so the Pauli-principle limits the spin to $\sigma' = -\sigma$ because this means that the spatial extent of the interaction is very small. This allows a rewrite of the Hamiltonian (2.26) to

$$\mathcal{H} = \sum_{\mathbf{k}\sigma} (\varepsilon_{\mathbf{k}} - \mu) c^{\dagger}_{\mathbf{k}\sigma} c_{\mathbf{k}\sigma} + \sum_{\mathbf{k}\mathbf{k}'} V_{\mathbf{k}\mathbf{k}'} c^{\dagger}_{\mathbf{k}\uparrow} c^{\dagger}_{-\mathbf{k}\downarrow} c_{-\mathbf{k}'\downarrow} c_{\mathbf{k}'\uparrow}, \tag{2.27}$$

where $V_{\mathbf{k}\mathbf{k}'}$ is now attractive within a thin shell around the Fermi surface and zero otherwise. This is very much like the Cooper problem with an attraction that works between all electrons in a thin shell around the Fermi surface instead of just between two.

However, this Hamiltonian is still too complicated to be treated exactly and the Cooper problem result (2.25) is a strong indication that perturbation theory is not the right choice for an approximate treatment. The way to do this is via a mean-field approach that we will go through in more detail in chapter 3. In essence the approach is to assume that the fluctuations around the statistical average of operators is small and use this to reduce the many-body problem to a self-consistent one-particle problem. Pairs of operators are replaced by their statistical averages plus fluctuations around the average $c_{-\mathbf{k}'\downarrow} c_{\mathbf{k}'\uparrow} = \langle c_{-\mathbf{k}'\downarrow} c_{\mathbf{k}'\uparrow} \rangle + \delta_{\mathbf{k}'}$ and terms of order $O(\delta^2_{\mathbf{k}'})$ are neglected. The quantity $\Delta_{\mathbf{k}} \equiv -\sum_{\mathbf{k}'} V_{\mathbf{k}\mathbf{k}'} \langle c_{-\mathbf{k}'\downarrow} c_{\mathbf{k}'\uparrow} \rangle$ is defined and is often called the superconducting gap for reasons that will become clear. This mean-field approximation gives a Hamiltonian that is quadratic in the creation and annihilation operators

$$\mathcal{H} = \sum_{\mathbf{k},\sigma} (\varepsilon_{\mathbf{k}} - \mu) c^{\dagger}_{\mathbf{k}\sigma} c_{\mathbf{k}\sigma} - \sum_{\mathbf{k}} \left[\Delta_{\mathbf{k}} c^{\dagger}_{\mathbf{k}\uparrow} c^{\dagger}_{-\mathbf{k}\downarrow} + \Delta^{\dagger}_{\mathbf{k}} c_{-\mathbf{k}\downarrow} c_{\mathbf{k}\uparrow} \right] + E_0, \tag{2.28}$$

where E_0 is a constant energy term we can ignore for now. This is a large simplification in that the Hamiltonian can now be diagonalized in a new set of fermionic operators. The diagonal form makes it simple to find expressions for thermodynamic quantities and thereby find $\Delta_{\mathbf{k}}$ in terms of other variables. In short this leads to a diagonal form of (2.28) which is then given by

$$\mathcal{H} = \sum_{\mathbf{k},\sigma} E_{\mathbf{k}} \gamma^{\dagger}_{\mathbf{k}\sigma} \gamma_{\mathbf{k}\sigma} + E_0^{'}, \tag{2.29}$$

where $E_{\mathbf{k}} = \sqrt{(\varepsilon_{\mathbf{k}} - \mu)^2 + \Delta^2_{\mathbf{k}}}$ and $\gamma, \gamma^{\dagger}$ are fermionic operators. In this diagonal form of the Hamiltonian we see that $\Delta_{\mathbf{k}}$ appears as a gap in the excitation spectrum on the Fermi-surface

CHAPTER 3

PHYSICAL MODEL

3.1 System

We are investigating quantum quenches in superconducting systems without inversion symmetry. In particular we are going to look at the possibility of suddenly changing the magnitude of a particular type of spin-orbit interaction. The general system is built from electrons hopping on a square lattice with inversion symmetry, then an inversion-symmetry breaking term is added and finally a pairing interactions between electrons that allows for the formation of Cooper-pairs. As a starting point, we find suitable equations describing the system justifying the equations and approximations used. This is followed by deriving equations of motion for relevant quantities we will need in the investigation of the quench-responses and a numerical scheme for solving the equations.

3.1.1 Non-interacting system

We start out by considering a system of non-interacting electrons on a two dimensional square lattice

$$H = \sum_{i,j,\sigma} t_{i,j} c^\dagger_{i\sigma} c_{j\sigma} - \sum_{i,\sigma} c^\dagger_{i\sigma} c_{i\sigma} \mu, \tag{3.1}$$

where c and $c^\dagger$ are fermionic creation and annihilation operators i and j indicate lattice sites, $t_{i,j}$ is the hopping matrix element which we refer to as the hopping amplitude and $\sigma = \downarrow\uparrow$ is the spin. Using a tight binding approximation we include only nearest neighbour hopping and define a single hopping amplitude $t_{\langle i,j\rangle} \equiv -t$, writing $\langle i,j\rangle$ to indicate that only nearest neighbours are to be summed over. This gives us

$$H = -t \sum_{\langle i,j\rangle} \sum_{\sigma} c^\dagger_{i\sigma} c_{j\sigma} - \sum_{i,\sigma} c^\dagger_{i\sigma} c_{i\sigma}\mu, \tag{3.2}$$

going to momentum-space will allow us to work in a diagonal basis, we first introduce Fourier-transformed operators on the lattice

$$c_i = \frac{1}{\sqrt{N}} \sum_{\mathbf{k}} \mathrm{e}^{i\mathbf{k}\cdot\mathbf{r_i}} c_{\mathbf{k}}, \tag{3.3}$$

where N is the number of lattice-sites, $\mathbf{k}$ is the momentum vector and $\mathbf{r}_i$ is the position vector of lattice-soite i. This lets us write

$$\begin{aligned}
H &= -t\frac{1}{N} \sum_{\langle i,j\rangle} \sum_{\sigma} \sum_{\mathbf{k},\mathbf{k}'} \mathrm{e}^{-i\mathbf{k}\cdot\mathbf{r_j}} \mathrm{e}^{i\mathbf{k}'\cdot\mathbf{r_i}} c^\dagger_{\mathbf{k}\sigma} c_{\mathbf{k}'\sigma} - \frac{1}{N} \sum_{i,\sigma} \sum_{\mathbf{k}} \mathrm{e}^{i\mathbf{k}\cdot(\mathbf{r_i}-\mathbf{r_i})} c^\dagger_{\mathbf{k}\sigma} c_{\mathbf{k}\sigma}\mu \\
&= -t\frac{1}{N} \sum_{\langle i,j\rangle} \sum_{\sigma} \sum_{\mathbf{k},\mathbf{k}'} \mathrm{e}^{-i\mathbf{k}\cdot(\mathbf{r_i}+\boldsymbol{\delta})} \mathrm{e}^{i\mathbf{k}'\cdot\mathbf{r_i}} c^\dagger_{\mathbf{k}\sigma} c_{\mathbf{k}'\sigma} - \sum_{\mathbf{k},\sigma} c^\dagger_{\mathbf{k}\sigma} c_{\mathbf{k}\sigma}\mu \\
&= -t\frac{1}{N} \sum_{\langle i,j\rangle} \sum_{\sigma} \sum_{\mathbf{k},\mathbf{k}'} \mathrm{e}^{-i\mathbf{k}\cdot\boldsymbol{\delta}_{ij}} \mathrm{e}^{i(\mathbf{k}'-\mathbf{k})\cdot\mathbf{r_i}} c^\dagger_{\mathbf{k}\sigma} c_{\mathbf{k}'\sigma} - \sum_{\mathbf{k},\sigma} c^\dagger_{\mathbf{k}\sigma} c_{\mathbf{k}\sigma}\mu \\
&= -t\frac{1}{N} \sum_{\mathbf{k},\mathbf{k}',\sigma} N\delta_{\mathbf{k},\mathbf{k}'} \left(\sum_{<i,j>} \mathrm{e}^{-i\mathbf{k}\cdot\boldsymbol{\delta}_{ij}} \right) c^\dagger_{\mathbf{k}\sigma} c_{\mathbf{k}'\sigma} - \sum_{\mathbf{k}\sigma} c^\dagger_{\mathbf{k}\sigma} c_{\mathbf{k}\sigma}\mu \\
&= \sum_{\mathbf{k},\sigma} (\varepsilon(\mathbf{k}) - \mu) c^\dagger_{\mathbf{k}\sigma} c_{\mathbf{k}\sigma},
\end{aligned} \tag{3.4}$$

where the momentum sum over $\mathbf{k}$ is restricted to the first Brillouin zone and we defined $\varepsilon(\mathbf{k}) \equiv -t \sum_{\langle i,j\rangle} \mathrm{e}^{-i\mathbf{k}\cdot\boldsymbol{\delta}_{ij}}$ as the kinetic energy. This is evaluated on the square lattice with lattice constant $a = 1$

$$-t \sum_{<i,j>} \mathrm{e}^{-i\mathbf{k}\cdot\boldsymbol{\delta}_{ij}} = -t\left(\mathrm{e}^{-i\mathbf{k}\cdot\hat{x}} + \mathrm{e}^{-i\mathbf{k}\cdot(-\hat{x})} + \mathrm{e}^{-i\mathbf{k}\cdot\hat{y}} + \mathrm{e}^{-i\mathbf{k}\cdot(-\hat{y})}\right) \tag{3.5}$$

$$= -2t(\cos(k_x) + \cos(k_y)). \tag{3.6}$$

The key to make this into a non-centrosymmetric system is the introduction of an additional term that breaks inversion symmetry in the Hamiltonian. In a centrosymmetric system we will have $\varepsilon_{\mathbf{k}} = \varepsilon_{-\mathbf{k}}$ hold [9] for both spin-up and spin-down electrons, meaning that the band-structure will have a double degeneracy and be symmetric around $\mathbf{k} = 0$. When the inversion symmetry is broken this degeneracy is lifted everywhere except for at some points or lines of high symmetry and only $\varepsilon_{\mathbf{k}\uparrow} = \varepsilon_{-\mathbf{k}\downarrow}$ holds instead. We can understand this by considering that the lack of inversion symmetry means that the potential $V(\mathbf{k}) \neq V(-\mathbf{k})$, resulting in the electrons feeling a gradient in the potential. Note however that there is no electric current flowing despite the presence of an effective electric field. We introduce the term

$$H_0 = \sum_{\mathbf{k}} \sum_{\alpha,\beta} [(\varepsilon_{\mathbf{k}} - \mu)\delta_{\alpha,\beta} + \gamma(\mathbf{k}) \cdot \boldsymbol{\sigma}_{\alpha\beta}] c^{\dagger}_{\mathbf{k}\alpha} c_{\mathbf{k}\beta} \tag{3.7}$$

where $\boldsymbol{\sigma}$ is the vector of Pauli-matrices defined as

$$\boldsymbol{\sigma} = \begin{bmatrix} 0 & 1 \\ 1 & 0 \end{bmatrix} \hat{x} + \begin{bmatrix} 0 & -i \\ i & 0 \end{bmatrix} \hat{y} + \begin{bmatrix} 1 & 0 \\ 0 & -1 \end{bmatrix} \hat{z}, \tag{3.8}$$

and $\gamma(\mathbf{k}) = -\gamma(-\mathbf{k})$ is an inversion symmetry breaking term [10, 11] whose form depends on the specifics of the system.

We continue with a tight-binding approach on a square lattice and use a Rashba-type spin-orbit coupling (SOC) in 2D as the symmetry breaking term, resulting in an out of plane electric field. Meaning that

$$H_0 = \sum_{\mathbf{k},\alpha} (\varepsilon_{\mathbf{k}} - \mu) c^{\dagger}_{\mathbf{k}\alpha} c_{\mathbf{k}\alpha} + \alpha_{\mathrm{R}} E_z \sum_{\mathbf{k}} [(\sin(k_y) + i \sin(k_x)) c^{\dagger}_{\mathbf{k}\uparrow} c_{\mathbf{k}\downarrow}, + h.c.] \tag{3.9}$$

as shown in section A.

3.1.2 Relevance to physical systems

This serves to illustrate that while the symmetry breaking can occur naturally from the structure of the material, it can also in principle be possible to induce it, tune it and quench it by using an external field. The relevance of this to real systems is that in effectively 2 dimensional systems this can be done by applying a gate voltage to induce the required asymmetry and make the electrons feel a Rashba-interaction. It can also be achieved in the interfaces

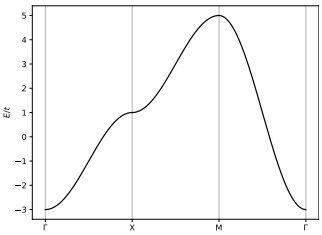

(a) Without SOC.

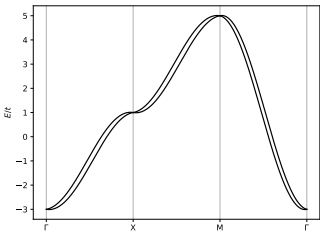

(b) With SOC.

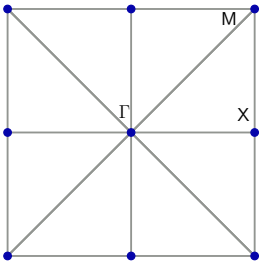

(c) Locations of the Γ, M and X points on the square lattice.

Figure 3.1: Tight binding dispersion for a square lattice without and with a Rashba SOC along high symmetry directions in the first Brillouin zone.

between heterostructures where a close to 2-dimensional electron gas experiences the Rashba-interaction. It will for be convenient to work in a diagonal basis where we end up with split pseudo-spin or so-called helicity bands for many calculations. In this basis

$$H_0 = \sum_{\mathbf{k},\lambda=\pm} \xi_{\mathbf{k}\lambda} \tilde{c}^\dagger_{\mathbf{k}\lambda} \tilde{c}_{\mathbf{k}\lambda}, \tag{3.10}$$

as derived in section B where we follow the same type of derivation that Børkje [12] does, with $\xi_{\mathbf{k}\lambda} = \varepsilon_{\mathbf{k}} - \mu + \lambda|\gamma_{\mathbf{k}}|$ giving

$$\xi_{\mathbf{k}\lambda} = -2t[\cos(k_x) + \cos(k_y)] - \mu + \lambda\alpha_{\mathrm{R}} E_z \sqrt{\sin^2(k_x) + \sin^2(k_y)}. \tag{3.11}$$

Note that λ is not a spin index, but a band-index. Now we can see that

the symmetry breaking term has lifted the degeneracy between the pseudo-spin bands by locking the spin for each momentum value $\mathbf{k}$ rather than letting it rotate freely, figure 3.1 illustrates the band structure without SOC and with SOC in the respective diagonal basis. The unitary transformation and the derivation of the above is given in B.

3.2 Pairing interaction

We will not concern ourselves with the specific microscopic origin of the pairing mechanism and write a general interaction Hamiltonian for superconductors in this band-basis

$$H_{int} = \frac{1}{2} \sum_{\mathbf{k}\mathbf{k}'\mathbf{q}} \sum_{\lambda_{1,2,3,4}} V_{\lambda_1\lambda_2\lambda_3\lambda_4}(\mathbf{k}, \mathbf{k}', \mathbf{q}) \tilde{c}^{\dagger}_{\mathbf{k}+\mathbf{q},\lambda_1} \tilde{c}^{\dagger}_{-\mathbf{k},\lambda_2} \tilde{c}_{-\mathbf{k}',\lambda_3} \tilde{c}_{\mathbf{k}'+\mathbf{q},\lambda_4}. \quad (3.12)$$

The examination is restricted to spatially homogeneous superconducting states in a weak-coupling limit. Furthermore we assume that the spin-orbit splitting is large compared to the size of the gaps. This strongly suppresses interband pairing as electrons would have to pair far away from their respective Fermi surfaces, this would incur a large energy cost and be unlikely. We therefore neglect interband pairing completely as it would be a small correction when the spin-orbit splitting is large, setting $\lambda_1 = \lambda_2 = \lambda$, $\lambda_3 = \lambda_4 = \lambda'$. The $\mathbf{q}$-dependence is also neglected for simplicity. This may not be valid for small spin-orbit splitting cases [13], but in the case of large spin-orbit splitting the depairing effect will be difficult to overcome [14]. We are then left with intraband pairing in both bands as well as the possibility of pair-hopping between bands shown in figure 3.2.

(a) Intraband scattering **(b)** Pair-hopping

Figure 3.2: Illustration of allowed interactions in the helicity bands from momentum $\mathbf{k}$ to $\mathbf{k}'$.

This leaves us with

$$H_{\text{int}} \approx -\frac{1}{2}\sum_{\mathbf{k}\mathbf{k}'}\sum_{\lambda,\lambda'} V_{\lambda\lambda'}(\mathbf{k},\mathbf{k}')\tilde{c}^{\dagger}_{\mathbf{k}\lambda}\tilde{c}^{\dagger}_{-\mathbf{k}\lambda}\tilde{c}_{-\mathbf{k}'\lambda'}\tilde{c}_{\mathbf{k}'\lambda'}, \tag{3.13}$$

where we write

$$V_{\lambda\lambda'}(\mathbf{k},\mathbf{k}') = t_{\lambda}(\mathbf{k})t^{*}_{\lambda'}(\mathbf{k}')\tilde{V}_{\lambda\lambda'}(\mathbf{k},\mathbf{k}'). \tag{3.14}$$

The motivation for splitting up $V_{\lambda\lambda'}(\mathbf{k},\mathbf{k}')$ into factors t and $\tilde{V}$ in the above is that this will allow us to write down a relation between the gap functions in the spin basis and the pseudospin basis in a particularly simple form later on. If we write $t_{\lambda}(\mathbf{k})c^{\dagger}_{-\mathbf{k}\lambda} = \mathcal{K}c^{\dagger}_{\mathbf{k}\lambda}$, where $\mathcal{K}$ is the time-reversal operator, then $\tilde{V}_{\lambda,\lambda'}(\mathbf{k},\mathbf{k}')$ becomes the pairing-interaction between time-reversed states.

We can then do a mean-field decoupling of the bands in the same way as for a normal BCS Hamiltonian. We rewrite the pairs of fermionic operators as the average plus fluctuations

$$\begin{aligned}\tilde{c}_{-\mathbf{k}'\lambda'}\tilde{c}_{\mathbf{k}'\lambda'} &= \langle\tilde{c}_{-\mathbf{k}'\lambda'}\tilde{c}_{\mathbf{k}'\lambda'}\rangle + (\tilde{c}_{-\mathbf{k}'\lambda'}\tilde{c}_{\mathbf{k}'\lambda'} - \langle\tilde{c}_{-\mathbf{k}'\lambda'}\tilde{c}_{\mathbf{k}'\lambda'}\rangle)\\ &\equiv \tilde{b}_{\mathbf{k}'\lambda'} + \delta\tilde{b}_{\mathbf{k}'\lambda'}\end{aligned} \tag{3.15}$$

and proceed to first order in the fluctuations. This gives

$$\begin{aligned}\tilde{c}^{\dagger}_{\mathbf{k}\lambda}\tilde{c}^{\dagger}_{-\mathbf{k}\lambda}\tilde{c}_{-\mathbf{k}'\lambda'}\tilde{c}_{\mathbf{k}'\lambda'} &= \left(\tilde{b}^{\dagger}_{\mathbf{k}\lambda} + \delta\tilde{b}^{\dagger}_{\mathbf{k}\lambda}\right)\left(\tilde{b}_{\mathbf{k}'\lambda'} + \delta\tilde{b}_{\mathbf{k}'\lambda'}\right)\\ &= \tilde{b}^{\dagger}_{\mathbf{k}\lambda}\tilde{b}_{\mathbf{k}'\lambda'} + \tilde{b}^{\dagger}_{\mathbf{k}\lambda}\delta\tilde{b}_{\mathbf{k}'\lambda'} + \tilde{b}_{\mathbf{k}'\lambda'}\delta\tilde{b}^{\dagger}_{\mathbf{k}\lambda} + \mathcal{O}(\delta b^2)\\ &\approx \tilde{b}^{\dagger}_{\mathbf{k}\lambda}\tilde{b}_{\mathbf{k}'\lambda'} + \tilde{b}^{\dagger}_{\mathbf{k}\lambda}\left(\tilde{c}_{-\mathbf{k}'\lambda'}\tilde{c}_{\mathbf{k}'\lambda'} - \tilde{b}_{\mathbf{k}'\lambda'}\right) + \tilde{b}_{\mathbf{k}'\lambda'}\left(\tilde{c}^{\dagger}_{\mathbf{k}\lambda}\tilde{c}^{\dagger}_{-\mathbf{k}\lambda} - \tilde{b}^{\dagger}_{\mathbf{k}\lambda}\right)\\ &= -\tilde{b}^{\dagger}_{\mathbf{k}\lambda}\tilde{b}_{\mathbf{k}'\lambda'} + \tilde{b}^{\dagger}_{\mathbf{k}\lambda}\tilde{c}_{-\mathbf{k}'\lambda'}\tilde{c}_{\mathbf{k}'\lambda'} + \tilde{b}_{\mathbf{k}'\lambda'}\tilde{c}^{\dagger}_{\mathbf{k}\lambda}\tilde{c}^{\dagger}_{-\mathbf{k}\lambda},\end{aligned} \tag{3.16}$$

by defining

$$\Delta_{\mathbf{k}\lambda} = \sum_{\mathbf{k}'\lambda'} V_{\lambda\lambda'}(\mathbf{k}\mathbf{k}')b_{\mathbf{k}'\lambda'}, \tag{3.17}$$

and ignoring the constant term for now we regain the usual mean-field terms for a multi-band superconductor.

Leaving us with

$$H_{MF} = -\frac{1}{2}\sum_{\mathbf{k}\lambda}(\Delta_{\mathbf{k}\lambda}\tilde{c}^{\dagger}_{\mathbf{k}\lambda}\tilde{c}^{\dagger}_{-\mathbf{k}\lambda} + \Delta^{\dagger}_{\mathbf{k}\lambda}\tilde{c}_{-\mathbf{k}\lambda}\tilde{c}_{\mathbf{k}\lambda}), \tag{3.18}$$

if we express the gaps as

$$\Delta_{\lambda}(\mathbf{k}) = t_{\lambda}(\mathbf{k})\tilde{\Delta}_{\lambda}(\mathbf{k}), \tag{3.19}$$

then the gaps also follow the self-consistency equation

$$\Delta_{\lambda}(\mathbf{k}) = \sum_{\mathbf{k}'\lambda'=\pm} V_{\lambda\lambda'}(\mathbf{k},\mathbf{k}')\langle\tilde{c}_{-\mathbf{k}'\lambda'}\tilde{c}_{\mathbf{k}'\lambda'}\rangle. \tag{3.20}$$

meaning that

$$\tilde{\Delta}_{\mathbf{k}\lambda} = t^{*}_{\lambda}(\mathbf{k})\sum_{\mathbf{k}'\lambda'=\pm} V_{\lambda\lambda'}(\mathbf{k},\mathbf{k}')\langle\tilde{c}_{-\mathbf{k}'\lambda'}\tilde{c}_{\mathbf{k}'\lambda'}\rangle. \tag{3.21}$$

Note that we follow the notation of Samokhin & Mineev [13] here and that Børkje [12] uses a different notation. Børkje uses $\tilde{\Delta}_{\lambda\mathbf{k}} = t_{\lambda\mathbf{k}}\chi_{\lambda\mathbf{k}}$ where $\chi_{\lambda\mathbf{k}}$ is the order parameter of time-reversed states $\tilde{c}_{\mathbf{k}\lambda}c_{\mathbf{k}\lambda}$ and $\chi_{\mathbf{k}\lambda} = \chi_{-\mathbf{k}\lambda}$. Samokhin & Mineev uses $\Delta_{\mathbf{k}\lambda} = t_{\lambda\mathbf{k}}\tilde{\Delta}_{\lambda\mathbf{k}}$, with $\tilde{\Delta}_{\lambda\mathbf{k}}$ being the order parameter of time-reversed states that transforms according to one of the irreducible representations of the space group [15]. This will aid us later in finding the form of the interaction potential and the equilibrium values of of our gaps.

In the non-centrosymmetric case we have mixing of even-parity singlet and odd-parity triplet pairing, in general this means that in the spin-basis

$$\Delta_{\alpha,\beta=\uparrow\downarrow}(\mathbf{k}) = \psi(\mathbf{k})(i\sigma_y)_{\alpha\beta} + \mathbf{d}(\mathbf{k})(i\boldsymbol{\sigma}\sigma_y)_{\alpha\beta}, \tag{3.22}$$

where

$$\psi(\mathbf{k}) = \frac{\tilde{\Delta}_{+}(\mathbf{k}) + \tilde{\Delta}_{-}(\mathbf{k})}{2} \tag{3.23}$$

and

$$\mathbf{d}(\mathbf{k}) = \frac{\tilde{\Delta}_{+}(\mathbf{k}) - \tilde{\Delta}_{-}(\mathbf{k})}{2}\hat{\gamma}(\mathbf{k}), \tag{3.24}$$

where $\hat{\gamma}(\mathbf{k}) = \gamma(\mathbf{k})/|\gamma(\mathbf{k})|$ and $\gamma(\mathbf{k})$ is defined in (3.7). The only part of the triplet gap that "survives" when the SOC is strong is the one parallel to $\hat{\gamma}(\mathbf{k})$ [11].

We can also invert the above relationships and express

$$\tilde{\Delta}_{\pm} = \psi(\mathbf{k}) \pm \hat{\gamma}(\mathbf{k}) \cdot \mathbf{d}(\mathbf{k}) \tag{3.25}$$

to illustrate that the mixing of singlet and triplet pairing can lead to nodes in the gaps.

So the quantities of interest in a quantum-quench scenario are clearly $\psi(\mathbf{k})$ and $\mathbf{d}(\mathbf{k})$. We can get these from calculating $\tilde{\Delta}_{+}(\mathbf{k}, t)$ and $\tilde{\Delta}_{-}(\mathbf{k}, t)$, which will be our goal in the following. Our strategy for obtaining these gaps will be presented in the next sections. We will need to find the Heisenberg equations of motion for the quantities we will define as the normal and anomalous Green's functions in the pseudo-spin basis and calculate the time evolution following the method used by Peronaci [16]. We also take our Hamiltonian in the pseudo-spin basis and do a Bogoliubov–Valatin transformation in each band to diagonalize it to assist in finding our initial values and analytical expressions for relevant quantities.

3.2.1 Interaction potential

So far we have not specified the form of the pairing-interaction beyond the restrictions form our approximations. We now turn our attention to this in equations (3.13) and (3.14). We remind ourselves of these equations

$$H_{int} \approx -\frac{1}{2} \sum_{\mathbf{k}\mathbf{k}'} \sum_{\lambda,\lambda'} V_{\lambda\lambda'}(\mathbf{k}, \mathbf{k}') \tilde{c}^{\dagger}_{\mathbf{k}\lambda} \tilde{c}^{\dagger}_{-\mathbf{k}\lambda} \tilde{c}_{-\mathbf{k}'\lambda'} \tilde{c}_{\mathbf{k}'\lambda'}, \tag{3.26}$$

and first note that when we write the interaction on the form in equation (3.14)

$$V_{\lambda\lambda'}(\mathbf{k}, \mathbf{k}') = t_{\lambda}(\mathbf{k}) t^{*}_{\lambda'}(\mathbf{k}') \tilde{V}_{\lambda\lambda'}(\mathbf{k}, \mathbf{k}'), \tag{3.27}$$

then the pairing between time-reversed states $\tilde{V}_{\lambda\lambda'}(\mathbf{k}, \mathbf{k}')$ must be even in both $\mathbf{k}$ and $\mathbf{k}'$ due to the anticommutation of fermionic operators. The reason for doing this is that while the full Hamiltonian is invariant under point-group operations, $\Delta_{\mathbf{k}\lambda}$ is not. It picks up a non-trivial phase-factor where the

dependence on $\mathbf{k}$ and the point group operation itself can not be eliminated as shown by Sergienko and Curnoe [15]. It turns out that when we define the gap as in equation (3.19) then $\tilde{\Delta}_{\mathbf{k}\lambda}$ transforms according to the irreducible representations of the point group. The physical explanation for this is that $\tilde{\Delta}_{\mathbf{k}\lambda}$ is the gap resulting from pairing time-reversed pairs of particles [11].

It follows that $\tilde{V}_{\lambda\lambda'}(\mathbf{k},\mathbf{k}')$ must be invariant under the point group operations of the underlying crystal symmetry group. Then we can further assume the pairing potential to have a factorized form

$$\tilde{V}_{\lambda\lambda'}(\mathbf{k},\mathbf{k}') = \sum_a V^a_{\lambda\lambda'} \sum_{i=1}^{d} \varphi_{a\lambda i}(\mathbf{k})\varphi^*_{a\lambda i}(\mathbf{k}'), \tag{3.28}$$

where a labels an irreducible representation, d is the dimension of each irreducible representation and $\varphi_{a\lambda i}(\mathbf{k})$ is a basis function of an irreducible representation of the point group of a crystal. As we are mostly interested in the pairing with the highest critical temperature, it is usually sufficient to look at the irreducible representation of the point group corresponding to the highest critical temperature. In a simple formulation we can therefore write the momentum dependence of the interaction matrix in terms of even basis functions of one irreducible representation,

$$\tilde{V}_{\lambda\lambda'}(\mathbf{k},\mathbf{k}') = V_{\lambda\lambda'} \sum_{i=1}^{d} \varphi_{\lambda i}(\mathbf{k})\varphi^*_{\lambda i}(\mathbf{k}'). \tag{3.29}$$

It can be shown by starting with the real-space representation and going to the band-basis [13] that for a BCS-like s-wave model with the approximations above, we get

$$\tilde{V}_{\lambda\lambda'}(\mathbf{k},\mathbf{k}') = \frac{V}{2}. \tag{3.30}$$

This means that the intraband pairing and the pair-scattering has the same coupling constant. This form of the coupling constant means that $\tilde{\Delta}_+ = \tilde{\Delta}_-$ from equation (3.20) as it becomes symmetrical. There will therefore be no triplet contribution to the order-parameter as we would expect in the simple s-wave case.

We can consider a slightly more general case which is where the matrix-elements of $\tilde{V}_{\lambda\lambda'}$ can give rise to triplet pairing, but is still simple in the sense that they are independent of $\mathbf{k}$ and $\mathbf{k}'$. To this end we can consider for our

model with a square 2 dimensional lattice the point group C_{4v} combined with a Rashba SOC and find that the unit representation A_1 is compatible with a pairing interaction that is particularly simple to deal with [17]

$$\tilde{V}(\mathbf{k},\mathbf{k}') = \frac{V_g}{2}(\sigma_0 + \sigma_x) + \frac{V_u}{2}(\sigma_0 - \sigma_x), \tag{3.31}$$

where V_g and V_u are constants that correspond to the even and odd parts of the interaction in the spin-basis, a full derivation of this can be found in [13]. What matters for the mixing of the singlet and triplet states is the relative size of these constants, equation (3.30) corresponds to $V_u = 0$ and $V_g \neq 0$.

We can rewrite this and let the diagonal parts be equal and described by a constant $\tilde{V}_{\lambda\lambda} = \tilde{V}^d$ and the off-diagonal parts be described by a constant $\tilde{V}^o$ that is in general different to $\tilde{V}^d$. This still allows equations (3.14) and (3.20) to give rise to mixtures of singlet and triplet states and our interaction-matrix takes the form

$$\begin{bmatrix} \tilde{V}^d & \tilde{V}^o \\ \tilde{V}^o & \tilde{V}^d \end{bmatrix}. \tag{3.32}$$

In particular, we can see in a similar way as above from equation (3.20) that the singlet part of the gap goes to zero when $\tilde{V}^o = -\tilde{V}^d$ leaving us with only a triplet part. Letting $\tilde{V}^o$ vary between $\pm\tilde{V}^d$ allows us to get mixtures of singlet and triplet pairing [11, 17]. This choice leads to basis functions that are $\mathbf{k}$ independent, meaning that our gap amplitudes will also be isotropic and independent of $\mathbf{k}$. This in turn leads to an isotropic singlet gap (3.23) and a triplet gap (3.24) with $\mathbf{k}$ dependence given entirely by $\hat{\gamma}(\mathbf{k})$ where $\hat{\gamma}(\mathbf{k})$ is proportional to $k_y\hat{\mathbf{x}} - k_x\hat{\mathbf{y}}$ for the Rashba interaction we have chosen.

Note that in general it is also possible for all four components in the matrix (3.32) to be different. The equations used in this thesis can accommodate this as well as different momentum dependencies than what is chosen here, we stick with the above interaction matrix to investigate the dynamics of singlet and triplet mixing in the simplest model.

In the following we will mostly refer to the ratio between the diagonal element ($\tilde{V}^d$) and off-diagonal element ($\tilde{V}^o$) when describing the interaction-matrix.

CHAPTER 4

EQUATIONS OF MOTION

4.1 Time dependence

So far everything we have done is completely time-independent and refers to systems in equilibrium. The quantities we are interested in examining are dynamical quantities, like the amplitude(Higgs)-modes and phase(Leggett)-modes of the order parameters. These are essentially oscillations in the amplitude of the order parameter in the case of the Higgs mode and oscillations in the relative phase of the two order parameters in a two-band system in the case of the Leggett mode. These quantities will be discussed in more detail in chapter 6 and 7. What we need to know at this time is that we want to find the time evolution of the order parameters. In the following section we will therefore derive a set of differential equations describing this. We will also need to develop a numerical scheme for solving this set of equations.

Our starting point for the equations of motion will the full mean field Hamiltonian we have derived so far

$$H = \sum_{\mathbf{k}\lambda} \xi_{\mathbf{k}\lambda} \tilde{c}^\dagger_{\mathbf{k}\lambda} \tilde{c}_{\mathbf{k}\lambda} - \frac{1}{2} \sum_{\mathbf{k}\lambda} (\Delta_{\mathbf{k}\lambda} \tilde{c}^\dagger_{\mathbf{k}\lambda} \tilde{c}^\dagger_{-\mathbf{k}\lambda} + \Delta^\dagger_{\mathbf{k}\lambda} \tilde{c}_{-\mathbf{k}\lambda} \tilde{c}_{\mathbf{k}\lambda}). \tag{4.1}$$

The quanties of interest are $\tilde{\Delta}_{\mathbf{k}\pm}(t)$, from which it follows that we need the quantities $\langle \tilde{c}_{-\mathbf{k}\pm}(t) \tilde{c}_{\mathbf{k}\pm}(t) \rangle$. It will turn out that this requires us to find the equations of motion for the following quantities which we with some abuse of notation call Green's functions

$$G_{\mathbf{k}\lambda}(t) = \langle \tilde{c}^\dagger_{\mathbf{k}\lambda}(t)\tilde{c}_{\mathbf{k}\lambda}(t)\rangle, \tag{4.2}$$

and

$$F_{\mathbf{k}\lambda}(t) = \langle \tilde{c}_{-\mathbf{k}\lambda}(t)\tilde{c}_{\mathbf{k}\lambda}(t)\rangle. \tag{4.3}$$

To get the initial conditions we then do a Bogoliubov–Valatin transformation to find the expectation values in the low temperature limit at the time $t = 0$.

4.1.1 Equations of motion

We start out by finding the equations of motion for the first pair of operators $\tilde{c}^\dagger_{\mathbf{k}\lambda}\tilde{c}_{\mathbf{k}\lambda}$

$$i\frac{d}{dt}\tilde{c}^\dagger_{\mathbf{k}\lambda}\tilde{c}_{\mathbf{k}\lambda} = [\tilde{c}^\dagger_{\mathbf{k}\lambda}\tilde{c}_{\mathbf{k}\lambda}, H] \tag{4.4}$$

and commute our operators across the Hamiltonian from left to right. The first term in the Hamiltonian in (4.1) does not contribute as number operators commute, and we focus on the last two terms giving contribution

$$\begin{aligned}
\tilde{c}^\dagger_{\mathbf{k}\lambda}\tilde{c}_{\mathbf{k}\lambda}\sum_{\mathbf{p}\mu}\Delta_{\mathbf{p}\mu}\tilde{c}^\dagger_{\mathbf{p}\mu}\tilde{c}^\dagger_{-\mathbf{p}\mu} &= \sum_{\mathbf{p}\mu}\Delta_{\mathbf{p}\mu}\tilde{c}^\dagger_{\mathbf{k}\lambda}\tilde{c}_{\mathbf{k}\lambda}\tilde{c}^\dagger_{\mathbf{p}\mu}\tilde{c}^\dagger_{-\mathbf{p}\mu} \\
&= \sum_{\mathbf{p}\mu}\Delta_{\mathbf{p}\mu}\tilde{c}^\dagger_{\mathbf{k}\lambda}(\delta_{\mathbf{k},\mathbf{p}}\delta_{\lambda,\mu} - c^\dagger_{\mathbf{p}\mu}\tilde{c}_{\mathbf{k}\lambda})\tilde{c}^\dagger_{-\mathbf{p}\mu} \\
&= \Delta_{\mathbf{k}\lambda}\tilde{c}^\dagger_{\mathbf{k}\lambda}\tilde{c}^\dagger_{-\mathbf{k}\lambda} - \sum_{\mathbf{p}\mu}\Delta_{\mathbf{p}\mu}\tilde{c}^\dagger_{\mathbf{k}\lambda}\tilde{c}^\dagger_{\mathbf{p}\mu}(\delta_{\lambda,\mu}\delta_{\mathbf{k},-\mathbf{p}} - \tilde{c}^\dagger_{-\mathbf{p}\mu}\tilde{c}_{\mathbf{k}\lambda}) \\
&= \Delta_{\mathbf{k}\lambda}\tilde{c}^\dagger_{\mathbf{k}\lambda}\tilde{c}^\dagger_{-\mathbf{k}\lambda} - \Delta_{-\mathbf{k}\lambda}\tilde{c}^\dagger_{\mathbf{k}\lambda}\tilde{c}^\dagger_{-\mathbf{k}\lambda} + \sum_{\mathbf{p}\mu}\Delta_{\mathbf{p}\mu}\tilde{c}^\dagger_{\mathbf{p}\mu}\tilde{c}^\dagger_{-\mathbf{p}\mu}\tilde{c}^\dagger_{\mathbf{k}\lambda}\tilde{c}_{\mathbf{k}\lambda} \\
&= 2\Delta_{\mathbf{k}\lambda}\tilde{c}^\dagger_{\mathbf{k}\lambda}\tilde{c}^\dagger_{-\mathbf{k}\lambda} + \sum_{\mathbf{p}\mu}\Delta_{\mathbf{p}\mu}\tilde{c}^\dagger_{\mathbf{p}\mu}\tilde{c}^\dagger_{-\mathbf{p}\mu}\tilde{c}^\dagger_{\mathbf{k}\lambda}\tilde{c}_{\mathbf{k}\lambda}
\end{aligned} \tag{4.5}$$

where the last line follows from the anti-commutation of fermions implying that $\Delta_{-\mathbf{k}\lambda} = -\Delta_{\mathbf{k}\lambda}$.

In the same way it follows that

$$\tilde{c}^\dagger_{\mathbf{k}\lambda}\tilde{c}_{\mathbf{k}\lambda}\sum_{\mathbf{p}\mu}\Delta^\dagger_{\mathbf{p}\mu}\tilde{c}_{-\mathbf{p}\mu}\tilde{c}_{\mathbf{p}\mu} = -2\Delta^\dagger_{\mathbf{k}\lambda}\tilde{c}_{-\mathbf{k}\lambda}\tilde{c}_{\mathbf{k}\lambda} + \sum_{\mathbf{p}\mu}\Delta^\dagger_{\mathbf{p}\mu}\tilde{c}_{-\mathbf{p}\mu}\tilde{c}_{\mathbf{p}\mu}\tilde{c}^\dagger_{\mathbf{k}\lambda}\tilde{c}_{\mathbf{k}\lambda} \tag{4.6}$$

giving us

$$i\frac{dG_{\mathbf{k}\lambda}(t)}{dt} = [\Delta^*_{\mathbf{k}\lambda}(t)F_{\mathbf{k}\lambda}(t) - F^*_{\mathbf{k}\lambda}(t)\Delta_{\mathbf{k}\lambda}(t)] \tag{4.7}$$

after taking the zero temperature expectation value. Next up, we look at the operators $\tilde{c}_{-\mathbf{k}\lambda}\tilde{c}_{\mathbf{k}\lambda}$

$$i\frac{d}{dt}\tilde{c}_{-\mathbf{k}\lambda}\tilde{c}_{\mathbf{k}\lambda} = [\tilde{c}_{-\mathbf{k}\lambda}\tilde{c}_{\mathbf{k}\lambda}, H] \tag{4.8}$$

and focus first on contributions from the kinetic term

$$\begin{aligned}
\tilde{c}_{-\mathbf{k}\lambda}\tilde{c}_{\mathbf{k}\lambda}\sum_{\mathbf{p}\mu}\xi_{\mathbf{p}\mu}\tilde{c}^\dagger_{\mathbf{p}\mu}\tilde{c}_{\mathbf{p}\mu} &= \sum_{\mathbf{p}\mu}\xi_{\mathbf{p}\mu}\tilde{c}_{-\mathbf{k}\lambda}(\delta_{\mathbf{p},\mathbf{k}}\delta_{\lambda,\mu} - \tilde{c}^\dagger_{\mathbf{p}\mu}\tilde{c}_{\mathbf{k}\lambda})\tilde{c}_{\mathbf{p}\mu} \\
&= \xi_{\mathbf{k}\lambda}\tilde{c}_{-\mathbf{k}\lambda}\tilde{c}_{\mathbf{k}\lambda} - \sum_{\mathbf{p}\mu}\xi_{\mathbf{p}\mu}(\delta_{\lambda,\mu}\delta_{\mathbf{k},-\mathbf{p}} - \tilde{c}^\dagger_{\mathbf{p}\mu}\tilde{c}_{-\mathbf{k}\lambda})\tilde{c}_{\mathbf{k}\lambda}\tilde{c}_{\mathbf{p}\mu} \\
&= \xi_{\mathbf{k}\lambda}\tilde{c}_{-\mathbf{k}\lambda}\tilde{c}_{\mathbf{k}\lambda} - \xi_{-\mathbf{k}\lambda}\tilde{c}_{\mathbf{k}\lambda}\tilde{c}_{-\mathbf{k}\lambda} + \sum_{\mathbf{p}\mu}\xi_{\mathbf{p}\mu}\tilde{c}^\dagger_{\mathbf{p}\mu}\tilde{c}_{\mathbf{p}\mu}\tilde{c}_{-\mathbf{k}\lambda}\tilde{c}_{\mathbf{k}\lambda} \\
&= 2\xi_{\mathbf{k}\lambda}\tilde{c}_{-\mathbf{k}\lambda}\tilde{c}_{\mathbf{k}\lambda} + \sum_{\mathbf{p}\mu}\xi_{\mathbf{p}\mu}\tilde{c}^\dagger_{\mathbf{p}\mu}\tilde{c}_{\mathbf{p}\mu}\tilde{c}_{-\mathbf{k}\lambda}\tilde{c}_{\mathbf{k}\lambda}
\end{aligned} \tag{4.9}$$

where the last line follows from the anti-commutation of fermions and the symmetry $\xi_{\mathbf{k}\lambda} = \xi_{-\mathbf{k}\lambda}$ of the kinetic energy in the pseudu-spin basis. The last contribution comes from

$$
\begin{aligned}
\tilde{c}_{-\mathbf{k}\lambda}\tilde{c}_{\mathbf{k}\lambda}\sum_{\mathbf{p}\mu}\Delta_{\mathbf{p}\mu}\tilde{c}^{\dagger}_{\mathbf{p}\mu}\tilde{c}^{\dagger}_{-\mathbf{p}\mu} &= \sum_{\mathbf{p}\mu}\Delta_{\mathbf{p}\mu}\tilde{c}_{-\mathbf{k}\lambda}(\delta_{\mathbf{p},\mathbf{k}}\delta_{\lambda\mu}-\tilde{c}^{\dagger}_{\mathbf{p}\mu}\tilde{c}_{\mathbf{k}\lambda})\tilde{c}^{\dagger}_{-\mathbf{p}\mu}\\
&= \Delta_{\mathbf{k}\lambda}(1-c^{\dagger}_{-\mathbf{k}\lambda}\tilde{c}_{-\mathbf{k}\lambda})-\sum_{\mathbf{p}\mu}\Delta_{\mathbf{p}\mu}\tilde{c}_{-\mathbf{k}\lambda}c^{\dagger}_{\mathbf{p}\mu}(\delta_{\mathbf{k},-\mathbf{p}}\delta_{\lambda,\mu}-\tilde{c}^{\dagger}_{-\mathbf{p}\mu}\tilde{c}_{\mathbf{k}\lambda})\\
&= \Delta_{\mathbf{k}\lambda}(1-c^{\dagger}_{-\mathbf{k}\lambda}\tilde{c}_{-\mathbf{k}\lambda})-\Delta_{-\mathbf{k}\lambda}c_{-\mathbf{k}\lambda}c^{\dagger}_{-\mathbf{k}\lambda}+\sum_{\mathbf{p}\mu}\Delta_{\mathbf{p}\mu}\tilde{c}_{-\mathbf{k}\lambda}c^{\dagger}_{\mathbf{p}\mu}\tilde{c}^{\dagger}_{-\mathbf{p}\mu}\tilde{c}_{\mathbf{k}\lambda}\\
&= 2\Delta_{\mathbf{k}\lambda}(1-c^{\dagger}_{-\mathbf{k}\lambda}\tilde{c}_{-\mathbf{k}\lambda})+\sum_{\mathbf{p}\mu}\Delta_{\mathbf{p}\mu}(\delta_{-\mathbf{k},\mathbf{p}}\delta_{\lambda,\mu}-\tilde{c}^{\dagger}_{\mathbf{p}\mu}\tilde{c}_{-\mathbf{k}\lambda})\tilde{c}^{\dagger}_{-\mathbf{p}\mu}\tilde{c}_{\mathbf{k}\lambda}\\
&= 2\Delta_{\mathbf{k}\lambda}(1-c^{\dagger}_{-\mathbf{k}\lambda}\tilde{c}_{-\mathbf{k}\lambda})+\Delta_{-\mathbf{k}\lambda}\tilde{c}^{\dagger}_{\mathbf{k}\lambda}c_{\mathbf{k}\lambda}-\sum_{\mathbf{p}\mu}\Delta_{\mathbf{p}\mu}\tilde{c}^{\dagger}_{\mathbf{p}\mu}\tilde{c}_{-\mathbf{k}\lambda}\tilde{c}^{\dagger}_{-\mathbf{p}\mu}\tilde{c}_{\mathbf{k}\lambda}\\
&= 2\Delta_{\mathbf{k}\lambda}(1-c^{\dagger}_{-\mathbf{k}\lambda}\tilde{c}_{-\mathbf{k}\lambda})+\Delta_{-\mathbf{k}\lambda}\tilde{c}^{\dagger}_{\mathbf{k}\lambda}c_{\mathbf{k}\lambda}-\Delta_{\mathbf{k}\lambda}\tilde{c}^{\dagger}_{\mathbf{k}\lambda}c_{\mathbf{k}\lambda}+\\
&+\sum_{\mathbf{p}\mu}\Delta_{\mathbf{p}\mu}\tilde{c}^{\dagger}_{\mathbf{p}\mu}\tilde{c}^{\dagger}_{-\mathbf{p}\mu}\tilde{c}_{-\mathbf{k}\lambda}\tilde{c}_{\mathbf{k}\lambda}\\
&= 2\Delta_{\mathbf{k}\lambda}(1-c^{\dagger}_{-\mathbf{k}\lambda}\tilde{c}_{-\mathbf{k}\lambda})-2\Delta_{\mathbf{k}\lambda}\tilde{c}^{\dagger}_{\mathbf{k}\lambda}c_{\mathbf{k}\lambda}+\sum_{\mathbf{p}\mu}\Delta_{\mathbf{p}\mu}\tilde{c}^{\dagger}_{\mathbf{p}\mu}\tilde{c}^{\dagger}_{-\mathbf{p}\mu}\tilde{c}_{-\mathbf{k}\lambda}\tilde{c}_{\mathbf{k}\lambda}\\
&= 2\Delta_{\mathbf{k}\lambda}(1-2c^{\dagger}_{-\mathbf{k}\lambda}\tilde{c}_{-\mathbf{k}\lambda})+\sum_{\mathbf{p}\mu}\Delta_{\mathbf{p}\mu}\tilde{c}^{\dagger}_{\mathbf{p}\mu}\tilde{c}^{\dagger}_{-\mathbf{p}\mu}\tilde{c}_{-\mathbf{k}\lambda}\tilde{c}_{\mathbf{k}\lambda}
\end{aligned}
$$

giving us

$$
i\frac{dF_{\mathbf{k}\lambda}(t)}{dt} = 2\xi_{\mathbf{k}\lambda}F_{\mathbf{k}\lambda}(t)+\Delta_{\mathbf{k}\lambda}(2G_{\mathbf{k}\lambda}(t)-1) \tag{4.10}
$$

after taking the expectation value. Which is on the same form as the equations in [18].

This leaves us with a coupled set of differential equations for the equations of motion

$$
i\frac{dF_{\mathbf{k}\lambda}(t)}{dt} = 2\xi_{\mathbf{k}\lambda}F_{\mathbf{k}\lambda}(t)+\Delta_{\mathbf{k}\lambda}(2G_{\mathbf{k}\lambda}(t)-1) \tag{4.11a}
$$

$$
i\frac{dG_{\mathbf{k}\lambda}(t)}{dt} = [\Delta^{*}_{\mathbf{k}\lambda}(t)F_{\mathbf{k}\lambda}(t)-F^{*}_{\mathbf{k}\lambda}(t)\Delta_{\mathbf{k}\lambda}(t)]. \tag{4.11b}
$$

We note that while the equations of motion appear uncoupled in this form, they are in fact coupled through the gap-equations

$$
\Delta_{\mathbf{k}\lambda} = \sum_{\mathbf{k}'\lambda'}V_{\mathbf{k}\mathbf{k}'\lambda\lambda'}F_{\mathbf{k}'\lambda'}, \tag{4.12}
$$

and we now need to find the initial conditions.

4.1.2 Bogoliubov-Valantin transform

To proceed further we do a change of basis to diagonalize the mean-field Hamiltonian

$$H = \sum_{\mathbf{k}\lambda} \xi_{\mathbf{k}\lambda} \tilde{c}^\dagger_{\mathbf{k}\lambda} \tilde{c}_{\mathbf{k}\lambda} - \frac{1}{2} \sum_{\mathbf{k}\lambda} (\Delta_{\mathbf{k}\lambda} \tilde{c}^\dagger_{\mathbf{k}\lambda} \tilde{c}^\dagger_{-\mathbf{k}\lambda} + \Delta^\dagger_{\mathbf{k}\lambda} \tilde{c}_{-\mathbf{k}\lambda} \tilde{c}_{\mathbf{k}\lambda}). \tag{4.13}$$

In order to do this, a Bogoliubov-Valantin transform is introduced to our system of effectively spinless fermions

$$\gamma_{\mathbf{k}\lambda} = u_{\mathbf{k}\lambda} \tilde{c}_{\mathbf{k}\lambda} - v_{\mathbf{k}\lambda} \tilde{c}^\dagger_{-\mathbf{k}\lambda}. \tag{4.14}$$

We start out by making sure that our new quasi-particle operators $\gamma, \gamma^\dagger$ are fermions, then we express our Hamiltonian in terms of them to find the conditions on the coefficients u, v for it to be diagonalized. Dropping the band-index for now (as all operators in the following are in the same band) we check that this transform preserves the commutation relations

$$\begin{aligned}
\{\gamma_{\mathbf{k}}, \gamma^\dagger_{\mathbf{k}}\} &= (u_{\mathbf{k}\lambda} \tilde{c}_{\mathbf{k}\lambda} - v_{\mathbf{k}\lambda} \tilde{c}^\dagger_{-\mathbf{k}\lambda})(u^*_{\mathbf{k}\lambda} \tilde{c}^\dagger_{\mathbf{k}\lambda} - v^*_{\mathbf{k}\lambda} \tilde{c}_{-\mathbf{k}\lambda}) + \\
&+ (u^*_{\mathbf{k}\lambda} \tilde{c}^\dagger_{\mathbf{k}\lambda} - v^*_{\mathbf{k}\lambda} \tilde{c}_{-\mathbf{k}\lambda})(u_{\mathbf{k}\lambda} \tilde{c}_{\mathbf{k}\lambda} - v_{\mathbf{k}\lambda} \tilde{c}^\dagger_{-\mathbf{k}\lambda}) \\
&= |u_{\mathbf{k}}|^2 (1 - \tilde{c}^\dagger_{\mathbf{k}} \tilde{c}_{\mathbf{k}}) + |u_{\mathbf{k}}|^2 \tilde{c}^\dagger_{\mathbf{k}} \tilde{c}_{\mathbf{k}} + |v_{\mathbf{k}}|^2 \tilde{c}^\dagger_{-\mathbf{k}} \tilde{c}_{-\mathbf{k}} + |v_{\mathbf{k}}|^2 (1 - \tilde{c}^\dagger_{-\mathbf{k}} \tilde{c}_{-\mathbf{k}}) + \\
&- u_{\mathbf{k}} v^*_{\mathbf{k}} \tilde{c}_{\mathbf{k}} \tilde{c}_{-\mathbf{k}} + u^*_{\mathbf{k}} v_{\mathbf{k}} \tilde{c}^\dagger_{-\mathbf{k}} \tilde{c}^\dagger_{\mathbf{k}} - u_{\mathbf{k}} v^*_{\mathbf{k}} \tilde{c}_{-\mathbf{k}} \tilde{c}_{\mathbf{k}} + u^*_{\mathbf{k}} v_{\mathbf{k}} \tilde{c}^\dagger_{\mathbf{k}} \tilde{c}^\dagger_{-\mathbf{k}} \\
&= |u_{\mathbf{k}}|^2 + |v_{\mathbf{k}}|^2
\end{aligned} \tag{4.15}$$

which gives us the correct anti-commutator $\{\gamma_{\mathbf{k}}, \gamma^\dagger_{\mathbf{k}}\} = 1$ with the standard choices of $u_{\mathbf{k}} = \cos(\theta_{\mathbf{k}})$, $v_{\mathbf{k}} = \sin(\theta_{\mathbf{k}})$ and $\theta_{-\mathbf{k}} = -\theta_{\mathbf{k}}$. The other anti-commutators

$$\{\gamma_{\mathbf{k}}, \gamma_{\mathbf{k}'}\} = \{\gamma^\dagger_{\mathbf{k}}, \gamma^\dagger_{\mathbf{k}'}\} = 0 \tag{4.16}$$

follow directly from the anti-commutation of the band-operators.

With the check completed we can proceed, the band indices are reintroduced and we express our band-operators in terms of our new fermions

$$\tilde{c}_{\mathbf{k}\lambda} = u^*_{\mathbf{k}\lambda} \gamma_{\mathbf{k}\lambda} + v_{\mathbf{k}\lambda} \gamma^\dagger_{-\mathbf{k}\lambda} \tag{4.17}$$

$$\tilde{c}^{\dagger}_{-\mathbf{k}\lambda} = u_{\mathbf{k}\lambda}\gamma^{\dagger}_{-\mathbf{k}\lambda} - v^{*}_{\mathbf{k}\lambda}\gamma_{\mathbf{k}\lambda}. \tag{4.18}$$

Now we want to express the quadratic terms in the Hamiltonian with our new operators with the goal of removing off-diagonal terms

$$\begin{aligned}\tilde{c}^{\dagger}_{\mathbf{k}\lambda}\tilde{c}_{\mathbf{k}\lambda} &= (u_{\mathbf{k}\lambda}\gamma^{\dagger}_{\mathbf{k}\lambda} + v^{*}_{\mathbf{k}\lambda}\gamma_{-\mathbf{k}\lambda})(u^{*}_{\mathbf{k}\lambda}\gamma_{\mathbf{k}\lambda} + v_{\mathbf{k}\lambda}\gamma^{\dagger}_{-\mathbf{k}\lambda}) \\ &= |u_{\mathbf{k}\lambda}|^2\gamma^{\dagger}_{\mathbf{k}\lambda}\gamma_{\mathbf{k}\lambda} + u_{\mathbf{k}\lambda}v_{\mathbf{k}\lambda}\gamma^{\dagger}_{\mathbf{k}\lambda}\gamma^{\dagger}_{-\mathbf{k}\lambda} + u^{*}_{\mathbf{k}\lambda}v^{*}_{\mathbf{k}\lambda}\gamma_{-\mathbf{k}\lambda}\gamma_{\mathbf{k}\gamma} + |v_{\mathbf{k}\lambda}|^2\gamma_{-\mathbf{k}\lambda}\gamma^{\dagger}_{-\mathbf{k}\lambda},\end{aligned} \tag{4.19}$$

$$\begin{aligned}\tilde{c}^{\dagger}_{\mathbf{k}\lambda}\tilde{c}^{\dagger}_{-\mathbf{k}\lambda} &= (u_{\mathbf{k}\lambda}\gamma^{\dagger}_{\mathbf{k}\lambda} + v^{*}_{\mathbf{k}\lambda}\gamma_{-\mathbf{k}\lambda})(u_{\mathbf{k}\lambda}\gamma^{\dagger}_{-\mathbf{k}\lambda} - v^{*}_{\mathbf{k}\lambda}\gamma_{\mathbf{k}\lambda}) \\ &= u^2_{\mathbf{k}\lambda}\gamma^{\dagger}_{\mathbf{k}\lambda}\gamma^{\dagger}_{-\mathbf{k}\lambda} - (v^{*}_{\mathbf{k}\lambda})^2\gamma_{-\mathbf{k}\lambda}\gamma_{\mathbf{k}\lambda} + u_{\mathbf{k}\lambda}v^{*}_{\mathbf{k}\lambda}(\gamma_{-\mathbf{k}\lambda}\gamma^{\dagger}_{-\mathbf{k}\lambda} - \gamma^{\dagger}_{\mathbf{k}\lambda}\gamma_{\mathbf{k}\lambda}),\end{aligned} \tag{4.20}$$

$$\begin{aligned}\tilde{c}_{-\mathbf{k}\lambda}\tilde{c}_{\mathbf{k}\lambda} &= (u^{*}_{\mathbf{k}\lambda}\gamma_{-\mathbf{k}\lambda} - v_{\mathbf{k}\lambda}\gamma^{\dagger}_{\mathbf{k}\lambda})(u^{*}_{\mathbf{k}\lambda}\gamma_{\mathbf{k}\lambda} + v_{\mathbf{k}\lambda}\gamma^{\dagger}_{-\mathbf{k}\lambda}) \\ &= (u^{*}_{\mathbf{k}\lambda})^2\gamma_{-\mathbf{k}\lambda}\gamma_{\mathbf{k}\lambda} - v^2_{\mathbf{k}\lambda}\gamma^{\dagger}_{\mathbf{k}\lambda}\gamma^{\dagger}_{-\mathbf{k}\lambda} + u^{*}_{\mathbf{k}\lambda}v_{\mathbf{k}\lambda}(\gamma_{-\mathbf{k}\lambda}\gamma^{\dagger}_{-\mathbf{k}\lambda} - \gamma^{\dagger}_{\mathbf{k}\lambda}\gamma_{\mathbf{k}\lambda}).\end{aligned} \tag{4.21}$$

The coefficients of the undesired off-diagonal terms can now be gathered up

$$\gamma^{\dagger}_{\mathbf{k}\lambda}\gamma^{\dagger}_{-\mathbf{k}\lambda} : \xi_{\mathbf{k}\lambda}u_{\mathbf{k}\lambda}v_{\mathbf{k}\lambda} - \frac{1}{2}\Delta_{\mathbf{k}\lambda}u^2_{\mathbf{k}\lambda} + \frac{1}{2}\Delta^{*}_{\mathbf{k}\lambda}v^2_{\mathbf{k}\lambda}, \tag{4.22}$$

$$\gamma_{-\mathbf{k}\lambda}\gamma_{\mathbf{k}\lambda} : \xi_{\mathbf{k}\lambda}u^{*}_{\mathbf{k}\lambda}v^{*}_{\mathbf{k}\lambda} + \frac{1}{2}(v^{*}_{\mathbf{k}\lambda})^2\Delta_{\mathbf{k}\lambda} - \frac{1}{2}(u^{*}_{\mathbf{k}\lambda})^2\Delta^{*}_{\mathbf{k}\lambda}. \tag{4.23}$$

We want these to vanish, as they are simply conjugate equations we pick one, set the coefficient equations equal to zero and solve for the ratio $v_{\mathbf{k}\lambda}/u_{\mathbf{k}\lambda}$

$$2\xi_{\mathbf{k}\lambda}\frac{v_{\mathbf{k}\lambda}}{u_{\mathbf{k}\lambda}} - \Delta^{*}_{\mathbf{k}\lambda}\left(\frac{v_{\mathbf{k}\lambda}}{u_{\mathbf{k}\lambda}}\right)^2 + \Delta_{\mathbf{k}\lambda} = 0 \tag{4.24}$$

$$\implies \frac{v_{\mathbf{k}\lambda}}{u_{\mathbf{k}\lambda}} = \frac{-\xi_{\mathbf{k}\lambda} \pm \sqrt{\xi^2_{\mathbf{k}\lambda} + |\Delta_{\mathbf{k}\lambda}|^2}}{\Delta^{*}_{\mathbf{k}\lambda}} \tag{4.25}$$

it follows from our above definitions of $u_{\mathbf{k}\lambda}, v_{\mathbf{k}\lambda}$ that since $|u_{\mathbf{k}\lambda}|^2 + |v_{\mathbf{k}\lambda}|^2 = 1$

$$|u_{\mathbf{k}\lambda}|^2 = \frac{1}{1+\left|\frac{u_{\mathbf{k}\lambda}}{v_{\mathbf{k}\lambda}}\right|^2} = \frac{|\Delta_{\mathbf{k}\lambda}|^2}{2|\Delta_{\mathbf{k}\lambda}|^2 + 2\xi_{\mathbf{k}\lambda}^2 \mp 2\xi_{\mathbf{k}\lambda}\sqrt{\xi_{\mathbf{k}\lambda}^2 + |\Delta_{\mathbf{k}\lambda}|^2}} \tag{4.26}$$

to ensure that the BCS-ground state is a minimum energy state we choose the positive solution for the above equation and so

$$\begin{aligned}
|u_{\mathbf{k}\lambda}|^2 &= \frac{1}{1+\left|\frac{u_{\mathbf{k}\lambda}}{v_{\mathbf{k}\lambda}}\right|^2} = \frac{1}{2}\frac{|\Delta_{\mathbf{k}\lambda}|^2}{|\Delta_{\mathbf{k}\lambda}|^2 + \xi_{\mathbf{k}\lambda}^2 - \xi_{\mathbf{k}\lambda}\sqrt{\xi_{\mathbf{k}\lambda}^2 + |\Delta_{\mathbf{k}\lambda}|^2}} \\
&= \frac{1}{2}\frac{|\Delta_{\mathbf{k}\lambda}|^2(\sqrt{\xi_{\mathbf{k}\lambda}^2 + |\Delta_{\mathbf{k}\lambda}|^2} + \xi_{\mathbf{k}\lambda})}{|\Delta_{\mathbf{k}\lambda}|^2(\sqrt{\xi_{\mathbf{k}\lambda}^2 + |\Delta_{\mathbf{k}\lambda}|^2} + \xi_{\mathbf{k}\lambda}) - \xi_{\mathbf{k}\lambda}|\Delta_{\mathbf{k}\lambda}|^2} \\
&= \frac{1}{2}\frac{\sqrt{\xi_{\mathbf{k}\lambda}^2 + |\Delta_{\mathbf{k}\lambda}|^2} + \xi_{\mathbf{k}\lambda}}{\sqrt{\xi_{\mathbf{k}\lambda}^2 + |\Delta_{\mathbf{k}\lambda}|^2}} \\
&= \frac{1}{2}\left(1 + \frac{\xi_{\mathbf{k}\lambda}}{\sqrt{\xi_{\mathbf{k}\lambda}^2 + |\Delta_{\mathbf{k}\lambda}|^2}}\right).
\end{aligned} \tag{4.27}$$

From the above it follows that

$$|v_{\mathbf{k}\lambda}|^2 = \frac{1}{2}\left(1 - \frac{\xi_{\mathbf{k}\lambda}}{\sqrt{\xi_{\mathbf{k}\lambda}^2 + |\Delta_{\mathbf{k}\lambda}|^2}}\right) \tag{4.28}$$

Now we take a look at the coefficients of the diagonal terms, ignoring any terms that appear without operators as we are not concerned about the zero-point of the energy at the moment

$$\gamma_{\mathbf{k}\lambda}^\dagger \gamma_{\mathbf{k}\lambda} : \xi_{\mathbf{k}\lambda}|u_{\mathbf{k}\lambda}|^2 + \frac{1}{2}\Delta_{\mathbf{k}\lambda}u_{\mathbf{k}\lambda}v_{\mathbf{k}\lambda}^* + \frac{1}{2}\Delta_{\mathbf{k}\lambda}^* u_{\mathbf{k}\lambda}^* v_{\mathbf{k}\lambda}, \tag{4.29}$$

$$\gamma_{-\mathbf{k}\lambda}^\dagger \gamma_{-\mathbf{k}\lambda} : -\xi_{\mathbf{k}\lambda}|v_{\mathbf{k}\lambda}|^2 + \frac{1}{2}\Delta_{\mathbf{k}\lambda}u_{\mathbf{k}\lambda}v_{\mathbf{k}\lambda}^* + \frac{1}{2}\Delta_{\mathbf{k}\lambda}^* u_{\mathbf{k}\lambda}^* v_{\mathbf{k}\lambda}. \tag{4.30}$$

And so we get by using the relations above for the coefficients of our diagonalized Hamiltonian

$$\begin{aligned}
&\xi_{\mathbf{k}\lambda}(|u_{\mathbf{k}\lambda}|^2 - |v_{\mathbf{k}\lambda}|^2) + \Delta_{\mathbf{k}\lambda} u_{\mathbf{k}\lambda} v^*_{\mathbf{k}\lambda} + \Delta^*_{\mathbf{k}\lambda} u^*_{\mathbf{k}\lambda} v_{\mathbf{k}\lambda} \\
=&\frac{\xi^2_{\mathbf{k}\lambda}}{\sqrt{\xi^2_{\mathbf{k}\lambda} + |\Delta_{\mathbf{k}\lambda}|^2}} + \left(1 + \frac{\xi_{\mathbf{k}\lambda}}{\sqrt{\xi^2_{\mathbf{k}\lambda} + |\Delta_{\mathbf{k}\lambda}|^2}}\right)(\sqrt{\xi^2_{\mathbf{k}\lambda} + |\Delta_{\mathbf{k}\lambda}|^2} - \xi_{\mathbf{k}\lambda}) \\
&= (\sqrt{\xi^2_{\mathbf{k}\lambda} + |\Delta_{\mathbf{k}\lambda}|^2}, \qquad (4.31)
\end{aligned}$$

where we can now define

$$E_{\mathbf{k}\lambda} = \sqrt{\xi^2_{\mathbf{k}\lambda} + |\Delta_{\mathbf{k}\lambda}|^2}, \qquad (4.32)$$

which is unsurprisingly on the same form as the result for a regular BCS superconductor.

This allows us to rewrite our Hamiltonian as

$$H = \sum_{\mathbf{k}\lambda} E_{\mathbf{k}\lambda} \tilde{\gamma}^\dagger_{\mathbf{k}\lambda} \tilde{\gamma}_{\mathbf{k}\lambda} + E_0, \qquad (4.33)$$

where $E_0 = -1/2\xi_{\mathbf{k}\lambda} + 1/2E_{\mathbf{k}\lambda} - 1/2\Delta_{\mathbf{k}\lambda}\langle \tilde{c}^\dagger_{\mathbf{k}\lambda} \tilde{c}^\dagger_{-\mathbf{k}\lambda}\rangle$. Letting us find the initial values we need for our set of differential equations in the low temperature limit as

$$\langle \tilde{c}^\dagger_{\mathbf{k}\lambda} \tilde{c}_{\mathbf{k}\lambda}\rangle = \frac{1}{2}\left(1 - \frac{\xi_{\mathbf{k}\lambda}}{E_{\mathbf{k}\lambda}}\right) \qquad (4.34)$$

$$\langle \tilde{c}_{-\mathbf{k}\lambda} \tilde{c}_{\mathbf{k}\lambda}\rangle = \frac{1}{2}\frac{\Delta_{\mathbf{k}\lambda}}{E_{\mathbf{k}\lambda}}. \qquad (4.35)$$

This gives us self-consistent equations for $\Delta_{\mathbf{k}\lambda}$ and $\tilde{\Delta}_{\mathbf{k}\lambda}$ by inserting this result in the relations in (3.19) and (3.20).

In total we end up with

$$G_{\mathbf{k}\lambda}(0) = \frac{1}{2}\left(1 - \frac{\xi_{\mathbf{k}\lambda}}{E_{\mathbf{k}\lambda}(0)}\right) \qquad (4.36a)$$

$$F_{\mathbf{k}\lambda}(0) = \frac{\Delta_{\mathbf{k}\lambda}(0)}{2E_{\mathbf{k}\lambda}(0)} \qquad (4.36b)$$

$$\Delta_{\mathbf{k}\lambda}(0) = \sum_{\mathbf{k}'\lambda'} V_{\mathbf{k}\mathbf{k}'\lambda\lambda'} F_{\mathbf{k}'\lambda'}(0), \qquad (4.36c)$$

after explicitly specifying that we are dealing with the values at time $t = 0$.

4.1.3 Numerics

The system of equations (4.12) is in general an equation for $8N$ numbers which can be written as arrays on a grid for numerical solving. N is the number of grid points (lattice points), we get $4N$ from $G_{\mathbf{k}\lambda}$ and $F_{\mathbf{k}\lambda}$, which are both complex in general. For the initial gap calculations grid points in a thin energy band around the Fermi-levels of the bands are selected based on the energy $E < |\xi_{\mathbf{k}\lambda} - \omega_0|$. It is important to divide the initial grid into small enough pieces such that one ends up with enough points lying in the thin bands. The equations of motion do not couple to any points outside of those selected, so the points selected in the manner explained above are the only ones needed for the calculations.

When calculating the initial conditions the self-consistency equation (4.36c) may have more than one solution, in that case the free energy must be calculated for each solution and the solution that minimizes the energy is chosen. A fourth/fifth order adaptive Runge-Kutta method is used to propagate the differential equations in time and offers some speedup over a regular fourth order method.

For driving the system out of equilibrium a variation on a common quench-protocol is used. For quenching in the spin-orbit interaction, we start with the ground state of the Hamiltonian at $t = 0$ (4.1) and calculate the time evolution of the system using the same Hamiltonian with a different electric field strength E_z which effectively changes the strength of the spin-orbit interaction. This method of quenching appears to raise an issue compared to the more standard quench in the interaction strength as we are changing $\xi_{\mathbf{k}\lambda}$ in the quench and we would therefore change the position of the energy bands used in the self consistent gap calculations. In the numerical calculations we have no good way of coupling to new points or deciding how such a coupling should take place. Therefore we choose to propagate the equations by coupling at the same momentum-values as before the quench as an approximation. The justification for this being that as long as the quenches in the SOC are small compared to the other energies in the expression for $\xi_{\mathbf{k}\lambda}$ the moving of the bands would be a very small effect. In the following calculations the quenches are at most of the order of $\delta\alpha/t \approx 10^{-4}$ and in most cases much smaller.

CHAPTER 5

THE SPECTRAL FUNCTION

The spectral function (2.18) is in general a difficult quantity to calculate for an interacting many-body system. In almost all cases this can only be done in certain limiting cases, in this thesis we will follow the method of Peronaci, Schiró and Capone by using a sudden-approximation where we approximate the time-dependence by assuming that the parameters in the Hamiltonian instantly changes from it's initial values to some other values at the time $t = 0$ [18]. We remind ourselves from equation (2.19) that the lesser Green's function is directly related to the spectral function. In the following we therefore focus on calculating the lesser Green's function.

5.1 Definitions and preliminaries

We would like to do these calculations in a simple basis, however when we are discussing the spectral function and try to relate it to possible experiments it is important to remember what would actually be measured. In a real experiment one would measure electrons, and so we need to see how the spectral function in our band-basis relates to the electron basis. To see this, we first look at the normal spin-up component of the lesser Green's function in the spin-basis defined as

$$G^{<}_{\uparrow\uparrow\mathbf{k}}(t,t') = i\langle c^{\dagger}_{\mathbf{k}\uparrow}(t')c_{\mathbf{k}\uparrow}(t)\rangle. \tag{5.1}$$

Projecting (5.1) onto the pseudo-spin basis,

$$c^\dagger_{\mathbf{k}\uparrow}(t')c_{\mathbf{k}\uparrow}(t) = \frac{1}{\sqrt{2}}\left(\tilde{c}^\dagger_{\mathbf{k}+}(t') + \tilde{c}_{\mathbf{k}-}(t')\right)\frac{1}{\sqrt{2}}\left(\tilde{c}^\dagger_{\mathbf{k}+}(t) + \tilde{c}_{\mathbf{k}-}(t)\right), \tag{5.2}$$

we end up with a simple form

$$G^<_{\uparrow\uparrow\mathbf{k}}(t,t') = \frac{1}{2}G^<_{+\mathbf{k}}(t,t') + \frac{1}{2}G^<_{-\mathbf{k}}(t,t'). \tag{5.3}$$

where the Green's function in the spin-basis is simply a linear combination of the band-basis Green's functions.

Similarly, we can look at the other components of the lesser Green's function and project them on the same pseudo-spin basis

$$c^\dagger_{\mathbf{k}\uparrow}(t')c_{\mathbf{k}\downarrow}(t) = \frac{1}{\sqrt{2}}\left(\tilde{c}^\dagger_{\mathbf{k}+}(t') + \tilde{c}_{\mathbf{k}+}(t')\right)\frac{1}{\sqrt{2}}\Lambda_{\mathbf{k}}\left(\tilde{c}^\dagger_{\mathbf{k}+}(t) - \tilde{c}_{\mathbf{k}-}(t)\right), \tag{5.4}$$

giving

$$G^<_{\uparrow\downarrow\mathbf{k}}(t,t') = \frac{1}{2}\Lambda_{\mathbf{k}}G^<_{+\mathbf{k}}(t,t') - \frac{1}{2}\Lambda_{\mathbf{k}}G^<_{-\mathbf{k}}(t,t') \tag{5.5}$$

which is in perfect agreement with the results in [17].

Following [16] we approximate the non-equilibrium Greens function and use this to look at the spectral weight associated with the negative frequency peaks in the low temperature limit. We use a sudden change in the order-parameter and SOC to implement a time-dependent Bogolubov-Valantin transform. The calculation is rather long and tedious and can be found in appendix B.1. In essence we diagonalize the initial and final state Hamiltonians in two bases reminiscent of Nambu spinors $\psi^\dagger = (\tilde{c}^\dagger_{\mathbf{k}\gamma}, \tilde{c}_{-\mathbf{k}\gamma})$.

The final result is given by

$$\frac{Z^-_{\mathbf{k}\text{neq}}}{Z_{\mathbf{k}\text{eq}}} \approx \left(\frac{1 - \frac{\epsilon_{\mathbf{k}}}{E_{\mathbf{k}}}}{1 - \frac{\epsilon_{\mathbf{k}}}{E_{\mathbf{k}f}}}\right)\left(\frac{1}{2} + \frac{\epsilon^2_{\mathbf{k}} + \gamma^2_{\mathbf{k}}\Delta_{st}\Delta_i}{2E_{\mathbf{k}}E_{\mathbf{k}i}}\right), \tag{5.6}$$

where Z is the spectral weight associated with a frequency peak so that

$$-\frac{i}{\pi}G^<_{\mathbf{k}} = Z^-_{\mathbf{k}neq}\delta(\omega + E_{\mathbf{k}}) + Z^+_{\mathbf{k}neq}\delta(\omega - E_{\mathbf{k}}). \tag{5.7}$$

Note that we have suppressed the band-indices in equation (5.6) and (5.7) as all terms are in the same band.

CHAPTER 6

THE SINGLE BAND CASE

In this chapter we present numerical results for a single band model with a quench in the interaction strength where the results are known from previous literature. This will serve as a test of the numerical calculations and as a point of comparison for the model used in this thesis.

6.1 Model

The model used is the well known mean-field Hamiltonian

$$\mathcal{H} = \sum_{\mathbf{k}\sigma} \varepsilon_{\mathbf{k}} c^{\dagger}_{\mathbf{k}\sigma} c_{\mathbf{k}\sigma} - \sum_{\mathbf{k}} \left(\Delta_{\mathbf{k}}(t) c^{\dagger}_{\mathbf{k}\uparrow} c^{\dagger}_{-\mathbf{k}\downarrow} + \Delta^{*}_{\mathbf{k}}(t) c_{-\mathbf{k}\downarrow} c_{\mathbf{k}\uparrow} \right) \tag{6.1}$$

where

$$\Delta_{\mathbf{k}} = V \gamma_{\mathbf{k}} \sum_{\mathbf{p}} \gamma^{*}_{\mathbf{p}} \langle c_{-\mathbf{p}\downarrow}(t) c_{\mathbf{p}\uparrow}(t) \rangle \tag{6.2}$$

and $\gamma_{\mathbf{k}}$ is a factor containing the symmetry of the gap which is $\gamma_{\mathbf{k}} = 1$ for the s-wave case and $\gamma = (k_x^2 - k_y^2)/|k|^2$ in the d-wave case. This model has very similar equations of motion to our two band case (4.12) following the

mean-field Hamiltonian (6.1).

$$i\frac{dF_{\mathbf{k}}(t)}{dt} = 2\varepsilon_{\mathbf{k}}F_{\mathbf{k}}(t) + \Delta_{\mathbf{k}}(2G_{\mathbf{k}}(t) - 1) \tag{6.3a}$$

$$i\frac{dG_{\mathbf{k}}(t)}{dt} = [\Delta^*_{\mathbf{k}}(t)F_{\mathbf{k}}(t) - F^*_{\mathbf{k}}(t)\Delta_{\mathbf{k}}(t)] \tag{6.3b}$$

$$\Delta_{\mathbf{k}} = V\sum_{\mathbf{k}'} F_{\mathbf{k}'}, \tag{6.3c}$$

and initial conditions

$$G_{\mathbf{k}}(0) = \frac{1}{2}\left(1 - \frac{\varepsilon_{\mathbf{k}}}{E_{\mathbf{k}}(0)}\right) \tag{6.4a}$$

$$F_{\mathbf{k}}(0) = \frac{\Delta_{\mathbf{k}}(0)}{2E_{\mathbf{k}}(0)} \tag{6.4b}$$

$$\Delta_{\mathbf{k}}(0) = V\sum_{\mathbf{p}} \gamma^*_{\mathbf{p}}F_{\mathbf{p}}(0), \tag{6.4c}$$

where the quench is performed by suddenly changing the potential V from an initial value V_i to some final value V_f. Furthermore, we remind ourselves of the non equilibrium spectral weight (B.48)

$$\frac{Z^-_{\mathbf{k}neq}}{Z_{\mathbf{k}eq}} \approx \left(\frac{1 - \frac{\epsilon_{\mathbf{k}}}{E_{\mathbf{k}}}}{1 - \frac{\epsilon_{\mathbf{k}}}{E_{\mathbf{k}f}}}\right)\left(\frac{1}{2} + \frac{\epsilon^2_{\mathbf{k}} + \gamma^2_{\mathbf{k}}\Delta_{st}\Delta_i}{2E_{\mathbf{k}}E_{\mathbf{k}i}}\right) \tag{6.5}$$

which is notably on the form of an equilibrium superconductor at finite temperature with the thermal factor $n(\pm E_{\mathbf{k}})$ replaced by a different factor in the last bracket.

6.2 Results

The results are presented in terms of a quench parameter given by Δ_i/Δ_f where Δ_i and Δ_f are the equilibrium values corresponding to the initial and final values of the pairing potential V_i and V_f.

We start out by considering the Higgs mode (amplitude mode) of the gap, the Higgs mode is defined as fluctuations in the amplitude of the order parameter and is illustrated in the top figure in 6.1. A quench changes the free energy landscape in a non-adiabatic way leading to such oscillations illustrated in the bottom figure in 6.1. It is also possible to have oscillations in the phase of the order parameter, these oscillations will not be important here because

for the single-band case there is no energy associated with phase fluctuations. For two-bands however there can be energy associated with fluctuations in the relative phase between the bands, we get back to these fluctuations in the next chapter instead.

In figure 6.2 we can observe a key difference in the dynamics, where the s-wave model exhibits persistent oscillations the d-wave model experiences quick damping. In figure 6.3 this is shown for a range of quench parameters where the s-wave behavior can be divided into persistent oscillations, damping to a stationary value and exponential decay. The decay to a vanishing gap is attributed to dephasing of the Cooper pairs [19]. The d-wave model does not experience the persistent oscillations, but is always quickly damped. It is important to note that this damping is not because of scattering processes or any real dissipation mechanism, such mechanisms are not included in the model Hamiltonian. The system persists in a non-equilibrium state even though the oscillations are damped and the stationary value of the gap is reached as a result of destructive interference between different momenta [18]. This disappearance of the persistent oscillations is explained physically by Peronaci [16] as an effect of the nodal lines giving a fast dephasing because of the presence of zero energy modes along the nodal lines.

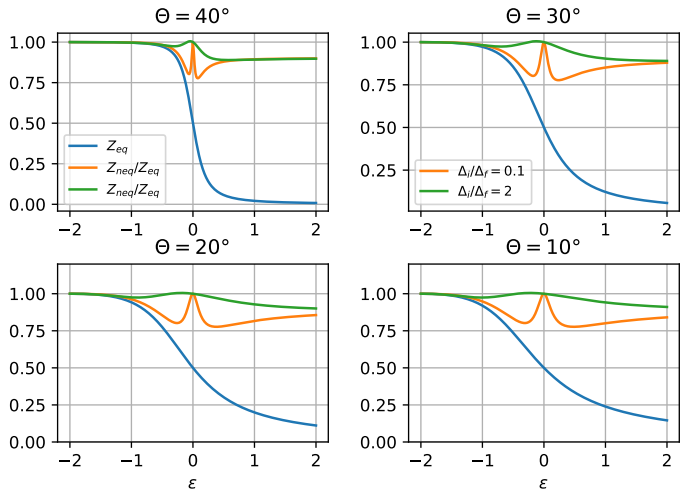

Figure 6.4: Plot of the spectral weight Z_{eq} and the ratio Z_{neq}/Z_{eq} as a function of $\epsilon_{\mathbf{k}}$ for different angles in $\mathbf{k}$ space and for two different quenches for a d-wave system.

In figure 6.4 the equilibrium spectral weight and the ratio between the

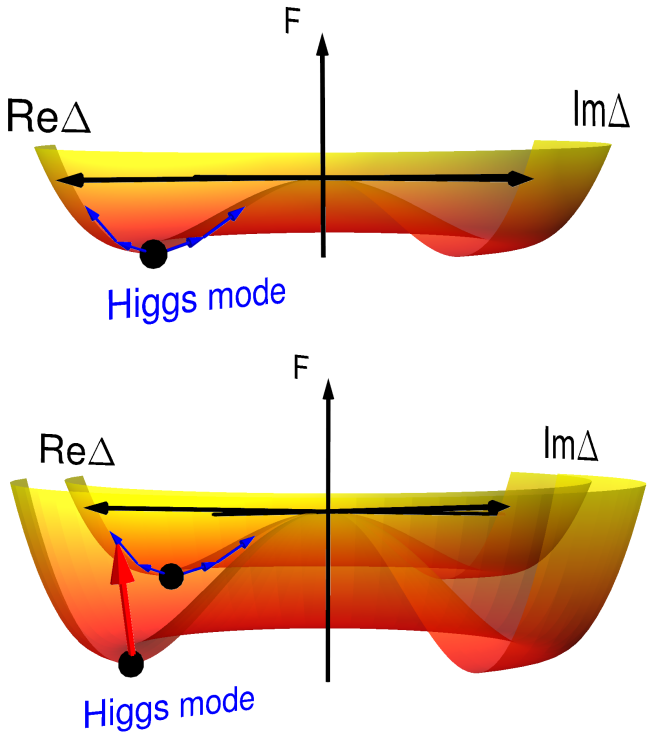

Figure 6.1: A schematic illustration of the Higgs mode represented on the Mexican-hat free energy potential as a function of the order parameter (top). Illustration of a non-adiabatic excitation for a one band superconductor. This results in oscillations of $|\Delta|$ around a new minimum of the free energy F (bottom).

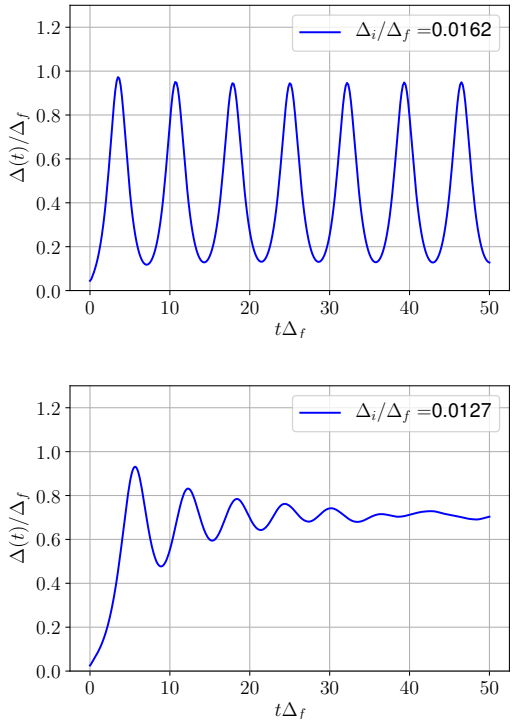

Figure 6.2: Gap dynamics after quenches from a weak to a much stronger interaction in the s-wave (top) and d-wave (bottom) case.

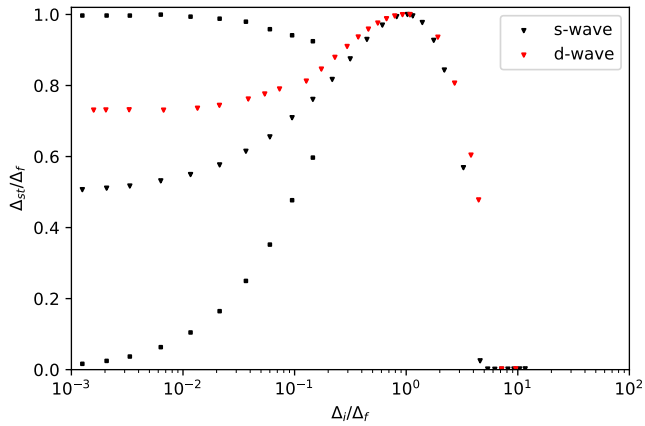

Figure 6.3: Plot of the steady state gap Δ_{st}/Δ_f as a function of the quench parameter Δ_i/Δ_f. The black squares indicate the extrema of the undamped oscillations in the s-wave case.

non-equilibrium and equilibrium spectral weight is shown for a d-wave system. Plots for the s-wave system are omitted as they correspond to $\Theta = 0$ and are very similar to the $\Theta = 10°$ case as $\gamma = (k_x^2 - k_y^2)/|k|^2$ approaches 1 as $\mathbf{k} \to k_x\hat{x}$. One observation we can make is that the transition becomes sharper as we approach a nodal line where the gap becomes smaller. For the equilibrium spectral weight we approach a step function as we approach the nodal line. We can expect this from the equations, when we approach a gapless system $\Delta_{\mathbf{k}} \to 0$ the equilibrium spectral weight equation $Z_{\mathbf{k}eq} = 1/2 \cdot (1 - \epsilon_{\mathbf{k}}/E_{\mathbf{k}}) \to 1/2 \cdot (1 - \epsilon_{\mathbf{k}}/|\epsilon_{\mathbf{k}}|)$ approaches a step-function.

CHAPTER 7
RESULTS

In this chapter we will present the numerical results for our model in a similar way as was done for the single band model in chapter 6. We start out by considering the gap dynamics, then we look at the spectral features and finish with a discussion on how the results can be connected to experiments. Each result section is divided into three different parts based on the relative size of the singlet and triplet gaps in equilibrium where. The first part will be for a singlet dominated gap, the second for a gap where the singlet and triplet parts have similar amplitudes and lastly a gap where the triplet amplitude dominates.

Before moving on to the results there is one additional feature of the model that needs to be introduced. As the model used in this thesis is effectively a two-band model we get in addition to the Higgs mode presented in chapter 6 another collective mode called the Leggett or relative-phase mode [20]. Unlike the phase mode of a one-band superconductor which is not associated with an energy cost, the Leggett mode does have an associated cost because of the coupling between the bands as illustrated in figure 7.1. Furthermore, Krull et al. [21] found that for a two-band superconductor out of equilibrium the Higgs and Leggett modes are strongly coupled and propose a pump-probe type experiment for measuring these modes.

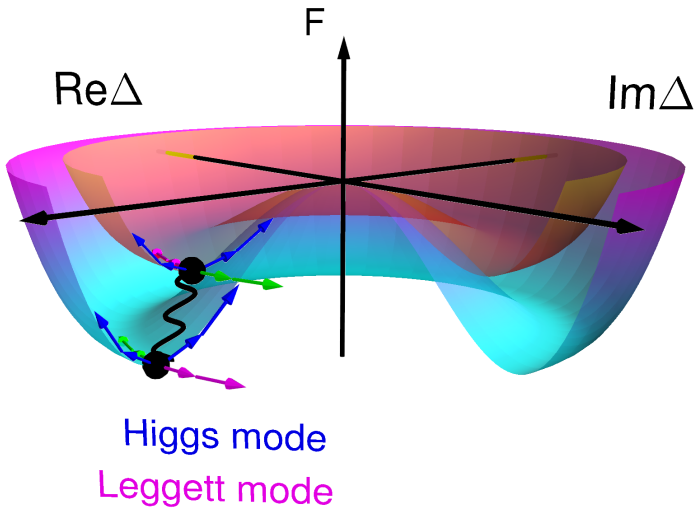

Figure 7.1: Illustration of the Leggett(relative phase) mode for a two-band system where the green and pink arrows indicate the legget mode, while the black wavy line indicates coupling between the bands. The two Mexican hat potentials are for two different bands in this picture as opposed to the same potential at different times shown in figure 6.1.

7.1 Gap dynamics

In this section will be looking at the gap-dynamics out of equilibrium after a quench. We start out by considering a singlet-dominated gap with a quench in the pairing interaction and compare the results to a similar quench for a one-band s-wave model as a test of the numerics of of our two-band model. Then we move on to quenches in the spin-orbit interaction for the different scenarios. The interaction matrix will be specified by the ratio of off-diagonal to diagonal elements $\tilde{V}^o/\tilde{V}^d = r$. We note that like in the previous chapter we work in a collisionless approximation where there is no dissipation mechanism and the gaps do not settle into a thermal equilibrium. Therefore the calculated gap $\Delta(t)$ does not in general settle towards the equilibrium value Δ_f that we would expect in a real material at large times, emphasizing that the equations are not valid at large times. However, the system can still settle into a metastable state despite the absence of dissipation mechanisms. This is because a stationary state can be reached through decoherence between $\mathbf{k}$-modes that are excited differently by the quench. If we include coupling to an external heat bath and the system in question is continuously cooled however, then we would expect that the system will relax to it's equilibrium value at long times [22]. It can also be shown from the equations of motion for a one-band BCS pairing problem similar to that in chapter 5 that inclusion of a damping term relaxes the system to the ground state [19].

7.1.1 Singlet dominated gap with interaction quench

The first scenario we are looking at is a quench in the pairing interaction when the system is strongly dominated by singlet pairing. In figure 7.2 we see behavior very similar to what we saw in chapter 6 with persistent oscillations of a similar nature in the singlet amplitude. The two bands are very similar in both amplitude and dynamical behavior and they almost overlap, the triplet amplitude is very small compared to the singled amplitude. This should perhaps not be very surprising as this scenario is not very different from the conventional single band scenario. The Leggett-mode is essentially non-existent for these quenches and the two bands oscillate in phase. Only the out of phase mode has an energy cost associated with it, this can be seen from the Hamiltonian if one writes $\Delta_\lambda = \mathrm{e}^{i\theta_\lambda}|\Delta_\lambda|$ and looks at the terms in the free energy where we end up with a term proportional to $\cos(\theta_+ - \theta_-)$.

7.1.2 Singlet dominated gap with spin-orbit quench

The next scenario to look at is similarly to the previous one strongly dominated by the singlet pairing, the difference being that we do the quench in the SOC

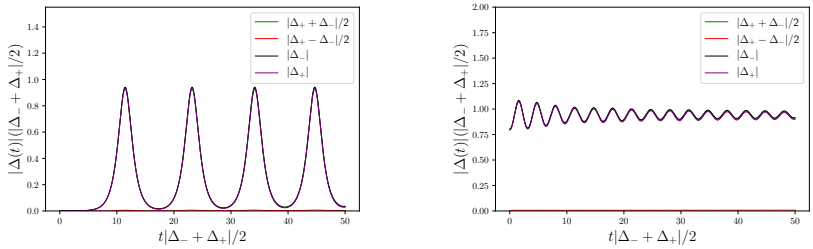

Figure 7.2: Time dynamics of a singlet dominated gap after a quench in the interaction strength, $\Delta_i/\Delta_f \approx 10^{-3}$ on the left and $\Delta_i/\Delta_f \approx 1/2$ on the right where Δ is defined as $|\Delta_- + \Delta_+|/2$. The interaction matrix is specified by $r = 8/10$. While a triplet component is present its amplitude is negligible in magnitude compared to the singlet amplitude. The lines for $|\Delta_+|$, $|\Delta_-|$ and $|\Delta_+ - \Delta_-|/2$ essentially overlap here.

instead of the interaction potential. When doing quenches in this regime we need to be careful not to quench the strength of the SOC too low as that would bring the spin-orbit splitting of the bands into a regime of small band-splitting. In those cases our model may not be valid as we may need to consider inter-band pairing and more as discussed in chapter 3. To avoid such issues we stay in a range of parameters where $\alpha_R E_z/\Delta_\lambda \sim 10^3 - 10^5$ as they are given in equation (3.9).

We are now ready to look at the first quenches. Figure 7.3 shows the same system as in the previous section with a quench in the SOC parameter instead of the interaction. Using Δ_i/Δ_f to classify the quench strength is no longer the obvious choice as this contains no direct reference to the quench parameter any more. This is in contrast to the of the interaction strength quench. We instead choose to refer to the quench strength in terms of $\delta\alpha/\Delta_i$ where $\delta\alpha$ is the change in the SOC interaction, there is still a reference to Δ_f in that we still normalize the plots to it.

The first observation we can make is that things mostly look quite normal, there are no large surprises compared to interaction quenches except for some small bumps in the triplet amplitude in the topmost plots. In the bottom plots the singlet amplitude still dominates, but not to the same extent and we see a clearer oscillation in the triplet amplitude. One possible explanation for why this should happen is that changing the strength of the SOC-interaction has a different effect on the density of states in the two bands compared to the change we get from a uniform change in the interaction strength. It can be shown that at least near the critical temperature T_C the ratio between

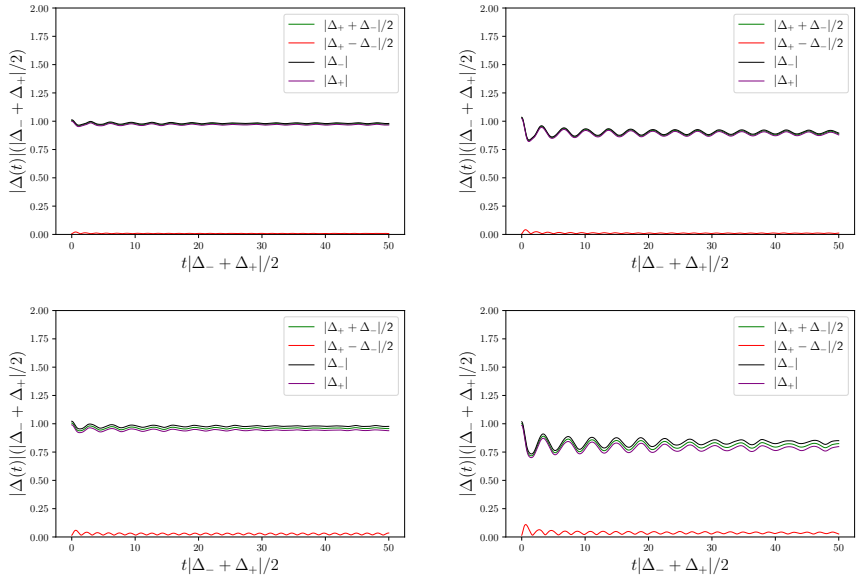

Figure 7.3: Time dynamics of a singlet dominated gap after a quench in the spin-orbit interaction strength, $\delta\alpha/\Delta_i \approx 10^{-1}$ on the left and $\delta\alpha/\Delta_i \approx 2$ on the right where Δ is defined as $|\Delta_- + \Delta_+|/2$. The interaction matrix is specified by $r = 8/10$ for the top and $r = 6/10$ for the bottom.

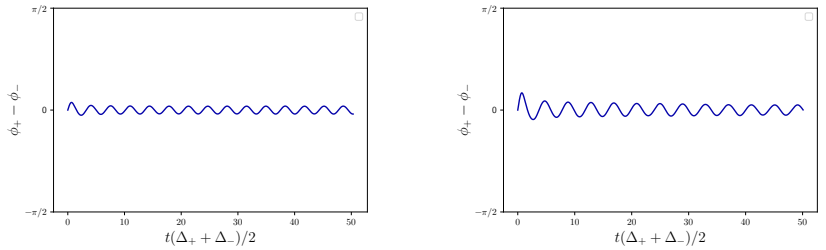

Figure 7.4: Time dynamics of the Leggett mode of the gaps after a quench in the spin-orbit interaction strength. The phase angle of each band is denoted by $\phi_\pm$, the parameters correspond to those in the top of 7.3.

triplet and singlet amplitudes depend in a non-trivial way on both the density of states in each band and on the relative size of the various parts of the interaction matrix [17].

A Leggett mode also starts to emerge as we can see in figure 7.4, and a Fourier transform as seen in figure 7.5 reveal that they are dominated by the same frequency. This is similar to what is observed in [21] and in [23] where the frequency content of both the Higgs modes and the Legget mode is similar out of equilibrium at strong interband couplings after a quench in the interband coupling strength.

We also plot some phase-diagrams, similar to figure 2 in [18]. In figures 7.6 and 7.7 we can see the results so far. Figure 7.6 shows the singlet gap for our two-band model with both diagonal and off-diagonal interaction elements, a) shows a very similar behavior to the one observed by Peronaci, Schiró, and Capone [16] except for a small bump before decreasing again at large ratios of Δ_i/Δ_f. The results for the triplet part shows a similar behavior again. Figure 7.7 shows the behavior for spin-orbit quenches, for the singlet amplitude we see a quite consistent decrease as the quench increases in magnitude, however, the triplet part increases in a similar way to what we observed in the interaction quench in figure 7.6. A possible explanation for this increase in the triplet amplitude is that even though the bands are coupled and respond in a similar way, they do not in general respond identically to the quenches. A difference in response will have a tendency to increase the triplet amplitude as this depends on the difference. This makes another question arise, why do we see the amplitude start to decrease again after the rise in figure 7.7 b)? We can understand this by considering that the quenches tend to make both bands stabilize at a lower value and tend towards zero as the quench becomes large. This ends up decreasing the difference between the bands and the triplet

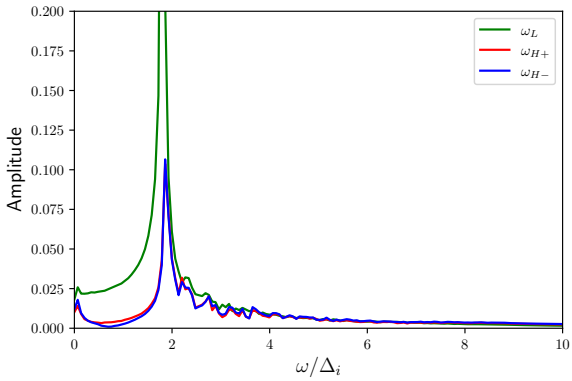

Figure 7.5: Fourier transform of the Higgs and Leggett mode oscillations after a quench in the SOC at $r = 6/10$.

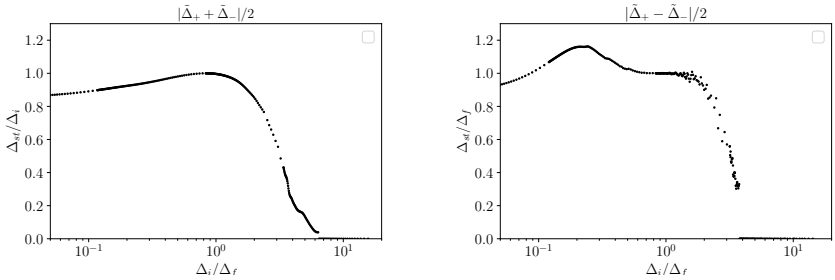

Figure 7.6: A quench in the interaction strength V for $r = 6/10$. a) Singlet. b) Triplet.

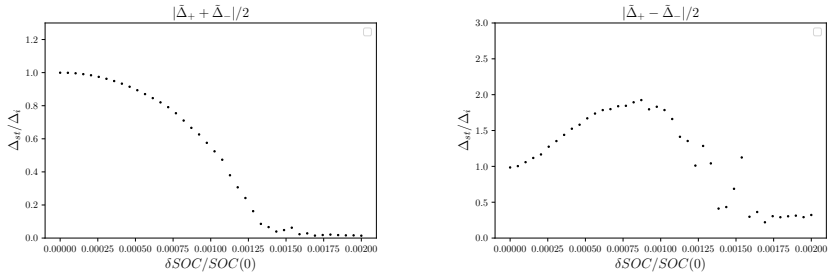

Figure 7.7: A quench in the SOC strength for $r = 6/10$. a) Singlet. b) Triplet as a function of the change on spin-orbit interaction relative to the magnitude at $t = 0$. The size of the gap is taken relative to the initial value of the gap as the final value Δ_f differs very little from the initial one for quenches of these sizes.

amplitude in turn starts to reduce. One cause of this can be that the quenches cause a dephasing effect [24] where the anomalous Green's functions no longer are in phase, we will get back to this in the next section.

7.1.3 Significantly mixed states

In this subsection we will look at quenches in states where the mixing of singlet and tripled amplitudes is more significant, and we will look into how mixed states arise from the equations. Figure 7.8 and 7.9 shows some of the same trends as the what was seen in the previous section, but clearer. This mixing of singlet and tripled amplitudes is strongest when the magnitude of the inter-band term $\tilde{V}^o$ is small compared to the intra-band term, meaning that $|r|$ is small. To see why, an expression for the ratio of triplet to singlet mixing close to the critical temperature (T_C) in this model is given by Mineev and Sigrist [17] can be rewritten in our notation as

$$r_{\text{mix}} = \frac{2\tilde{V}^o N_- + \tilde{V}^d(N_+ - N_-) - \sqrt{(\tilde{V}^d)^2(N_+ - N_-)^2 + 4N_+N_-(\tilde{V}^o)^2}}{2\tilde{V}^o N_- - \tilde{V}^d(N_+ - N_-) + \sqrt{(\tilde{V}^d)^2(N_+ - N_-)^2 + 4N_+N_-(\tilde{V}^o)^2}}, \tag{7.1}$$

where $N_\pm$ is the density of states of the two bands. The limiting cases of this expression while derived close to T_C gives some insight into what to expect. Firstly for the cases discussed in chapter 3, if the diagonal and off-diagonal elements are equal $\tilde{V}^o = \tilde{V}^d$ that makes $r_{\text{mix}} = 0$, meaning that there is no

triplet amplitude. Similarly we can set the off-diagonal coupling to be equal in magnitude and opposite in sign $\tilde{V}^o = -\tilde{V}^d$ and see that $r_{\text{mix}}^{-1} = 0$ meaning that there is no singlet amplitude. The last limiting case is when there is no off-diagonal coupling where we can see that $r_{\text{mix}} = 1$. This expression can also give a hint as to why how a change in the SOC strength would be able to change the triplet/singlet ratio as the expression can be sensitive to density of states $N_\pm$ in the two bands even if the interaction strengths are held constant. However, we also need to consider that the equations of motion depend directly on $\xi_{\lambda\mathbf{k}}$ (4.11a), (4.11b) and that we in the self consistent equation (4.12) couple the dependency of both bands. Here we remind ourselves of the form of these equations

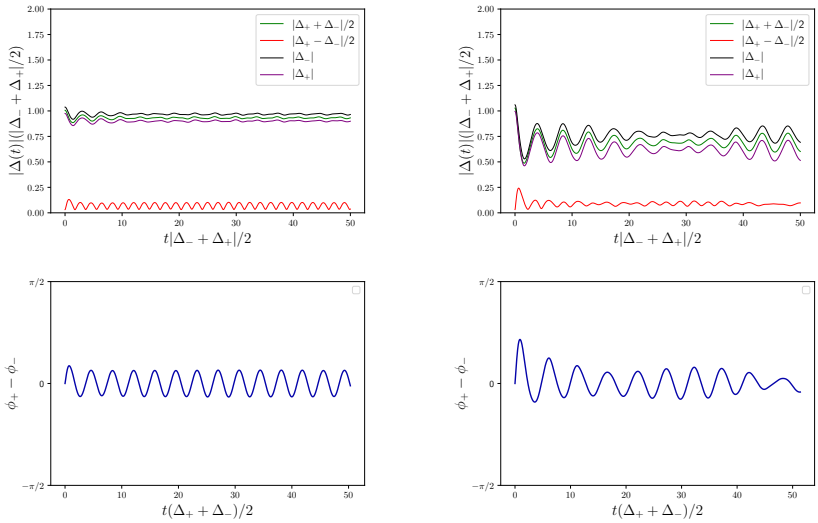

Figure 7.8: Time dynamics of a mixed gap after a quench in the SOC strength. The interaction matrix is specified by $r = 4/10$. The triplet amplitude shows up as much more significant than in the previous cases. Higgs-modes on shown on top with corresponding Leggett modes on the bottom.

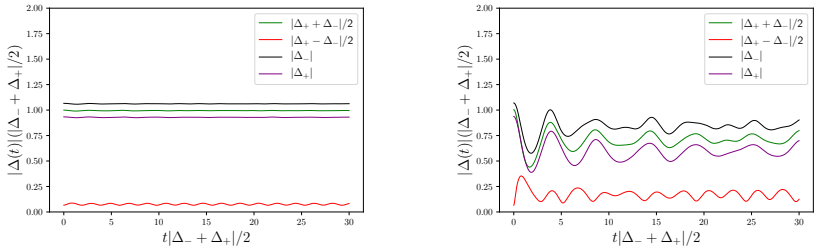

Figure 7.9: Time dynamics of a mixed gap after a quench in the SOC strength. The interaction matrix is specified by $r = 2/10$. The triplet amplitude shows up as much more significant than in the previous cases.

$$i\frac{dF_{\mathbf{k}\lambda}(t)}{dt} = 2\xi_{\mathbf{k}\lambda}F_{\mathbf{k}\lambda}(t) + \Delta_{\mathbf{k}\lambda}(2G_{\mathbf{k}\lambda}(t) - 1) \tag{7.2a}$$

$$i\frac{dG_{\mathbf{k}\lambda}(t)}{dt} = [\Delta^*_{\mathbf{k}\lambda}(t)F_{\mathbf{k}\lambda}(t) - F^*_{\mathbf{k}\lambda}(t)\Delta_{\mathbf{k}\lambda}(t)] \tag{7.2b}$$

$$\Delta_{\mathbf{k}\lambda} = \sum_{\mathbf{k}'\lambda'} V_{\mathbf{k}\mathbf{k}'\lambda\lambda'}F_{\mathbf{k}'\lambda'}, \tag{7.2c}$$

noting that we also still sum over the same points in $\mathbf{k}-$space as there is no coupling to new $\mathbf{k}$ values in our set of equations. In contrast to the equilibrium situation where we would calculate a new set of points around the Fermi-surface in $\mathbf{k}-$space for the two bands.

When the quench is done in $\xi_{\mathbf{k}\lambda}$ we must also consider the form for $\xi_{\mathbf{k}\lambda}$ given in (3.11), which we remind ourselves of here

$$\xi_{\mathbf{k}\lambda} = -2t[\cos(k_x) + \cos(k_y)] - \mu + \lambda\alpha_{\mathrm{R}}E_z\sqrt{\sin^2(k_x) + \sin^2(k_y)}. \tag{7.3}$$

The quench parameter therefore gets weighted differently for different values of $\mathbf{k}$ in $\xi_{\mathbf{k}\lambda}$. As the equations of motion gives us the imaginary change in the Green's functions, this difference in quenches for the different values of $\mathbf{k}$ can be a factor that drives the different $F_{\mathbf{k}\lambda}$ functions out of phase from each other. In this context we can look at the phase of the gap for different quench strengths and in figure 7.10 see that the phase changes much more rapidly as the quench grows larger.

We also see the emergence of different oscillation modes, somewhat similar to what was found by Krull et al. [25] and Cui et al. [23]. Cui et al. uses an

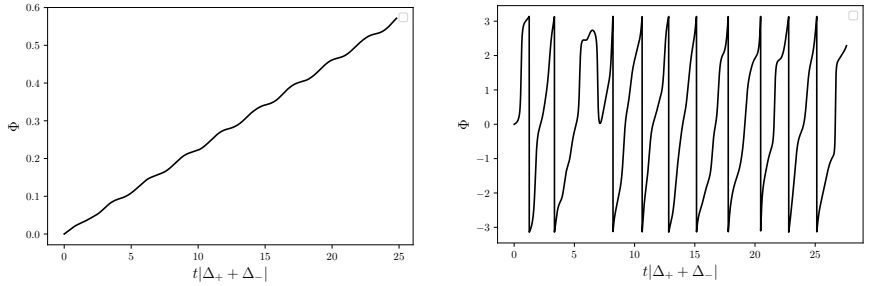

Figure 7.10: Time dynamics of the phase angle for the singlet part of the gap $\Delta_+ + \Delta_-$ as a function of time for a small and a large quench in the SOC.

effective interaction matrix with the same inter-band interaction $V_{11} = V_{22}$, and the same intra-band interaction $V_{12} = V_{21}$ that still gives an effective asymmetric effective interaction as differing density of states is imposed on the two bands. If identical densities of state are imposed around the Fermi level in both bands in the standard two band model then the standard two-band model self-consistent gap equation gets solutions on the form $\Delta_1 = \pm\Delta_2$. The spin-orbit coupled model used in this thesis differs in the band-splitting. We also note that the phase-difference and complex-valued nature of the gaps can lead to more complicated behavior in the singlet and triplet amplitudes $|\Delta_+ \pm \Delta_-|/2$.

7.1.4 Triplet dominated gap with spin-orbit quench

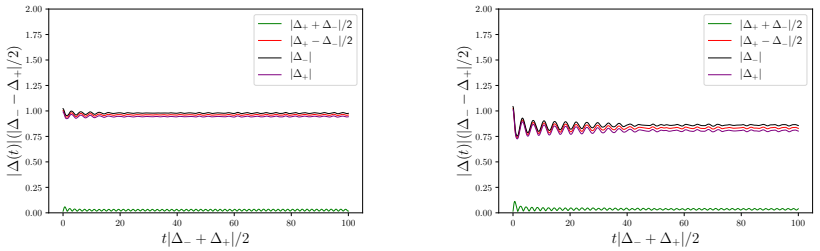

Figure 7.11: Time dynamics of a triplet dominated gap after a quench in the SOC strength. The interaction matrix is specified by $r = -6/10$.

The final scenario to look at is the triplet dominated case. This case however does not offer much in terms of new and interesting behavior compared to the

previous cases of a singlet dominated gap and a significantly mixed gap. This is because it in broad terms behaves very much like the singlet dominated gap with the roles of the triplet and singlet gaps exchanged. We can look back at the gap equation (4.12) and the discussion in chapter 3 where we essentially see the singlet and triplet gaps exchange roles as the sign of the off-diagonal part of the interaction matrix changes.

7.2 Spectral features

In this subsection we will look at how the quenches in the previous sections may show up in the spectral features that could be measured. We will use the results from appendix B.1 given in chapter 5 to plot approximations of the change in spectral weight for the two bands.

The SOC and the square lattice leads to a distortion of the Fermi-surface which is reflected in the equilibrium spectral weight shown in figure 7.12a). We also get a splitting of the bands in momentum space due to the SOC (figure 7.12b)). For ease of comparison we therefore use the single-particle kinetic energy in each band $\xi_{\pm}$rather than the momentum $\mathbf{k}$ for comparison of the spectral weights. The energy units are scaled to $t/1000$ to allow details of the sharp transition in figure 7.12 to be seen. We specify the form of the interaction matrix (3.32) by the ratio between the off-diagonal and diagonal elements $\tilde{V}^o/\tilde{V}^d = r$. We note that care should be taken when trying to interpret spectral features of the two bands individually as they are inherently coupled in this model. Due to the very sudden changes happening over very small areas in $\mathbf{k}$-space however, this is not as big of concern as it may seem at first.

In figure 7.13 we see the spectral weights in the two bands for different quenches in the whole interaction matrix. These are qualitatively similar to the results in [18] for a single angle in k-space in a d-wave superconductor, and importantly identical in each band. This does not have to be the case in a multi-band approach, by quenching in different parameters and using different initial conditions for the bands they can exhibit different time dynamics and final behavior [23].

Figure 7.14 shows the spectral weights in the two bands for quenches in the SOC interaction strength. Here we see more interesting features. In particular we observe the change in band-splitting as a direct result of the change in SoC as we get a new Fermi-level observed from the peaks of the non-equilibrium spectral weights moving away from $\xi_{\pm} = 0$. We also observe that the bands do not in general respond in an identical way to a change in the SoC, in contrast to the interaction quench in figure 7.13.

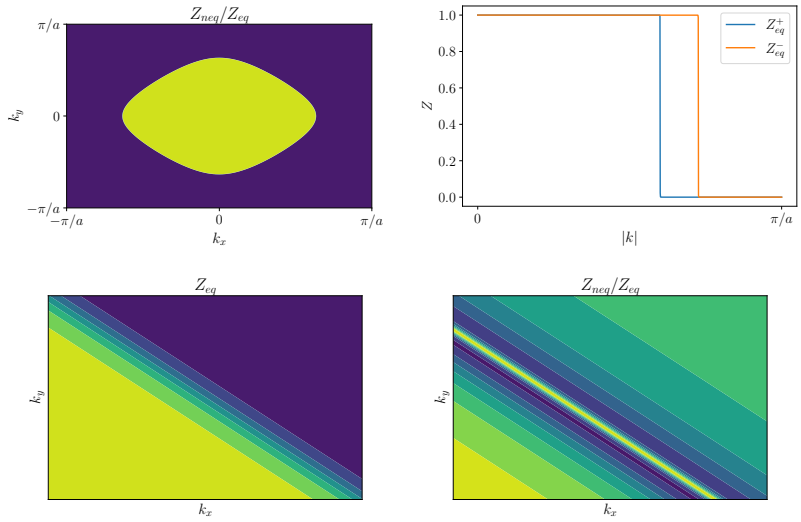

Figure 7.12: From top left to bottom right, a) example of equilibrium spectral weight of a single band in the first BZ, b) equilibrium spectral weight of both bands along a single direction in the first BZ, c) detail of the sharp transition in a), d) detail of the ratio of non-equilibrium to equilibrium weight. Momenta are normalized to the grid-spacing a.

When quenching the SOC in a scenario where the singlet and triplet components are of comparable size, as in figure 7.15, a striking difference is observed where the spectral weight of one band is enhanced even when moving far away from the Fermi-level. Qualitatively some of the features can be expected from the equations for the equilibrium and non-equilibrium spectral weights

$$Z^{eq}_{\mathbf{k}} \propto 1 - \frac{\xi_{\mathbf{k}}}{\sqrt{\xi^2_{\mathbf{k}} + \Delta^2_{\mathbf{k}}}}. \tag{7.4}$$

We expect the spectral weight to approach a step-function as a function of $\xi_{\mathbf{k}}$ as $\Delta^2_{\mathbf{k}} \to 0$ and for it to flatten out and approach a constant as $\Delta^2_{\mathbf{k}} \to \infty$. Qualitatively we can make some sense of the spectral weights in figure 7.14 by considering that the $+$-band and $-$-band do not respond identically to quenches. In 7.15 we can note that when $|r|$ gets very small we are effectively removing coupling between the bands as we can write the coupling $\tilde{V}^o = r\tilde{V}^d$.

The reasoning behind presenting the spectral weights in the band-basis as opposed to the original spin-basis may be questioned here as in any real

measurement one would measure for instance electrons. Note however that equations (5.3) and (5.5) allows us to easily get the spectral weights in the spin-basis from these spectral weights, and that the band-splitting means that the interesting features are centered at different momenta. Presenting the spectral weights in the band-basis therefore allows us to look at the features in more convenient way without loosing the connection to the spin-basis.

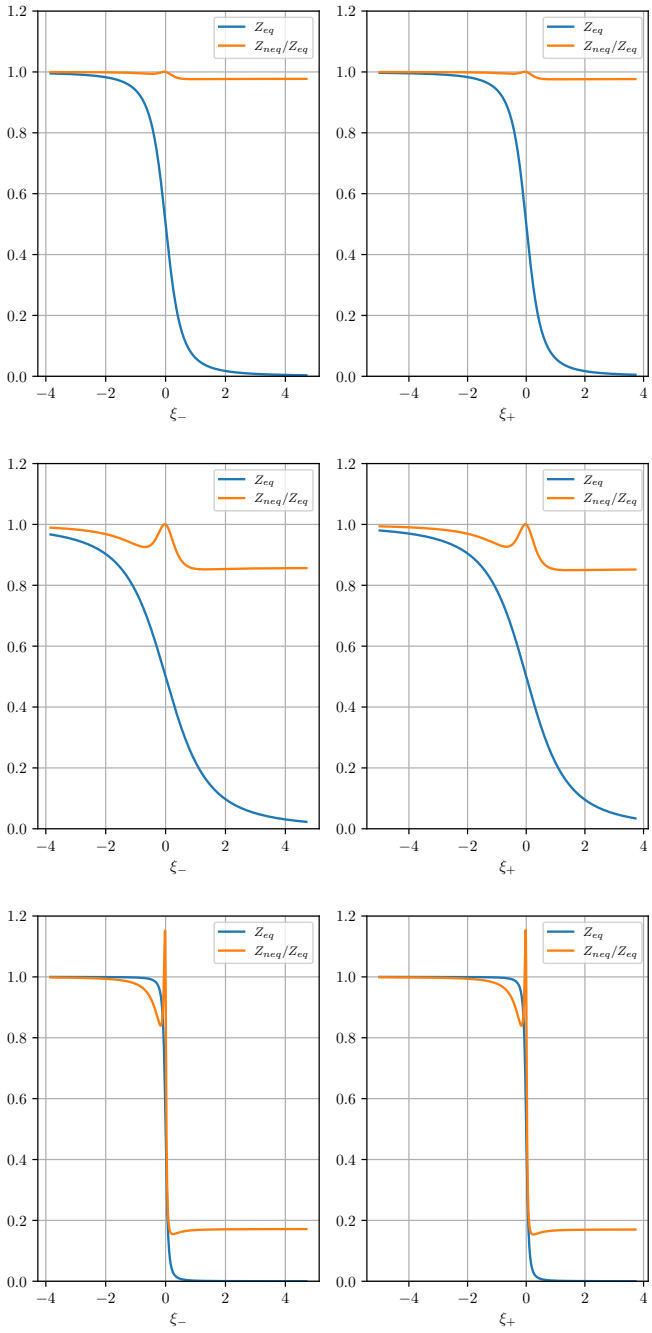

Figure 7.13: Spectral weight after successively stronger quenches in the interaction strength (top left to bottom right). An interaction matrix with $r = 6/10$ was used.

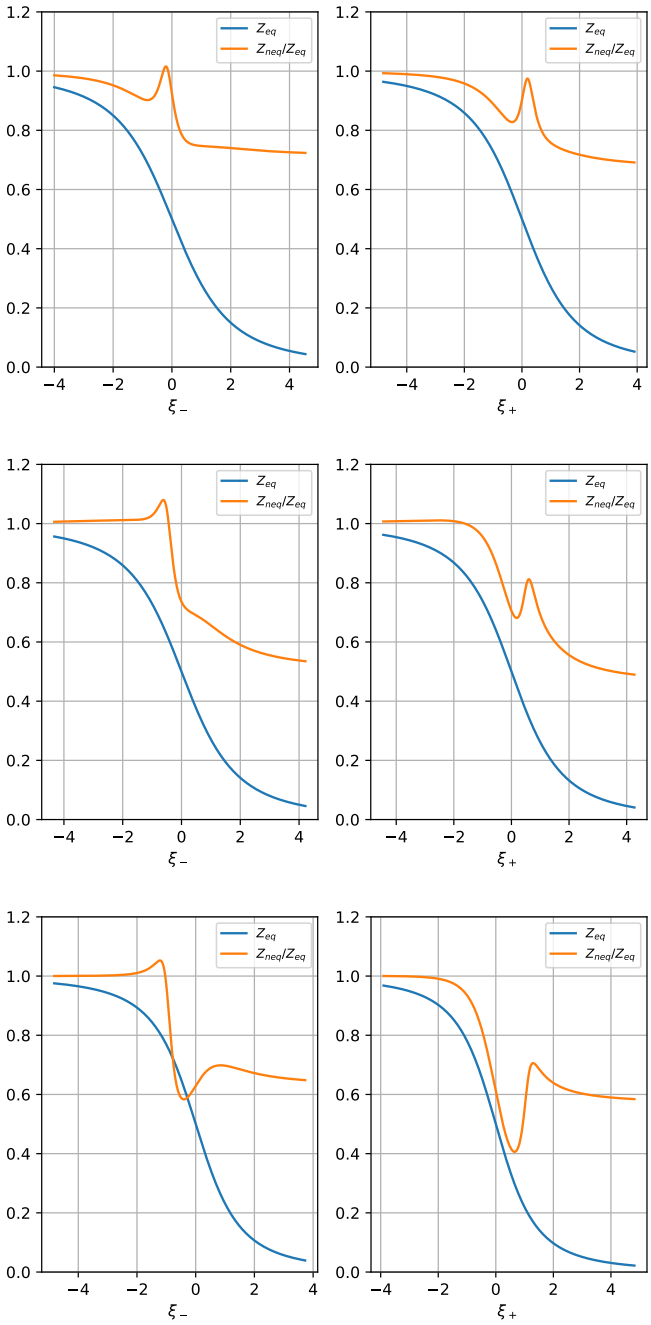

Figure 7.14: Spectral weight after successively stronger quenches in the SoC in a system dominated by singlet pairing (top left to bottom right). An interaction matrix with $r = 6/10$ was used.

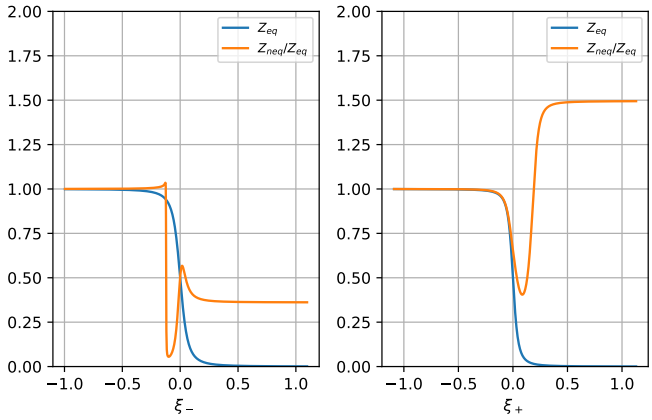

Figure 7.15: Spectral weights after quenching the SOC in a system where singlet and triplet components are of similar size. An interaction matrix with $r = 1/20$ was used.

7.3 Connections to experiments

In this section we will present connections between the theoretical work and experimental methods. We attempt to justify the approximations used to arrive at the analytical and numerical results.

We start out with a discussion of the quench. The easiest way to look at quenches is to consider a Hamiltonian with explicit dependence on a parameter $\lambda(t)$. The quench then describes the time evolution of of the parameter as a result of some external perturbation. In cold atom systems this can be changed more or less directly, inter-particle interactions are tunable via Feshbach resonance where the Bose-Einstein condensate-BCS crossover has been subject of much study [26]. It is also possible to directly induce and tune the spin-orbit coupling in such systems, allowing great experimental control over the system parameters [27]. In these systems one can consider the Hamiltonian to be directly changed.

However, in a solid state system the situation can be interpreted in a different way. We can ask if we are given a time-independent Hamiltonian for the material in question $\mathcal{H}(\lambda_f)$, how will a particular excited non-equilibrium state $|\psi(\lambda_i)\rangle$ evolve. At first glance this appears to create a new challenge in that we now need to accurately describe an excited state in a solid. It will turn out that this is not as big of a problem as it first appears to be as long as some details of the excitation process can be neglected. We have previously stated that the ARPES signal can be related to the spectral function by the relation in equation (2.19) at equilibrium. The specification that this relation holds at equilibrium is made because the distribution function for occupied states is known in equilibrium, while out of equilibrium the distribution is not in general given by the Fermi-Dirac distribution. This leads to a generalization of the time-resolved ARPES signal shown in [28] where Peronaci further shows that including the details of the quench-pulse only leads to a smearing the the delta function peaks appearing [18]. Furthermore, we justify our use of a sudden approximation in the derivation of the non-equilibrium spectral weight in the same way by the fast dynamics observed of the gaps. Our $\tilde{\Delta}_\pm$ at equilibrium are on the order of allows us to estimate sufficiently short time scales on the order of before the average value of the gaps relaxes to their steady state values.

7.3.1 Connections to physical systems

In this section we will give a brief discussion of possible systems where this model can be relevant for describing the dynamics of the system.

The first and perhaps most obvious system would be an analogue to the high temperature cuprates. If we have a non-centrosymmetric superconducting

compound where one can describe the superconductivity happening primarily in layers and where a major effect of the rest of the crystal structure is to provide a symmetry-breaking field. In such systems one can imagine inducing a quench by giving the material a mechanical shock, distorting the crystal-lattice and changing the strength of the symmetry-breaking field briefly.

Another possible system is a centrosymmetric thin-film superconductor where the spin-orbit interaction could be tuned by the application of a gate voltage. Such systems have been realized experimentally in several cases, but to the authors knowledge no quenching experiments have been attempted.

Interfaces between heterostructures also provide possibilities for an effectively 2d electron gas that gets the symmetry-breaking from the interface between different crystal lattices. Most relevant are the experimental setups where this can be tuned using an external electric field [29].

Yet another possibility are in globally centrosymmetric systems where one can have locally non-centrosymmetric behaviour [30].

7.4 Extensions

A few obvious extensions of the model are possible. The form of the equations of motion that is derived is general and factors describing different material symmetries can be calculated and investigated. The inclusion of an external magnetic field in the normal-state part of the equations which would lead to a shift in the $\mathbf{k}$ dependence of the gaps. This could also be combined with allowing for non-zero center of mass momentum giving rise to possible Fulde-Ferrel-Larkin-Ovchinnikov states. The model can also be extended to incorporate a full 3 dimensional system to investigate different classes of materials, like many of those introduced in [11], this would however be more computationally expensive.

BIBLIOGRAPHY

[1] H. Bruus and K. Flensberg. *Many-Body Quantum Theory in Condensed Matter Physics: An Introduction (Oxford Graduate Texts)*. Number August. Oxford University Press, 2004. ISBN 0198566336.

[2] A. L. Fetter and J. D. Walecka. *Quantum Theory of Many-Particle Systems*. Dover Publications, June 2003. ISBN 0486428273.

[3] G. D. Mahan. Many-particle physics, 3e, 2008.

[4] D. I. E. Abriskosov A. A., Gorkov L. P. *Methods of quantum field theory in statistical physics*. Dover, 1963. ISBN 9780486632285.

[5] R. Comin and A. Damascelli. ChemInform Abstract: ARPES. A Probe of Electronic Correlations. *ChemInform*, 44(25):no–no, 2013. doi:10.1002/chin.201325188.

[6] A. F. Kemper, M. A. Sentef, B. Moritz, T. P. Devereaux, and J. K. Freericks. Review of the Theoretical Description of Time-Resolved Angle-Resolved Photoemission Spectroscopy in Electron-Phonon Mediated Superconductors. *Annalen der Physik*, 529(9):1–11, 2017. doi:10.1002/andp.201600235.

[7] S. A. Fossheim Kristian. *Superconductivity: Physics and Applications*. Wiley, 2004. ISBN 9780470844526. doi:10.1002/0470020784.

[8] W. Kohn and J. M. Luttinger. New mechanism for superconductivity. *Phys. Rev. Lett.*, 15:524–526, Sep 1965. doi:10.1103/PhysRevLett.15.524.

[9] D. V. Berkov. Theory of magnetism. *Zeitschrift für Physikalische Chemie*, 198(1-2):275–276, 1997. doi:10.1524/zpch.1997.198.part_1_2.275a.

[10] L. P. Gor'kov and E. I. Rashba. Superconducting 2d system with lifted spin degeneracy: Mixed singlet-triplet state. *Physical Review Letters*, 87 (3):37004–1–37004–4, 2001. doi:10.1103/PhysRevLett.87.037004.

[11] M. Smidman, M. B. Salamon, H. Q. Yuan, and D. F. Agterberg. Superconductivity and spin-orbit coupling in non-centrosymmetric materials: A review. *Reports on Progress in Physics*, 80(3):1–57, 2017. doi:10.1088/1361-6633/80/3/036501.

[12] K. Børkje. Using Josephson junctions to determine the pairing state of superconductors without crystal inversion symmetry. *Physical Review B - Condensed Matter and Materials Physics*, 76(18):1–16, 2007. doi:10.1103/PhysRevB.76.184513.

[13] K. V. Samokhin and V. P. Mineev. Gap structure in noncentrosymmetric superconductors. *Physical Review B - Condensed Matter and Materials Physics*, 77(10):1–9, 2008. doi:10.1103/PhysRevB.77.104520.

[14] K. V. Samokhin, E. S. Zijlstra, and S. K. Bose. CePt3Si: An unconventional superconductor without inversion center. *Physical Review B - Condensed Matter and Materials Physics*, 69(9):1–9, 2004. doi:10.1103/PhysRevB.69.094514.

[15] I. A. Sergienko and S. H. Curnoe. Order parameter in seperconductors with nondegenerate bands. *Physical Review B - Condensed Matter and Materials Physics*, 70(21):1–8, 2004. doi:10.1103/PhysRevB.70.214510.

[16] F. Peronaci. Transient dynamics of unconventional superconductors. 2016.

[17] V. P. Mineev and M. Sigrist. Introduction to superconductivity in metals without inversion center. pages 1–17, 2009, http://arxiv.org/abs/0904.2962.

[18] F. Peronaci, M. Schiró, and M. Capone. Transient Dynamics of d -Wave Superconductors after a Sudden Excitation. *Physical Review Letters*, 115 (25), 2015. doi:10.1103/PhysRevLett.115.257001.

[19] R. A. Barankov, L. S. Levitov, and B. Z. Spivak. Collective Rabi oscillations and solitons in a time-dependent BCS pairing problem. *Physical Review Letters*, 93(16):1–4, 2004. doi:10.1103/PhysRevLett.93.160401.

[20] A. J. Leggett. Number-Phase Fluctuations in Two-Band Superconductors. *Progress of Theoretical Physics*, 36(5):901–930, 11 1966. doi:10.1143/PTP.36.901.

[21] H. Krull, N. Bittner, G. S. Uhrig, D. Manske, and A. P. Schnyder. Coupling of Higgs and Leggett modes in non-equilibrium superconductors. *Nature Communications*, 7(May), 2016. doi:10.1038/ncomms11921.

[22] E. A. Yuzbashyan and M. Dzero. Dynamical vanishing of the order parameter in a fermionic condensate. *Physical Review Letters*, 96(23):1–4, 2006. doi:10.1103/PhysRevLett.96.230404.

[23] T. Cui, M. Schütt, P. P. Orth, and R. M. Fernandes. Postquench gap dynamics of two-band superconductors. *Physical Review B*, 100(14):1–18, 2019. doi:10.1103/PhysRevB.100.144513.

[24] R. A. Barankov and L. S. Levitov. Synchronization in the BCS pairing dynamics as a critical phenomenon. *Physical Review Letters*, 96(23):1–4, 2006. doi:10.1103/PhysRevLett.96.230403.

[25] H. Krull, N. Bittner, G. S. Uhrig, D. Manske, and A. P. Schnyder. Coupling of Higgs and Leggett modes in non-equilibrium superconductors. *Nature Communications*, 7(May), 2016. doi:10.1038/ncomms11921.

[26] I. Bloch, J. Dalibard, and W. Zwerger. Many-body physics with ultracold gases. *Reviews of Modern Physics*, 80(3):885–964, 2008. doi:10.1103/RevModPhys.80.885.

[27] K. Jiménez-García, L. J. Leblanc, R. A. Williams, M. C. Beeler, C. Qu, M. Gong, C. Zhang, and I. B. Spielman. Tunable spin-orbit coupling via strong driving in ultracold-atom systems. *Physical Review Letters*, 114 (12):1–5, 2015. doi:10.1103/PhysRevLett.114.125301.

[28] J. K. Freericks, H. R. Krishnamurthy, and T. Pruschke. Theoretical description of time-resolved photoemission spectroscopy: Application to pump-probe experiments. *Physical Review Letters*, 102(13):3–6, 2009. doi:10.1103/PhysRevLett.102.136401.

[29] A. D. Caviglia, M. Gabay, S. Gariglio, N. Reyren, C. Cancellieri, and J. M. Triscone. Tunable Rashba Spin-Orbit Interaction at Oxide Interfaces. *Physical Review Letters*, 104(12):1–4, 2010. doi:10.1103/PhysRevLett.104.126803.

[30] D. Maruyama, M. Sigrist, and Y. Yanase. Locally non-centrosymmetric superconductivity in multilayer systems. *Journal of the Physical Society of Japan*, 81(3), 2012. doi:10.1143/JPSJ.81.034702.

[31] A. Altland and B. D. Simons. *Condensed Matter Field Theory*. Cambridge University Press, Cambridge, 2010. ISBN 9780511789984. doi:10.1017/CBO9780511789984.

APPENDIX A

RASHBA-TYPE SOC

We start with a Rashba-type spin-orbit coupling assuming $\mathbf{k} = (kx, ky, 0)$ and $\mathbf{E} = \mathrm{E}_z\hat{z}$:

$$\mathcal{H}_R = \alpha_R E_z[k_y\sigma_x - k_x\sigma_y], \tag{A.1}$$

and want to write it in second quantized form, more specifically we want it to fit into our tight-binding model with discrete lattice sites in a crystal. We will use Wannier-functions and assume that the Wannier functions are strongly localized at the ionic sites, meaning that $\langle\varphi(\mathbf{r} - \mathbf{R_i})|\varphi(\mathbf{r} - \mathbf{R_j})\rangle = \delta_{i,j}$, where $\varphi(\mathbf{r})$ is a Wannier orbital.

We therefore start out with

$$\begin{aligned}\mathcal{H} &= \sum_{i,j,\sigma,\sigma'}\int d^3r\varphi^\dagger(\mathbf{r} - \mathbf{R_i})\chi_\sigma\alpha_R E_z[k_y\sigma_x - k_x\sigma_y]\chi_{\sigma'}\varphi(\mathbf{r} - \mathbf{R_j})c^\dagger_{i\sigma}c_{j\sigma'} \\ &= \alpha_R\mathrm{E}_z\sum_{i,j,\sigma,\sigma'}\int d^3r\varphi^\dagger(\mathbf{r} - \mathbf{R_i})[k_y\sigma^x_{\sigma\sigma'} - k_x\sigma^y_{\sigma\sigma'}]\varphi(\mathbf{r} - \mathbf{R_j})c^\dagger_{i\sigma}c_{j\sigma'}\end{aligned} \tag{A.2}$$

where χ is the spin eigenfunction of the electron, and $\sigma^x_{\sigma\sigma'}$ is shorthand for $\chi_\sigma\sigma_x\chi_{\sigma'}$. Now we rewrite $k_x = -id/dx$, on the lattice we interpret this as a finite difference. On a square lattice with lattice constant $a = 1$

$$\frac{d}{dx}\varphi(\mathbf{r}) = \varphi(\mathbf{r} + \hat{x}) - \varphi(\mathbf{r}), \tag{A.3}$$

we start with

$$
\begin{aligned}
&- i \sum_{i,j,\sigma,\sigma'} \int d^3 r \varphi^\dagger(\mathbf{r}-\mathbf{R_i}) \sigma^x_{\sigma\sigma'} (\varphi(\mathbf{r}-\mathbf{R_j}+\hat{y}) - \varphi(\mathbf{r}-\mathbf{R_j})) c^\dagger_{i\sigma} c_{j\sigma'} \\
&= -i \sum_{i,j} (\delta_{\sigma\uparrow}\delta_{\sigma'\downarrow} + \delta_{\sigma\downarrow}\delta_{\sigma'\uparrow})(\delta_{i,j+\delta y} - \delta_{i,j}) c^\dagger_{i\sigma} c_{j\sigma'} \\
&= -i \sum_{i,j} (c^\dagger_{i\uparrow} c_{j\downarrow} + c^\dagger_{i\downarrow} c_{j\uparrow})(\delta_{i,j+\delta y} - \delta_{i,j}) \\
&= -i \sum_{i} (c^\dagger_{i\uparrow} c_{i-\delta y\downarrow} - c^\dagger_{i\uparrow} c_{i\downarrow} + c^\dagger_{i\downarrow} c_{i-\delta y\uparrow} - c^\dagger_{i\downarrow} c_{i\uparrow})
\end{aligned} \tag{A.4}
$$

and the second part follows in the same manner

$$
\begin{aligned}
&i \sum_{i,j,\sigma,\sigma'} \int d^3 r \varphi^\dagger(\mathbf{r}-\mathbf{R_i}) \sigma^y_{\sigma\sigma'} (\varphi(\mathbf{r}-\mathbf{R_j}+\hat{x}) - \varphi(\mathbf{r}-\mathbf{R_j})) c^\dagger_{i\sigma} c_{j\sigma'} \\
&= i \sum_{i,j} (\delta_{i,j+\delta x} - \delta_{i,j}) i(\delta_{\sigma,\downarrow}\delta_{\sigma',\uparrow} - \delta_{\sigma,\uparrow}\delta_{\sigma',\downarrow}) c^\dagger_{i\sigma} c_{j\sigma'} \\
&= -\sum_{i,j} (\delta_{i,j+\delta x} - \delta_{i,j})(c^\dagger_{i\downarrow} c_{j\uparrow} - c^\dagger_{i\uparrow} c_{j\downarrow}) \\
&= -\sum_{i} (c^\dagger_{i\downarrow} c_{i-\delta x\uparrow} - c^\dagger_{i\uparrow} c_{i-\delta x\downarrow} - c^\dagger_{i\downarrow} c_{i\uparrow} + c^\dagger_{i\uparrow} c_{i\downarrow})
\end{aligned} \tag{A.5}
$$

finally giving

$$
\begin{aligned}
\mathcal{H} = -\alpha_R \mathrm{E}_z \sum_i (i[c^\dagger_{i\uparrow} c_{i-\delta y\downarrow} - c^\dagger_{i\uparrow} c_{i\downarrow} + c^\dagger_{i\downarrow} c_{i-\delta y\uparrow} - c^\dagger_{i\downarrow} c_{i\uparrow}] + \\
+ c^\dagger_{i\downarrow} c_{i-\delta x\uparrow} - c^\dagger_{i\uparrow} c_{i-\delta x\downarrow} - c^\dagger_{i\downarrow} c_{i\uparrow} + c^\dagger_{i\uparrow} c_{i\downarrow})
\end{aligned} \tag{A.6}
$$

we do a Fourier transform, where

$$
c_{i\sigma} = \frac{1}{\sqrt{N}} \sum_{\mathbf{k}} e^{i\mathbf{k}\cdot\mathbf{r}_i} c_{\mathbf{k}\sigma} \tag{A.7}
$$

where we get

$$
\mathcal{H} = -\alpha_R \mathrm{E}_z \sum_{\mathbf{k}} [i(\mathrm{e}^{-ik_y} - 1)(c^\dagger_{\mathbf{k}\uparrow} c_{\mathbf{k}\downarrow} + c^\dagger_{\mathbf{k}\downarrow} c_{\mathbf{k}\uparrow}) + (\mathrm{e}^{-ik_x} - 1)(c^\dagger_{\mathbf{k}\downarrow} c_{\mathbf{k}\uparrow} - c^\dagger_{\mathbf{k}\uparrow} c_{\mathbf{k}\downarrow})]. \tag{A.8}
$$

Central difference

It turns out that by choosing a central difference rather than a forward difference we can get our expression on a slightly more pleasing form, letting

$$\begin{aligned}\frac{d}{dx}\varphi(\mathbf{r}) &= \frac{\varphi(\mathbf{r}+\hat{x})-\varphi(\mathbf{r})}{2} - \frac{\varphi(\mathbf{r}-\hat{x})-\varphi(\mathbf{r})}{2} \\ &= \frac{\varphi(\mathbf{r}+\hat{x})-\varphi(\mathbf{r}-\hat{x})}{2},\end{aligned} \tag{A.9}$$

where the same process leads us to terms

$$\begin{aligned}&-\frac{i}{2}\sum_{i,j,\sigma,\sigma'}\int d^3r\varphi^\dagger(\mathbf{r}-\mathbf{R_i})\sigma^x_{\sigma\sigma'}(\varphi(\mathbf{r}-\mathbf{R_j}+\hat{y})-\varphi(\mathbf{r}-\mathbf{R_j}-\hat{y}))c^\dagger_{i\sigma}c_{j\sigma'} \\ &= -\frac{i}{2}\sum_{i,j}(\delta_{\sigma\uparrow}\delta_{\sigma'\downarrow}+\delta_{\sigma\downarrow}\delta_{\sigma'\uparrow})(\delta_{i,j-\delta y}-\delta_{i,j+\delta y})c^\dagger_{i\sigma}c_{j\sigma'} \\ &= -\frac{i}{2}\sum_{i,j}(c^\dagger_{i\uparrow}c_{j\downarrow}+c^\dagger_{i\downarrow}c_{j\uparrow})(\delta_{i,j-\delta y}-\delta_{i,j+\delta y}) \\ &= -\frac{i}{2}\sum_{i}(c^\dagger_{i\uparrow}c_{i+\delta y\downarrow}-c^\dagger_{i\uparrow}c_{i-\delta y\downarrow}+c^\dagger_{i\downarrow}c_{i+\delta y\uparrow}-c^\dagger_{i\downarrow}c_{i-\delta y\uparrow})\end{aligned} \tag{A.10}$$

which after a Fourier transform gives

$$\begin{aligned}&-\frac{i}{2}\sum_{\mathbf{k}}(c^\dagger_{\mathbf{k}\uparrow}c_{\mathbf{k}\downarrow}+c^\dagger_{\mathbf{k}\downarrow}c_{\mathbf{k}\uparrow})(\mathrm{e}^{ik_y}-e^{-ik_y}) \\ &= \frac{1}{2i}\sum_{\mathbf{k}}(c^\dagger_{\mathbf{k}\uparrow}c_{\mathbf{k}\downarrow}+c^\dagger_{\mathbf{k}\downarrow}c_{\mathbf{k}\uparrow})2i\sin(k_y) \\ &= \sum_{\mathbf{k}}(c^\dagger_{\mathbf{k}\uparrow}c_{\mathbf{k}\downarrow}+c^\dagger_{\mathbf{k}\downarrow}c_{\mathbf{k}\uparrow})\sin(k_y),\end{aligned} \tag{A.11}$$

and for the second term

$$\begin{aligned}
&\frac{i}{2}\sum_{i,j,\sigma,\sigma'}\int d^3r\varphi^\dagger(\mathbf{r}-\mathbf{R_i})\sigma^y_{\sigma\sigma'}(\varphi(\mathbf{r}-\mathbf{R_j}+\hat{x})-\varphi(\mathbf{r}-\mathbf{R_j}-\hat{x}))c^\dagger_{i\sigma}c_{j\sigma'}\\
&=\frac{i}{2}\sum_{i,j}(\delta_{i,j-\delta x}-\delta_{i,j+\delta x})i(\delta_{\sigma,\downarrow}\delta_{\sigma',\uparrow}-\delta_{\sigma,\uparrow}\delta_{\sigma',\downarrow})c^\dagger_{i\sigma}c_{j\sigma'}\\
&=-\frac{1}{2}\sum_{i,j}(\delta_{i,j-\delta x}-\delta_{i,j+\delta x})(c^\dagger_{i\downarrow}c_{j\uparrow}-c^\dagger_{i\uparrow}c_{j\downarrow})\\
&=-\frac{1}{2}\sum_{i}(c^\dagger_{i\downarrow}c_{i+\delta x\uparrow}-c^\dagger_{i\uparrow}c_{i+\delta x\downarrow}-c^\dagger_{i\downarrow}c_{i-\delta x\uparrow}+c^\dagger_{i\uparrow}c_{i-\delta x\downarrow})
\end{aligned}\tag{A.12}$$

which we can Fourier transform to give

$$\begin{aligned}
&-\frac{1}{2}\sum_{\mathbf{k}}[\mathrm{e}^{ik_x}(c^\dagger_{\mathbf{k}\downarrow}c_{\mathbf{k}\uparrow}-c^\dagger_{\mathbf{k}\uparrow}c_{\mathbf{k}\downarrow})-e^{-ik_x}(c^\dagger_{\mathbf{k}\downarrow}c_{\mathbf{k}\uparrow}-c^\dagger_{\mathbf{k}\uparrow}c_{\mathbf{k}\downarrow})]\\
&=i\sum_{\mathbf{k}}\sin(kx)(c^\dagger_{\mathbf{k}\uparrow}c_{\mathbf{k}\downarrow}-c^\dagger_{\mathbf{k}\downarrow}c_{\mathbf{k}\uparrow})).
\end{aligned}\tag{A.13}$$

Giving us a total Hamiltonian

$$\mathcal{H}=\alpha_R E_z\sum_{\mathbf{k}}[(\sin(k_y)+i\sin(k_x))c^\dagger_{\mathbf{k}\uparrow}c_{\mathbf{k}\downarrow}+(\sin(k_y)-i\sin(k_x))c^\dagger_{\mathbf{k}\downarrow}c_{\mathbf{k}\uparrow}].\tag{A.14}$$

APPENDIX B

PSEUDOSPIN BANDS

We follow Børkje [12] and let our Hamiltonian consist of two parts $\mathcal{H}_N + \mathcal{H}_{SC}$, a normal part, and one describing the superconducting pairing interaction and let

$$\mathcal{H}_N = \sum_{\mathbf{k}} \varphi_{\mathbf{k}}^\dagger [\varepsilon_{\mathbf{k}} - \mu + \mathbf{B}_{\mathbf{k}} \cdot \sigma] \varphi_{\mathbf{k}}, \tag{B.1}$$

where σ is the vector of Pauli-matrices, $\varepsilon_{\mathbf{k}}$ is the dispersion, μ is the chemical potential and $\varphi_{\mathbf{k}}^\dagger = (c_{\mathbf{k}\uparrow}^\dagger, c_{\mathbf{k}\downarrow}^\dagger)$.

We further define $\tilde{\varepsilon}_{\mathbf{k}} = \varepsilon_{\mathbf{k}} - \mu$ and let $\mathbf{B}_{\mathbf{k}} \cdot \sigma$ describe a Rashba-type spin-orbit coupling (SOC) with no $\hat{z}$-component for $\mathbf{B}_{\mathbf{k}}$. The eigenvalues of the Hamiltonian are readily found as $\xi_{\mathbf{k}} = \tilde{\varepsilon}_{\mathbf{k}} \pm |\mathbf{B}_{\mathbf{k}}|$ and the matrix we want to diagonalize takes the form

$$H = \begin{bmatrix} \tilde{\varepsilon}_{\mathbf{k}} & B_x - iB_y \\ B_x + iB_y & \tilde{\varepsilon}_{\mathbf{k}} \end{bmatrix}, \tag{B.2}$$

where we suppress the $\mathbf{k}$-index on the components of $\mathbf{B}_{\mathbf{k}}$ for ease of notation.

Meaning that we want to find the eigenvectors corresponding to the two eigenvalues by finding vectors such that

$$\begin{bmatrix} \mp|\mathbf{B}_{\mathbf{k}}| & B_x - iB_y \\ B_x + iB_y & \mp|\mathbf{B}_{\mathbf{k}}| \end{bmatrix} \begin{bmatrix} a \\ b \end{bmatrix} = \begin{bmatrix} 0 \\ 0 \end{bmatrix}, \tag{B.3}$$

which gives us eigenvectors proportional to

$$\mathbf{x_1} = \begin{bmatrix} 1 \\ \frac{B_x + iB_y}{|\mathbf{B_k}|} \end{bmatrix} \qquad \mathbf{x_2} = \begin{bmatrix} 1 \\ -\frac{B_x + iB_y}{|\mathbf{B_k}|} \end{bmatrix}. \tag{B.4}$$

As all entries have an absolute value of 1, a factor $1/\sqrt{2}$ keeps the transformation unitary. Denoting $(B_x + iB_y)/|\mathbf{B_k}| = \Lambda_\mathbf{k}$, we find

$$P = \frac{1}{\sqrt{2}} \begin{bmatrix} 1 & 1 \\ \Lambda_\mathbf{k} & -\Lambda_\mathbf{k} \end{bmatrix}, \tag{B.5}$$

where

$$P^{-1} H P = D, \tag{B.6}$$

where D is the diagonal matrix of eigenvalues. This gives us

$$P^{-1} = \frac{1}{\sqrt{2}} \begin{bmatrix} 1 & \frac{1}{\Lambda_\mathbf{k}} \\ 1 & -\frac{1}{\Lambda_\mathbf{k}} \end{bmatrix}. \tag{B.7}$$

Now we return to equation (B.1) and (B.2) and rewrite

$$\begin{aligned} \varphi^\dagger_\mathbf{k} H \varphi_\mathbf{k} &= \varphi^\dagger_\mathbf{k} P D P^{-1} \varphi_\mathbf{k} \\ &= (\varphi^\dagger_\mathbf{k} P) D (P^{-1} \varphi_\mathbf{k}) \\ &\equiv \tilde{\varphi}^\dagger_\mathbf{k} D \tilde{\varphi}_\mathbf{k}. \end{aligned} \tag{B.8}$$

We define $\tilde{\varphi}^\dagger_\mathbf{k} = (\tilde{c}^\dagger_{\mathbf{k}+}, \tilde{c}^\dagger_{\mathbf{k}-})$, using the same notation for the bands as [12] and further note that $1/\Lambda_\mathbf{k} = \Lambda^*_\mathbf{k}$, ending up with

$$\tilde{c}_{\mathbf{k}+} = \frac{1}{\sqrt{2}} \left(c_{\mathbf{k}\uparrow} + \Lambda^*_\mathbf{k} c_{\mathbf{k}\downarrow} \right) \tag{B.9}$$

$$\tilde{c}_{\mathbf{k}-} = \frac{1}{\sqrt{2}} \left(c_{\mathbf{k}\uparrow} - \Lambda^*_\mathbf{k} c_{\mathbf{k}\downarrow} \right), \tag{B.10}$$

noting in particular that the transformation is independent of the strength of the SOC and is dependent on $\mathbf{k}$ only through a phase-factor.

This lets us identify the factor $t_{\lambda\mathbf{k}}$ by using the action of the time-reversal operator $\mathcal{K}$ in the spin-basis and the pseudo-spin basis. $\mathcal{K} : \tilde{c}^\dagger_{\mathbf{k}\lambda} = t_{\lambda\mathbf{k}}\tilde{c}^\dagger_{-\mathbf{k}\lambda}$ and $\mathcal{K} : c^\dagger_{\mathbf{k}\sigma} = -\sigma c^\dagger_{-\mathbf{k}-\sigma}$.

$$\begin{aligned}\mathcal{K} : \tilde{c}^\dagger_{\mathbf{k}+} &= t_{+\mathbf{k}}\tilde{c}^\dagger_{-\mathbf{k}+} \\ &= \frac{t_{\lambda\mathbf{k}}}{\sqrt{2}}\left(c^\dagger_{-\mathbf{k}\uparrow} + \Lambda_{-\mathbf{k}}c^\dagger_{-\mathbf{k}\downarrow}\right) \\ &= \frac{t_{\lambda\mathbf{k}}}{\sqrt{2}}\left(c^\dagger_{-\mathbf{k}\uparrow} - \Lambda_{\mathbf{k}}c^\dagger_{-\mathbf{k}\downarrow}\right), \end{aligned} \tag{B.11}$$

$$\begin{aligned}\mathcal{K} : \tilde{c}^\dagger_{\mathbf{k}+} &= \frac{1}{\sqrt{2}}\left(\mathcal{K}c^\dagger_{\mathbf{k}\uparrow} + \mathcal{K}(\Lambda_{\mathbf{k}}c^\dagger_{\mathbf{k}\downarrow})\right) \\ &= \frac{1}{\sqrt{2}}\left(\mathcal{K}c^\dagger_{\mathbf{k}\uparrow} + \Lambda^*_{\mathbf{k}}\mathcal{K}c^\dagger_{\mathbf{k}\downarrow}\right) \\ &= \frac{1}{\sqrt{2}}\left(-c^\dagger_{-\mathbf{k}\downarrow} + \Lambda^*_{\mathbf{k}}c^\dagger_{-\mathbf{k}\uparrow}\right), \end{aligned} \tag{B.12}$$

giving us

$$t_{+\mathbf{k}} = \Lambda^*_{\mathbf{k}} \tag{B.13}$$

and

$$t_{-\mathbf{k}} = -\Lambda^*_{\mathbf{k}} = -t_{+\mathbf{k}} \tag{B.14}$$

B.1 Calculation of the spectral weight

The initial Hamiltonian is diagonalized in a basis $\bar{\Psi}_{\mathbf{k}\gamma} = (c^\dagger_{\mathbf{k}\gamma}, c_{-\mathbf{k}\gamma})$, where $\gamma = \pm$.

$$\Phi_{\mathbf{k}\gamma} = \exp(i\theta_{\mathbf{k}i}\tau_y)\Psi_{\mathbf{k}\gamma} \tag{B.15}$$

where $\Phi_{\mathbf{k}}$ diagonalizes the original Hamiltonioan with excitation energies $E_{\mathbf{k}\gamma i} = \sqrt{\varepsilon^2_{\mathbf{k}\gamma i} + \Delta^2_{\mathbf{k}\gamma i}}$.
In the same way we diagnoalize the Hamiltonain after the quench with another set of of fermions

$$\Upsilon_{\mathbf{k}\gamma} = \exp(i\theta_{\mathbf{k}\gamma}\tau_y)\Psi_{\mathbf{k}\gamma}, \tag{B.16}$$

where $\Upsilon_{\mathbf{k}\gamma}$ diagonalizes the final Hamiltonain with excitation energies $E_{\mathbf{k}\gamma st} = \sqrt{\varepsilon^2_{\mathbf{k}\gamma st} + \Delta^2_{\mathbf{k}\gamma st}}$. We can then write down a time-dependent transformation

$$\Psi_{\mathbf{k}\gamma}(t) = M_{\mathbf{k}\gamma}(t)\Phi_{\mathbf{k}\gamma}(0), \tag{B.17}$$

where we will be using the final quench Hamiltonian for the time evolution,

$$H = \sum_{\mathbf{k}\gamma} \overline{\Upsilon}_{\mathbf{k}\gamma} E_{\mathbf{k}\gamma}\tau_z \Upsilon_{\mathbf{k}\gamma} \tag{B.18}$$

$$= \sum_{\mathbf{k}\gamma} \overline{\Psi}_{\mathbf{k}\gamma} \exp(-i\theta_{\mathbf{k}\gamma}\tau_y) E_{\mathbf{k}\gamma}\tau_z \exp(i\theta_{\mathbf{k}\gamma}\tau_y)\Psi_{\mathbf{k}\gamma}. \tag{B.19}$$

As this is a constant Hamiltonian, we can use $\psi(t) = e^{i\hat{H}t}\psi(0)$ for the evolution of the Nambu spinors. Furthermore, our operator $\hat{H}$ is on the form $\hat{H} = PDP^{-1}$, where D is diagonal, allowing us to use $e^{\hat{H}} = Pe^{D}P^{-1}$.

We start out by using the properties of diagonalizable matrices to explicitly write out

$$\Psi(t) = e^{-i\hat{H}t}\Psi(0), \tag{B.20}$$

and do a change of basis to the Φ basis. Then we will set up the matrix $M_{k\gamma}(t)$ and compare coefficients to find the elements of the matrix. This will allow us to find the approximate time-evolution of the matrix-elements of the lesser Green's function, which can be related to the ARPES signal. In the following we drop the band index γ as this is always the same throughout the calculation.

$$\begin{aligned}
\Psi_{\mathbf{k}}(t) &= e^{i\hat{H}t}\Psi_{\mathbf{k}}(0) \\
&= e^{i\exp(-i\theta_{\mathbf{k}}\tau_y)E_{\mathbf{k}}\tau_z\exp(i\theta_{\mathbf{k}}\tau_y)t}\Psi_{\mathbf{k}}(0) \\
&= \exp(-i\theta_{\mathbf{k}}\tau_y)e^{iE_{\mathbf{k}}\tau_z t}\exp(i\theta_{\mathbf{k}}\tau_y)\Psi_{\mathbf{k}}(0) \\
&= \exp(-i\theta_{\mathbf{k}}\tau_y)e^{iE_{\mathbf{k}}\tau_z t}\exp(i\theta_{\mathbf{k}}\tau_y)\exp(-i\theta_{\mathbf{k}i}\tau_y)\Phi_{\mathbf{k}}(0) \\
&= \exp(-i\theta_{\mathbf{k}}\tau_y)e^{iE_{\mathbf{k}}\tau_z t}\exp(i(\theta_{\mathbf{k}}-\theta_{\mathbf{k}i})\tau_y)\Phi_{\mathbf{k}}(0) \\
&= (\mathbf{I}\cos(\theta_{\mathbf{k}}) - i\tau_y\sin(\theta_{\mathbf{k}}))e^{iE_{\mathbf{k}}\tau_z t}(\mathbf{I}\cos(\theta_{\mathbf{k}}-\theta_{\mathbf{k}i}) + i\tau_y\sin(\theta_{\mathbf{k}}-\theta_{\mathbf{k}i}))\Phi_{\mathbf{k}}(0) \\
&= (\mathbf{I}\cos(\theta_{\mathbf{k}}) - i\tau_y\sin(\theta_{\mathbf{k}}))(\mathbf{I}\cos(E_{\mathbf{k}}t) - i\tau_z\sin(E_{\mathbf{k}}t))(\mathbf{I}\cos(\theta_{\mathbf{k}}-\theta_{\mathbf{k}i}) + \\
&+ i\tau_y\sin(\theta_{\mathbf{k}}-\theta_{\mathbf{k}i}))\Phi_{\mathbf{k}}(0) \\
&= (\mathbf{I}\cos(\theta_{\mathbf{k}}) - i\tau_y\sin(\theta_{\mathbf{k}}))(\mathbf{I}\cos(E_{\mathbf{k}}t)\cos(\theta_{\mathbf{k}}-\theta_{\mathbf{k}i}) + i\tau_y\cos(E_{\mathbf{k}}t)\sin(\theta_{\mathbf{k}}-\theta_{\mathbf{k}i}) \\
&- i\tau_z\sin(E_{\mathbf{k}}t)\cos(\theta_{\mathbf{k}}-\theta_{\mathbf{k}i}) - i\tau_z i\tau_y\sin(E_{\mathbf{k}}t)\sin(\theta_{\mathbf{k}}-\theta_{\mathbf{k}i}))\Phi_{\mathbf{k}}(0),
\end{aligned} \tag{B.21}$$

we now focus on the calculation of the matrix M in

$$\Psi_{\mathbf{k}}(t) = M_{\mathbf{k}}(t)\Phi_{\mathbf{k}}(0) \tag{B.22}$$

$$\begin{aligned}
M_{\mathbf{k}}(t) &= (\mathbf{I}\cos(\theta_{\mathbf{k}}) - i\tau_y\sin(\theta_{\mathbf{k}}))(\mathbf{I}\cos(E_{\mathbf{k}}t)\cos(\theta_{\mathbf{k}} - \theta_{\mathbf{k}i}) + \\
&+ i\tau_y\cos(E_{\mathbf{k}}t)\sin(\theta_{\mathbf{k}} - \theta_{\mathbf{k}i}) - i\tau_z\sin(E_{\mathbf{k}}t)\cos(\theta_{\mathbf{k}} - \theta_{\mathbf{k}i}) \\
&- i\tau_x\sin(E_{\mathbf{k}}t)\sin(\theta_{\mathbf{k}} - \theta_{\mathbf{k}i}))\Phi_{\mathbf{k}}(0) \\
&= \mathbf{I}\cos(\theta_{\mathbf{k}})\cos(E_{\mathbf{k}}t)\cos(\theta_{\mathbf{k}} - \theta_{\mathbf{k}i}) - i\tau_y\sin(\theta_{\mathbf{k}})\cos(E_{\mathbf{k}}t)\cos(\theta_{\mathbf{k}} - \theta_{\mathbf{k}i}) + \\
&+ i\tau_y\cos(\theta_{\mathbf{k}})\cos(E_{\mathbf{k}}t)\sin(\theta_{\mathbf{k}} - \theta_{\mathbf{k}i}) + \tau_y^2\sin(\theta_{\mathbf{k}})\cos(E_{\mathbf{k}}t)\sin(\theta_{\mathbf{k}} - \theta_{\mathbf{k}i}) + \\
&- i\tau_z\cos(\theta_{\mathbf{k}})\sin(E_{\mathbf{k}}t)\cos(\theta_{\mathbf{k}} - \theta_{\mathbf{k}i}) - \tau_y\tau_z\sin(\theta_{\mathbf{k}})\sin(E_{\mathbf{k}}t)\cos(\theta_{\mathbf{k}} - \theta_{\mathbf{k}i}) + \\
&- i\tau_x\cos(\theta_{\mathbf{k}})\sin(E_{\mathbf{k}}t)\sin(\theta_{\mathbf{k}} - \theta_{\mathbf{k}i}) - \tau_y\tau_x\sin(\theta_{\mathbf{k}})\sin(E_{\mathbf{k}}t)\sin(\theta_{\mathbf{k}} - \theta_{\mathbf{k}i}) \\
&= \mathbf{I}\cos(\theta_{\mathbf{k}})\cos(E_{\mathbf{k}}t)\cos(\theta_{\mathbf{k}} - \theta_{\mathbf{k}i}) - i\tau_y\sin(\theta_{\mathbf{k}})\cos(E_{\mathbf{k}}t)\cos(\theta_{\mathbf{k}} - \theta_{\mathbf{k}i}) + \\
&+ i\tau_y\cos(\theta_{\mathbf{k}})\cos(E_{\mathbf{k}}t)\sin(\theta_{\mathbf{k}} - \theta_{\mathbf{k}i}) + \mathbf{I}\sin(\theta_{\mathbf{k}})\cos(E_{\mathbf{k}}t)\sin(\theta_{\mathbf{k}} - \theta_{\mathbf{k}i}) + \\
&- i\tau_z\cos(\theta_{\mathbf{k}})\sin(E_{\mathbf{k}}t)\cos(\theta_{\mathbf{k}} - \theta_{\mathbf{k}i}) - i\tau_x\sin(\theta_{\mathbf{k}})\sin(E_{\mathbf{k}}t)\cos(\theta_{\mathbf{k}} - \theta_{\mathbf{k}i}) + \\
&- i\tau_x\cos(\theta_{\mathbf{k}})\sin(E_{\mathbf{k}}t)\sin(\theta_{\mathbf{k}} - \theta_{\mathbf{k}i}) + i\tau_z\sin(\theta_{\mathbf{k}})\sin(E_{\mathbf{k}}t)\sin(\theta_{\mathbf{k}} - \theta_{\mathbf{k}i}) \\
&= \mathbf{I}\cos(E_{\mathbf{k}}t)(\cos(\theta_{\mathbf{k}})\cos(\theta_{\mathbf{k}} - \theta_{\mathbf{k}i}) + \sin(\theta_{\mathbf{k}})\sin(\theta_{\mathbf{k}} - \theta_{\mathbf{k}i})) + \\
&+ i\tau_y\cos(E_{\mathbf{k}}t)(\cos(\theta_{\mathbf{k}})\sin(\theta_{\mathbf{k}} - \theta_{\mathbf{k}i}) - \sin(\theta_{\mathbf{k}})\cos(\theta_{\mathbf{k}} - \theta_{\mathbf{k}i})) + \\
&+ i\tau_z\sin(E_{\mathbf{k}}t)(\sin(\theta_{\mathbf{k}})\sin(\theta_{\mathbf{k}} - \theta_{\mathbf{k}i}) - \cos(\theta_{\mathbf{k}})\cos(\theta_{\mathbf{k}} - \theta_{\mathbf{k}i})) + \\
&- i\tau_x\sin(E_{\mathbf{k}}t)(\cos(\theta_{\mathbf{k}})\sin(\theta_{\mathbf{k}} - \theta_{\mathbf{k}i}) + \sin(\theta_{\mathbf{k}})\cos(\theta_{\mathbf{k}} - \theta_{\mathbf{k}i})).
\end{aligned} \tag{B.23}$$

Component wise, this gives many expressions on the form of the trigonometric addition formulas,

$$\begin{aligned}
M_{\mathbf{k}11}(t) &= \cos(E_{\mathbf{k}}t)(\cos(\theta_{\mathbf{k}})\cos(\theta_{\mathbf{k}} - \theta_{\mathbf{k}i}) + \sin(\theta_{\mathbf{k}})\sin(\theta_{\mathbf{k}} - \theta_{\mathbf{k}i})) \\
&+ i\sin(E_{\mathbf{k}}t)(\sin(\theta_{\mathbf{k}})\sin(\theta_{\mathbf{k}} - \theta_{\mathbf{k}i}) - \cos(\theta_{\mathbf{k}})\cos(\theta_{\mathbf{k}} - \theta_{\mathbf{k}i})) \\
&= \cos(E_{\mathbf{k}}t)\cos(\theta_{\mathbf{k}} - (\theta_{\mathbf{k}} - \theta_{\mathbf{k}i})) \\
&- i\sin(E_{\mathbf{k}}t)(\cos(\theta_{\mathbf{k}})\cos(\theta_{\mathbf{k}} - \theta_{\mathbf{k}i}) - \sin(\theta_{\mathbf{k}})\sin(\theta_{\mathbf{k}} - \theta_{\mathbf{k}i})) \qquad \text{(B.24)} \\
&= \cos(E_{\mathbf{k}}t)\cos(\theta_{\mathbf{k}i}) - i\sin(E_{\mathbf{k}}t)\cos(\theta_{\mathbf{k}i} + \theta_{\mathbf{k}} - \theta_{\mathbf{k}i}) \\
&= \cos(E_{\mathbf{k}}t)\cos(\theta_{\mathbf{k}i}) - i\sin(E_{\mathbf{k}}t)\cos(2\theta_{\mathbf{k}} - \theta_{\mathbf{k}i}), \qquad \text{(B.25)}
\end{aligned}$$

from the symmetry of the Pauli-matrices we see that

$$M_{\mathbf{k}22}(t) = M^*_{\mathbf{k}11}(t). \tag{B.26}$$

Looking at the other components,

$$\begin{aligned}
M_{\mathbf{k}12}(t) &= \cos(E_{\mathbf{k}}t)(\cos(\theta_{\mathbf{k}})\sin(\theta_{\mathbf{k}}-\theta_{\mathbf{k}i}) - \sin(\theta_{\mathbf{k}})\cos(\theta_{\mathbf{k}}-\theta_{\mathbf{k}i})) \\
&\quad - i\sin(E_{\mathbf{k}}t)(\cos(\theta_{\mathbf{k}})\sin(\theta_{\mathbf{k}}-\theta_{\mathbf{k}i}) + \sin(\theta_{\mathbf{k}})\cos(\theta_{\mathbf{k}}-\theta_{\mathbf{k}i})) \\
&= -\cos(E_{\mathbf{k}}t)(\sin(\theta_{\mathbf{k}})\cos(\theta_{\mathbf{k}}-\theta_{\mathbf{k}i}) - \cos(\theta_{\mathbf{k}})\sin(\theta_{\mathbf{k}}-\theta_{\mathbf{k}i})) \\
&\quad - i\sin(E_{\mathbf{k}}t)\sin(\theta_{\mathbf{k}}-\theta_{\mathbf{k}i}+\theta_{\mathbf{k}}) \\
&= -\cos(E_{\mathbf{k}}t)\sin(\theta_{\mathbf{k}}-(\theta_{\mathbf{k}}-\theta_{\mathbf{k}i})) - i\sin(E_{\mathbf{k}}t)\sin(2\theta_{\mathbf{k}}-\theta_{\mathbf{k}i}) \\
&= -\cos(E_{\mathbf{k}}t)\sin(\theta_{\mathbf{k}i}) - i\sin(E_{\mathbf{k}}t)\sin(2\theta_{\mathbf{k}}-\theta_{\mathbf{k}i}), \qquad \text{(B.27)}
\end{aligned}$$

again we see from the symmetry that

$$M_{\mathbf{k}21}(t) = -M^*_{\mathbf{k}12}(t). \qquad \text{(B.28)}$$

Now we define the Nambu Green's function (GF) on the Keldysh contour,

$$G_{k\alpha\beta}(t,t') = -i\langle T_K \Psi_{k\alpha}(t)\overline{\Psi}_{k\beta}(t')\rangle \qquad \text{(B.29)}$$

and in particular the lesser GF, $G^<_{k\alpha\beta}(t,t') = -i\langle \Psi_{k\alpha}(t)\overline{\Psi}_{k\beta}(t')\rangle$, with normal component ($\alpha=\beta=1$)

$$G^<_{\mathbf{k}}(t,t') = i\langle c^\dagger_{k\uparrow}(t')c_{k\uparrow}(t)\rangle. \qquad \text{(B.30)}$$

This is related to the ARPES signal, typically probing the transition for transmission from occupied to empty states,

$$\begin{aligned}
G^<_{\mathbf{k}}(t,t') &= i\langle (M^*_{\mathbf{k}11}(t')\Phi^\dagger_{\mathbf{k}\uparrow} + M^*_{\mathbf{k}12}(t')\Phi_{-\mathbf{k}\downarrow})(M_{\mathbf{k}11}(t)\Phi_{\mathbf{k}\uparrow} + M_{\mathbf{k}12}(t)\Phi^\dagger_{-\mathbf{k}\downarrow})\rangle \\
&= i(M^*_{\mathbf{k}11}(t')M_{\mathbf{k}11}(t)\langle\Phi^\dagger_{\mathbf{k}\uparrow}\Phi_{\mathbf{k}\uparrow}\rangle + iM^*_{\mathbf{k}12}(t')M_{\mathbf{k}12}(t)\langle\Phi_{-\mathbf{k}\downarrow}\Phi^\dagger_{-\mathbf{k}\downarrow}\rangle \\
&= iM^*_{\mathbf{k}11}(t')M_{\mathbf{k}11}(t)n(E_{\mathbf{k}i}) + iM^*_{\mathbf{k}12}(t')M_{\mathbf{k}12}(t)(1-n(E_{\mathbf{k}i}) \qquad \text{(B.31)}
\end{aligned}$$

where the expectation value is taken in the initial Bogolubov vacuum, $n(E) = 1/(e^{\beta E}+1)$is the Fermi distribution and $\beta = 1/T$ is the inverse temperature of the initial state.

In equilibrium, with no quench $\Delta_i = \Delta_f$, we recover

$$
\begin{aligned}
G^<_{\mathbf{k}}(t,t') &= i(\cos(E_{\mathbf{k}i}t')\cos(\theta_{\mathbf{k}i}) + i\sin(E_{\mathbf{k}i}t')\cos(2\theta_{\mathbf{k}i}-\theta_{\mathbf{k}i}))\cdot \\
&\quad \cdot(\cos(E_{\mathbf{k}i}t)\cos(\theta_{\mathbf{k}i}) - i\sin(E_{\mathbf{k}i}t)\cos(2\theta_{\mathbf{k}i}-\theta_{\mathbf{k}i}))n(E_{\mathbf{k}i})n(E_{\mathbf{k}i}) \\
&\quad + i(-\cos(E_{\mathbf{k}i}t')\sin(\theta_{\mathbf{k}i}) + i\sin(E_{\mathbf{k}i}t')\sin(2\theta_{\mathbf{k}i}-\theta_{\mathbf{k}i}))\cdot \\
&\quad \cdot(-\cos(E_{\mathbf{k}i}t)\sin(\theta_{\mathbf{k}i}) - i\sin(E_{\mathbf{k}i}t)\sin(2\theta_{\mathbf{k}i}-\theta_{\mathbf{k}i}))(1-n(E_{\mathbf{k}i})) \\
&= i\cos(\theta_{\mathbf{k}i})(\cos(E_{\mathbf{k}i}t') + i\sin(E_{\mathbf{k}i}t'))\cdot \\
&\quad \cdot(\cos(E_{\mathbf{k}i}t) - i\sin(E_{\mathbf{k}i}t))\cos(\theta_{\mathbf{k}i})n(E_{\mathbf{k}i}) \\
&\quad + i\sin(\theta_{\mathbf{k}i})(-\cos(E_{\mathbf{k}i}t') + i\sin(E_{\mathbf{k}i}t'))\cdot \\
&\quad \cdot(-\cos(E_{\mathbf{k}i}t) - i\sin(E_{\mathbf{k}i}t))\sin(\theta_{\mathbf{k}i})(1-n(E_{\mathbf{k}i})) \\
&= i\cos^2(\theta_{\mathbf{k}i})n(E_{\mathbf{k}i})(\cos(E_{\mathbf{k}i}t') + i\sin(E_{\mathbf{k}i}t'))(\cos(E_{\mathbf{k}i}t) - i\sin(E_{\mathbf{k}i}t)) \\
&\quad + i\sin^2(\theta_{\mathbf{k}i})(1-n(E_{\mathbf{k}i}))(-\cos(E_{\mathbf{k}i}t') + i\sin(E_{\mathbf{k}i}t'))(-\cos(E_{\mathbf{k}i}t) - i\sin(E_{\mathbf{k}i}t)) \\
&= i\cos^2(\theta_{\mathbf{k}i})n(E_{\mathbf{k}i})e^{iE_{\mathbf{k}i}t'}e^{-iE_{\mathbf{k}i}t} \\
&\quad + i\sin^2(\theta_{\mathbf{k}i})(1-n(E_{\mathbf{k}i}))(-e^{-iE_{\mathbf{k}i}t'})(-e^{iE_{\mathbf{k}i}t}) \\
&= i\cos^2(\theta_{\mathbf{k}i})n(E_{\mathbf{k}i})e^{-iE_{\mathbf{k}i}(t-t')} + i\sin^2(\theta_{\mathbf{k}i})(1-n(E_{\mathbf{k}i}))e^{iE_{\mathbf{k}i}(t-t')}.
\end{aligned}
\tag{B.32}
$$

Fourier transforming then gives

$$
G^<_{\mathbf{k}}(\omega) = i\cos^2(\theta_{\mathbf{k}i})n(E_{\mathbf{k}i})\delta(\omega - E_{\mathbf{k}i}) + i\sin^2(\theta_{\mathbf{k}i})(1-n(E_{\mathbf{k}i}))\delta(\omega + E_{\mathbf{k}i}),
\tag{B.33}
$$

in the low temperature limit $n(E_{\mathbf{k}i}) \approx 0$ and only one peak gives significant contributions. In the end, this peak will be used to compare spectral weights. In the non-equilibrium case with the quench turned on the lesser Green's function will not depend only on the time difference $t - t'$, it will depend on both $t - t' \equiv \tau$ and on $t + t'$. In the subsequent Fourier transform it is therefore convenient to transform with respect to τ and leave τ and t as independent. We first calculate the non-equilibrium case

$$
\begin{aligned}
&G^{<}_{\mathbf{k}}(t,t') = i(\cos(E_{\mathbf{k}}t')\cos(\theta_{\mathbf{k}i}) + i\sin(E_{\mathbf{k}}t')\cos(2\theta_{\mathbf{k}} - \theta_{\mathbf{k}i}))\cdot \\
&\cdot(\cos(E_{\mathbf{k}}t)\cos(\theta_{\mathbf{k}i}) - i\sin(E_{\mathbf{k}}t)\cos(2\theta_{\mathbf{k}} - \theta_{\mathbf{k}i}))n(E_{\mathbf{k}i}) \\
&+ i(-\cos(E_{\mathbf{k}}t')\sin(\theta_{\mathbf{k}i}) + i\sin(E_{\mathbf{k}}t')\sin(2\theta_{\mathbf{k}} - \theta_{\mathbf{k}i}))\cdot \\
&\cdot(-\cos(E_{\mathbf{k}}t)\sin(\theta_{\mathbf{k}i}) - i\sin(E_{\mathbf{k}}t)\sin(2\theta_{\mathbf{k}} - \theta_{\mathbf{k}i}))(1 - n(E_{\mathbf{k}i}) \\
&= i\cos(E_{\mathbf{k}}t')\cos(E_{\mathbf{k}}t)(n(E_{\mathbf{k}i})\cos^2(\theta_{\mathbf{k}i}) + \sin^2(\theta_{\mathbf{k}i})(1 - n(E_{\mathbf{k}i})))+ \\
&+ i(-i\cos(E_{\mathbf{k}}t')\sin(E_{\mathbf{k}}t) + i\sin(E_{\mathbf{k}}t')\cos(E_{\mathbf{k}}t))\cos(2\theta_{\mathbf{k}} - \theta_{\mathbf{k}i})\cos(\theta_{\mathbf{k}i})n(E_{\mathbf{k}i}))+ \\
&+ i\sin(E_{\mathbf{k}}t')\sin(E_{\mathbf{k}}t)(\cos^2(2\theta_{\mathbf{k}} - \theta_{\mathbf{k}i})n(E_{\mathbf{k}i})) + \sin^2(2\theta_{\mathbf{k}} - \theta_{\mathbf{k}i})(1 - n(E_{\mathbf{k}i})))+ \\
&+ i(i\cos(E_{\mathbf{k}}t')\sin(E_{\mathbf{k}}t) - i\cos(E_{\mathbf{k}}t)\sin(E_{\mathbf{k}}t'))\sin(\theta_{\mathbf{k}i})\sin(2\theta_{\mathbf{k}} - \theta_{\mathbf{k}i})(1 - n(E_{\mathbf{k}i})) \\
&= i\frac{1}{2}(\cos(E_{\mathbf{k}}(t' + t)) + \cos(E_{\mathbf{k}}(t' - t)))(\cos^2(\theta_{\mathbf{k}i}) - \sin^2(\theta_{\mathbf{k}i}))(n(E_{\mathbf{k}i}) + \sin^2(\theta_{\mathbf{k}i}))+ \\
&+ i\frac{1}{2}(\cos(E_{\mathbf{k}}(t - t')) - \cos(E_{\mathbf{k}}(t' + t)))(\cos^2(2\theta_{\mathbf{k}} - \theta_{\mathbf{k}i}) - \sin^2(2\theta_{\mathbf{k}} - \theta_{\mathbf{k}i}))n(E_{\mathbf{k}i})+ \\
&+ \sin^2(2\theta_{\mathbf{k}} - \theta_{\mathbf{k}i})) - i(i\sin(E_{\mathbf{k}}(t - t'))\cos(2\theta_{\mathbf{k}} - \theta_{\mathbf{k}i})\cos(\theta_{\mathbf{k}i})n(E_{\mathbf{k}i}))+ \\
&+ i(i\sin(E_{\mathbf{k}}(t - t'))\sin(2\theta_{\mathbf{k}} - \theta_{\mathbf{k}i})\sin(\theta_{\mathbf{k}i})(1 - n(E_{\mathbf{k}i}))) \\
&= i\frac{1}{4}(e^{2iE_{\mathbf{k}}t}e^{-iE_{\mathbf{k}}(t-t')} + e^{-2iE_{\mathbf{k}}t}e^{iE_{\mathbf{k}}(t-t')} + e^{-iE_{\mathbf{k}}(t-t')} + e^{E_{\mathbf{k}}(t-t')}).\\
&\cdot(\cos^2(\theta_{\mathbf{k}i}) - \sin^2(\theta_{\mathbf{k}i}))(n(E_{\mathbf{k}i}) + \sin^2(\theta_{\mathbf{k}i}))+ \\
&+ i\frac{1}{4}(e^{iE_{\mathbf{k}}(t-t')} + e^{-E_{\mathbf{k}}(t-t')} - e^{2iE_{\mathbf{k}}t}e^{-iE_{\mathbf{k}}(t-t'))} - e^{-2iE_{\mathbf{k}}t}e^{iE_{\mathbf{k}}(t-t')}).\\
&\cdot(\cos^2(2\theta_{\mathbf{k}} - \theta_{\mathbf{k}i}) - \sin^2(2\theta_{\mathbf{k}} - \theta_{\mathbf{k}i}))n(E_{\mathbf{k}i}) + \sin^2(2\theta_{\mathbf{k}} - \theta_{\mathbf{k}i}))+ \\
&- i\frac{1}{2}(e^{iE_{\mathbf{k}}(t-t')} - e^{-iE_{\mathbf{k}}(t-t')})\cos(2\theta_{\mathbf{k}} - \theta_{\mathbf{k}i})\cos(\theta_{\mathbf{k}i})n(E_{\mathbf{k}i}))+ \\
&+ i\frac{1}{2}(e^{iE_{\mathbf{k}}(t-t')} - e^{-iE_{\mathbf{k}}(t-t')})\sin(2\theta_{\mathbf{k}} - \theta_{\mathbf{k}i})\sin(\theta_{\mathbf{k}i})(1 - n(E_{\mathbf{k}i}))) \qquad \text{(B.34)}
\end{aligned}
$$

At this point we will try to make the expression somewhat more manageable, we look at the coefficients of each term containing time dependence separately. Starting with the coefficients of $ie^{2iE_{\mathbf{k}}t}e^{-iE_{\mathbf{k}}(t-t')}$ and $ie^{-2iE_{\mathbf{k}}t}e^{iE_{\mathbf{k}}(t-t')}$, denoting it $C_{\mathbf{k}}$

$$
\begin{aligned}
C_{\mathbf{k}} &= \frac{1}{4}(\cos^2(\theta_{\mathbf{k}i}) - \sin^2(\theta_{\mathbf{k}i}))(n(E_{\mathbf{k}i}) + \sin^2(\theta_{\mathbf{k}i}))+ \\
&\quad - \frac{1}{4}(\cos^2(2\theta_{\mathbf{k}} - \theta_{\mathbf{k}i}) - \sin^2(2\theta_{\mathbf{k}} - \theta_{\mathbf{k}i}))n(E_{\mathbf{k}i}) + \sin^2(2\theta_{\mathbf{k}} - \theta_{\mathbf{k}i})) \\
&\quad = \frac{1}{4}(\cos^2(\theta_{\mathbf{k}i}) - \cos^2(2\theta_{\mathbf{k}} - \theta_{\mathbf{k}i})) + \frac{1}{4}(1 - n(E_{\mathbf{k}i}))(\sin^2(2\theta_{\mathbf{k}}) - \sin^2(2\theta_{\mathbf{k}} - \theta_{\mathbf{k}i}))), \qquad \text{(B.35)}
\end{aligned}
$$

next, the coefficients of $ie^{iE_{\mathbf{k}}(t-t')}$, denoting it $A_{\mathbf{k}}$

$$\begin{aligned}
A_{\mathbf{k}} &= \frac{1}{4}(\cos^2(\theta_{\mathbf{k}i}) - \sin^2(\theta_{\mathbf{k}i}))(n(E_{\mathbf{k}i}) + \sin^2(\theta_{\mathbf{k}i}))+ \\
&+ \frac{1}{4}(\cos^2(2\theta_{\mathbf{k}} - \theta_{\mathbf{k}i}) - \sin^2(2\theta_{\mathbf{k}} - \theta_{\mathbf{k}i}))n(E_{\mathbf{k}i}) + \sin^2(2\theta_{\mathbf{k}} - \theta_{\mathbf{k}i}))+ \\
&- \frac{1}{2}\cos(2\theta_{\mathbf{k}} - \theta_{\mathbf{k}i})\cos(\theta_{\mathbf{k}i})n(E_{\mathbf{k}i}))+ \\
&+ \frac{1}{2}\sin(2\theta_{\mathbf{k}} - \theta_{\mathbf{k}i})\sin(\theta_{\mathbf{k}i})(1 - n(E_{\mathbf{k}i})))\\
&= \frac{1}{4}(1 - n(E_{\mathbf{k}i}))(\sin(\theta_{\mathbf{k}i}) + \sin(2\theta_{\mathbf{k}} - \theta_{\mathbf{k}i}))^2+ \\
&+ \frac{1}{4}n(E_{\mathbf{k}i})(\cos(\theta_{\mathbf{k}i}) - \cos(2\theta_{\mathbf{k}} - \theta_{\mathbf{k}i}))^2, \qquad \text{(B.36)}
\end{aligned}$$

and finally, the coefficient of $ie^{-iE_{\mathbf{k}}(t-t')}$, denoting it $B_{\mathbf{k}}$, can be seen from the symmetry between $A_{\mathbf{k}}$ and $B_{\mathbf{k}}$

$$\begin{aligned}
B_{\mathbf{k}} &= \frac{1}{4}n(E_{\mathbf{k}i})(\cos(\theta_{\mathbf{k}i}) + \cos(2\theta_{\mathbf{k}} - \theta_{\mathbf{k}i}))^2+ \\
&+ \frac{1}{4}(1 - n(E_{\mathbf{k}i}))(\sin(\theta_{\mathbf{k}i}) - \sin(2\theta_{\mathbf{k}} - \theta_{\mathbf{k}i}))^2. \qquad \text{(B.37)}
\end{aligned}$$

Now we can write down the lesser GF in a form suitable for Fourier transformation

$$G^<_{\mathbf{k}}(t,t') = i(A_{\mathbf{k}} + C_{\mathbf{k}}e^{2iE_{\mathbf{k}}t})e^{-iE_{\mathbf{k}}(t-t')} + i(B_{\mathbf{k}} + C_{\mathbf{k}}e^{-2iE_{\mathbf{k}}t})e^{iE_{\mathbf{k}}(t-t')}, \qquad \text{(B.38)}$$

giving us

$$G^<_{\mathbf{k}}(\omega,t) = i(A_{\mathbf{k}} + C_{\mathbf{k}}e^{2iE_{\mathbf{k}}t})\delta(\omega + E_{\mathbf{k}}) + i(B_{\mathbf{k}} + C_{\mathbf{k}}e^{-2iE_{\mathbf{k}}t})\delta(\omega - E_{\mathbf{k}}). \qquad \text{(B.39)}$$

We do a time-average over the time t as the coefficients in front of the delta functions are not positive definite. We care about this being positive as the spectral function can be physically interpreted as a probability measure [31]. The coefficient functions $C_{\mathbf{k}}e^{\pm 2iE_{\mathbf{k}}t}$ are oscillating and disappear in the averaging

$$G^<_{\mathbf{k}}(\omega) = \lim_{t\to\infty}\frac{1}{t}\int_0^t dT G^<_{\mathbf{k}}(\omega,T), \qquad \text{(B.40)}$$

giving us

$$Z_{\mathbf{k}neq} = -\frac{1}{\pi}\,\mathrm{Im}(G^{<}_{\mathbf{k}}), \tag{B.41}$$

letting us write

$$-\frac{i}{\pi}G^{<}_{\mathbf{k}} = Z^{-}_{\mathbf{k}neq}\delta(\omega + E_{\mathbf{k}}) + Z^{+}_{\mathbf{k}neq}\delta(\omega - E_{\mathbf{k}}). \tag{B.42}$$

We can now focus on the negative frequency peak in a single band and compare the equilibrium and non-equilibrium case for some final gap Δ_f,

$$\begin{aligned}\frac{Z^{-}_{\mathbf{k}neq}}{Z_{\mathbf{k}eq}} = &\frac{\frac{1}{4}(1-n(E_{\mathbf{k}i}))(\sin(\theta_{\mathbf{k}i}) + \sin(2\theta_{\mathbf{k}} - \theta_{\mathbf{k}i}))^2}{\sin^2(\theta_{\mathbf{k}f})(1-n(E_{\mathbf{k}f}))} + \\ &+ \frac{\frac{1}{4}n(E_{\mathbf{k}i})(\cos(\theta_{\mathbf{k}i}) - \cos(2\theta_{\mathbf{k}} - \theta_{\mathbf{k}i}))^2}{\sin^2(\theta_{\mathbf{k}f})(1-n(E_{\mathbf{k}f}))}.\end{aligned} \tag{B.43}$$

In the low temperature limit the Fermi-Dirac distributions $n(E_{\mathbf{k}}) \approx 0$, defining $A_i \equiv \sin(\theta_{\mathbf{k}i})$, $A \equiv \sin(\theta_{\mathbf{k}})$, $B_i \equiv \cos(\theta_{\mathbf{k}i})$ and $B \equiv \cos(\theta_{\mathbf{k}})$ we write

$$\begin{aligned}\frac{Z^{-}_{\mathbf{k}neq}}{Z_{\mathbf{k}eq}} &\approx \frac{1}{4}\frac{(\sin(\theta_{\mathbf{k}i}) + \sin(2\theta_{\mathbf{k}} - \theta_{\mathbf{k}i}))^2}{\sin^2(\theta_{\mathbf{k}f})} \\ &= \frac{A_i^2 + 2A_i\sin(2\theta_{\mathbf{k}} - \theta_{\mathbf{k}i}) + \sin^2(2\theta_{\mathbf{k}} - \theta_{\mathbf{k}i})}{4\sin^2(\theta_{\mathbf{k}f})} \\ &= \frac{A_i^2 + 2A_i(\sin(2\theta_{\mathbf{k}})B_i - \cos(2\theta_{\mathbf{k}})A_i) + (\sin(2\theta_{\mathbf{k}})B_i - \cos(2\theta_{\mathbf{k}})A_i)^2}{4\sin^2(\theta_{\mathbf{k}f})} \\ &= \frac{A_i^2 + 2A_i(2ABB_i - (B^2 - A^2)A_i) + (2ABB_i - (B^2 - A^2)A_i)^2}{4\sin^2(\theta_{\mathbf{k}f})} \\ &= \frac{A_i^2 + 4A_iB_iAB - 2A_i^2B^2 + 2A_i^2A^2 + 4A^2B^2B_i^2}{4\sin^2(\theta_{\mathbf{k}f})} + \\ &+ \frac{A_i^2(B^2 - A^2)^2 - 4ABB_i(B^2 - A^2)A_i}{4\sin^2(\theta_{\mathbf{k}f})} \\ &= \frac{A_i^2(1 - 2B^2 + 2A^2 + B^4 + A^4 - 2A^2B^2)}{4\sin^2(\theta_{\mathbf{k}f})} + \\ &+ \frac{4ABB_i(A_i + ABB_i - A_iB^2 + A_iA^2)}{4\sin^2(\theta_{\mathbf{k}f})},\end{aligned} \tag{B.44}$$

looking first at the coefficient of A_i^2

$$
\begin{aligned}
&1 - 2B^2 + 2A^2 + B^4 + A^4 - 2A^2B^2 \\
&= 1 - (1 + \frac{\epsilon_{\mathbf{k}}}{E_{\mathbf{k}}}) + (1 - \frac{\epsilon_{\mathbf{k}}}{E_{\mathbf{k}}}) + \frac{1}{4}(1 + \frac{\epsilon_{\mathbf{k}}}{E_{\mathbf{k}}})^2 + \frac{1}{4}(1 - \frac{\epsilon_{\mathbf{k}}}{E_{\mathbf{k}}})^2 - \frac{1}{2}(1 + \frac{\epsilon_{\mathbf{k}}}{E_{\mathbf{k}}})(1 - \frac{\epsilon_{\mathbf{k}}}{E_{\mathbf{k}}}) \\
&= 1 - 2\frac{\epsilon_{\mathbf{k}}}{E_{\mathbf{k}}} + \frac{1}{2} + \frac{1}{2}\frac{\epsilon_{\mathbf{k}}^2}{E_{\mathbf{k}}^2} - \frac{1}{2} + \frac{1}{2}\frac{\epsilon_{\mathbf{k}}^2}{E_{\mathbf{k}}^2} \\
&= \left(1 - \frac{\epsilon_{\mathbf{k}}}{E_{\mathbf{k}}}\right)^2 ,
\end{aligned}
\tag{B.45}
$$

giving

$$
\begin{aligned}
\frac{Z^{-}_{\mathbf{k}neq}}{Z_{\mathbf{k}eq}} &\approx \frac{A_i^2\left(1-\frac{\epsilon_\mathbf{k}}{E_\mathbf{k}}\right)^2 + 4ABB_i(A_i(A^2-B^2+1)+ABB_i)}{4\sin^2(\theta_{\mathbf{k}f})} \\
&= \frac{A_i^2\left(1-\frac{\epsilon_\mathbf{k}}{E_\mathbf{k}}\right)^2 + 4ABB_i(A_i(A^2-B^2+A^2+B^2)+ABB_i)}{4\sin^2(\theta_{\mathbf{k}f})} \\
&= \frac{A_i^2\left(1-\frac{\epsilon_\mathbf{k}}{E_\mathbf{k}}\right)^2 + 4ABB_i(A_i\left(1-\frac{\epsilon_\mathbf{k}}{E_\mathbf{k}}\right)+ABB_i)}{4\sin^2(\theta_{\mathbf{k}f})} \\
&= \frac{A_i^2\left(1-\frac{\epsilon_\mathbf{k}}{E_\mathbf{k}}\right)^2 + 4ABB_iA_i\left(1-\frac{\epsilon_\mathbf{k}}{E_\mathbf{k}}\right)+2\left(1-\frac{\epsilon_\mathbf{k}}{E_\mathbf{k}}\right)B^2B_i^2}{4\sin^2(\theta_{\mathbf{k}f})} \\
&= \frac{1-\frac{\epsilon_\mathbf{k}}{E_\mathbf{k}}}{1-\frac{\epsilon_\mathbf{k}}{E_{\mathbf{k}f}}}\frac{A_i^2\left(1-\frac{\epsilon_\mathbf{k}}{E_\mathbf{k}}\right)+4ABB_iA_i+2B^2B_i^2}{2} \\
&= \frac{1-\frac{\epsilon_\mathbf{k}}{E_\mathbf{k}}}{1-\frac{\epsilon_\mathbf{k}}{E_{\mathbf{k}f}}}\frac{A_i^2\left(1-\frac{\epsilon_\mathbf{k}}{E_\mathbf{k}}\right)+4ABB_iA_i+\left(1+\frac{\epsilon_\mathbf{k}}{E_\mathbf{k}}\right)B_i^2}{2} \\
&= \frac{1-\frac{\epsilon_\mathbf{k}}{E_\mathbf{k}}}{1-\frac{\epsilon_\mathbf{k}}{E_{\mathbf{k}f}}}\frac{\frac{1}{2}\left(1-\frac{\epsilon_\mathbf{k}}{E_{\mathbf{k}i}}\right)\left(1-\frac{\epsilon_\mathbf{k}}{E_\mathbf{k}}\right)+4ABB_iA_i+\frac{1}{2}\left(1+\frac{\epsilon_\mathbf{k}}{E_\mathbf{k}}\right)\left(1+\frac{\epsilon_\mathbf{k}}{E_{\mathbf{k}i}}\right)}{2} \\
&= \frac{1-\frac{\epsilon_\mathbf{k}}{E_\mathbf{k}}}{1-\frac{\epsilon_\mathbf{k}}{E_{\mathbf{k}f}}}\frac{1+\frac{\epsilon_\mathbf{k}}{E_\mathbf{k}}\frac{\epsilon_\mathbf{k}}{E_{\mathbf{k}i}}+4ABB_iA_i}{2} \\
&= \frac{1-\frac{\epsilon_\mathbf{k}}{E_\mathbf{k}}}{1-\frac{\epsilon_\mathbf{k}}{E_{\mathbf{k}f}}}\left(\frac{1}{2}+\frac{\frac{\epsilon_\mathbf{k}^2}{E_\mathbf{k}E_{\mathbf{k}i}}+4ABB_iA_i}{2}\right) \\
&= \frac{1-\frac{\epsilon_\mathbf{k}}{E_\mathbf{k}}}{1-\frac{\epsilon_\mathbf{k}}{E_{\mathbf{k}f}}}\left(\frac{1}{2}+\frac{\frac{\epsilon_\mathbf{k}^2}{E_\mathbf{k}E_{\mathbf{k}i}}+\sqrt{\left(1-\frac{\epsilon_\mathbf{k}}{E_\mathbf{k}}\right)\left(1+\frac{\epsilon_\mathbf{k}}{E_\mathbf{k}}\right)\left(1+\frac{\epsilon_\mathbf{k}}{E_{\mathbf{k}i}}\right)\left(1-\frac{\epsilon_\mathbf{k}}{E_{\mathbf{k}i}}\right)}}{2}\right) \\
&= \frac{1-\frac{\epsilon_\mathbf{k}}{E_\mathbf{k}}}{1-\frac{\epsilon_\mathbf{k}}{E_{\mathbf{k}f}}}\left(\frac{1}{2}+\frac{\frac{\epsilon_\mathbf{k}^2}{E_\mathbf{k}E_{\mathbf{k}i}}+\sqrt{\left(1-\frac{\epsilon_\mathbf{k}^2}{E_\mathbf{k}^2}\right)\left(1-\frac{\epsilon_\mathbf{k}^2}{E_{\mathbf{k}i}^2}\right)}}{2}\right). \qquad \text{(B.46)}
\end{aligned}
$$

Focusing on the square root, letting $F = \sqrt{\left(1-\frac{\epsilon_\mathbf{k}^2}{E_\mathbf{k}^2}\right)\left(1-\frac{\epsilon_\mathbf{k}^2}{E_{\mathbf{k}i}^2}\right)}$

$$
\begin{aligned}
F &= \sqrt{\left(1-\frac{\epsilon_{\mathbf{k}}^2}{\epsilon_{\mathbf{k}}^2+\Delta_{st}^2}\right)\left(1-\frac{\epsilon_{\mathbf{k}}^2}{\epsilon_{\mathbf{k}}^2+\Delta_{i}^2}\right)} \\
&= \sqrt{\left(\frac{\epsilon_{\mathbf{k}}^2+\Delta_{st}^2-\epsilon_{\mathbf{k}}^2}{\epsilon_{\mathbf{k}}^2+\Delta_{st}^2}\right)\left(\frac{\epsilon_{\mathbf{k}}^2+\Delta_{i}^2-\epsilon_{\mathbf{k}}^2}{\epsilon_{\mathbf{k}}^2+\Delta_{i}^2}\right)} \\
&= \sqrt{\left(\frac{\Delta_{st}^2}{\epsilon_{\mathbf{k}}^2+\Delta_{st}^2}\right)\left(\frac{\Delta_{i}^2}{\epsilon_{\mathbf{k}}^2+\Delta_{i}^2}\right)} \\
&= \frac{\Delta_{st}\Delta_i}{E_{\mathbf{k}}E_{\mathbf{k}i}},
\end{aligned}
\tag{B.47}
$$

where we have suppressed any k-dependence in $\Delta = \Delta_{\mathbf{k}} = \gamma_{\mathbf{k}}\Delta$ for ease of notation. This gives our final result

$$
\frac{Z^{-}_{\mathbf{k}neq}}{Z_{\mathbf{k}eq}} \approx \left(\frac{1-\frac{\epsilon_{\mathbf{k}}}{E_{\mathbf{k}}}}{1-\frac{\epsilon_{\mathbf{k}}}{E_{\mathbf{k}f}}}\right)\left(\frac{1}{2}+\frac{\epsilon_{\mathbf{k}}^2+\gamma_{\mathbf{k}}^2\Delta_{st}\Delta_i}{2E_{\mathbf{k}}E_{\mathbf{k}i}}\right). \tag{B.48}
$$

If we have nodes in the gaps it becomes possible to expand this around the nodal lines where $\gamma\Delta/\epsilon \ll 1$, approximating $E_{\mathbf{k}} = \sqrt{\epsilon_{\mathbf{k}}^2+\Delta^2\gamma_{\mathbf{k}}^2}$ as $\epsilon_{\mathbf{k}}\sqrt{1+\Delta^2\gamma_{\mathbf{k}}^2/\epsilon_{\mathbf{k}}^2} \approx \epsilon_{\mathbf{k}}(1+1/2\Delta^2\gamma_{\mathbf{k}}^2/\epsilon_{\mathbf{k}}^2)$

In the case with a quench in the spin-orbit coupling, the results are the same until equation (B.44) where we now get a difference between $\varepsilon_{\mathbf{k}i}, E_{\mathbf{k}i}$ and $\varepsilon_{\mathbf{k}st}, E_{\mathbf{k}st}$ in addition to the change in the gap size. In the following we continue the calculation from there with the SoC-quench included

$$
\begin{aligned}
\frac{Z^{-}_{\mathbf{k}neq}}{Z_{\mathbf{k}eq}} &\approx \frac{A_i^2\left(1-\frac{\epsilon_{\mathbf{k}st}}{E_{\mathbf{k}st}}\right)^2 + 4ABB_i(A_i(A^2-B^2+1)+ABB_i)}{4\sin^2(\theta_{\mathbf{k}f})} \\
&= \frac{A_i^2\left(1-\frac{\epsilon_{\mathbf{k}st}}{E_{\mathbf{k}st}}\right)^2 + 4ABB_i(A_i(A^2-B^2+A^2+B^2)+ABB_i)}{4\sin^2(\theta_{\mathbf{k}f})} \\
&= \frac{A_i^2\left(1-\frac{\epsilon_{\mathbf{k}st}}{E_{\mathbf{k}st}}\right)^2 + 4ABB_iA_i\left(1-\frac{\epsilon_{\mathbf{k}st}}{E_{\mathbf{k}st}}\right) + 2\left(1-\frac{\epsilon_{\mathbf{k}st}}{E_{\mathbf{k}st}}\right)B^2B_i^2}{4\sin^2(\theta_{\mathbf{k}f})} \\
&= \frac{1-\frac{\epsilon_{\mathbf{k}st}}{E_{\mathbf{k}st}}}{1-\frac{\epsilon_{\mathbf{k}f}}{E_{\mathbf{k}f}}}\frac{A_i^2\left(1-\frac{\epsilon_{\mathbf{k}st}}{E_{\mathbf{k}st}}\right) + 4ABB_iA_i + 2B^2B_i^2}{2} \\
&= \frac{1-\frac{\epsilon_{\mathbf{k}st}}{E_{\mathbf{k}st}}}{1-\frac{\epsilon_{\mathbf{k}f}}{E_{\mathbf{k}f}}}\frac{\frac{1}{2}\left(1-\frac{\epsilon_{\mathbf{k}i}}{E_{\mathbf{k}i}}\right)\left(1-\frac{\epsilon_{\mathbf{k}st}}{E_{\mathbf{k}st}}\right) + 4ABB_iA_i + \frac{1}{2}\left(1+\frac{\epsilon_{\mathbf{k}st}}{E_{\mathbf{k}st}}\right)\left(1+\frac{\epsilon_{\mathbf{k}i}}{E_{\mathbf{k}i}}\right)}{2} \\
&= \frac{1-\frac{\epsilon_{\mathbf{k}st}}{E_{\mathbf{k}st}}}{1-\frac{\epsilon_{\mathbf{k}f}}{E_{\mathbf{k}f}}}\frac{\left(1+\frac{\epsilon_{\mathbf{k}i}}{E_{\mathbf{k}i}}\frac{\epsilon_{\mathbf{k}st}}{E_{\mathbf{k}st}}\right) + 4ABB_iA_i}{2} \\
&= \frac{1-\frac{\epsilon_{\mathbf{k}st}}{E_{\mathbf{k}st}}}{1-\frac{\epsilon_{\mathbf{k}f}}{E_{\mathbf{k}f}}}\frac{\left(1+\frac{\epsilon_{\mathbf{k}i}}{E_{\mathbf{k}i}}\frac{\epsilon_{\mathbf{k}st}}{E_{\mathbf{k}st}}\right) + \sqrt{\left(1-\frac{\varepsilon^2_{\mathbf{k}st}}{E^2_{\mathbf{k}st}}\right)\left(1-\frac{\varepsilon^2_{\mathbf{k}i}}{E^2_{\mathbf{k}i}}\right)}}{2} \\
&= \frac{1-\frac{\epsilon_{\mathbf{k}st}}{E_{\mathbf{k}st}}}{1-\frac{\epsilon_{\mathbf{k}f}}{E_{\mathbf{k}f}}}\frac{\left(1+\frac{\epsilon_{\mathbf{k}i}}{E_{\mathbf{k}i}}\frac{\epsilon_{\mathbf{k}st}}{E_{\mathbf{k}st}}\right) + \sqrt{\frac{\Delta^2_{\mathbf{k}st}}{E^2_{\mathbf{k}st}}\frac{\Delta^2_{\mathbf{k}i}}{E^2_{\mathbf{k}i}}}}{2} \\
&= \frac{1-\frac{\epsilon_{\mathbf{k}st}}{E_{\mathbf{k}st}}}{1-\frac{\epsilon_{\mathbf{k}f}}{E_{\mathbf{k}f}}}\frac{\left(1+\frac{\epsilon_{\mathbf{k}i}}{E_{\mathbf{k}i}}\frac{\epsilon_{\mathbf{k}st}}{E_{\mathbf{k}st}}\right) + \frac{\Delta_{\mathbf{k}st}}{E_{\mathbf{k}st}}\frac{\Delta_{\mathbf{k}i}}{E_{\mathbf{k}i}}}{2} \\
&= \frac{1-\frac{\epsilon_{\mathbf{k}st}}{E_{\mathbf{k}st}}}{1-\frac{\epsilon_{\mathbf{k}f}}{E_{\mathbf{k}f}}}\left(\frac{1}{2}+\frac{\epsilon_{\mathbf{k}i}\epsilon_{\mathbf{k}st}+\Delta_{\mathbf{k}st}\Delta_{\mathbf{k}i}}{2E_{\mathbf{k}st}E_{\mathbf{k}i}}\right).
\end{aligned}
\tag{B.49}
$$

This can be expanded in a similar way if we have nodes to expand around where $\Delta_{\mathbf{k}}/\varepsilon_{\mathbf{k}} << 1$, taking care to check that this is correct both before and after the quench. We use the same approximation as above, and $E_{\mathbf{k}} \approx \epsilon_{\mathbf{k}}(1+1/2\Delta^2\gamma^2_{\mathbf{k}}/\epsilon^2_{\mathbf{k}})$, first assuming that $\epsilon_{\mathbf{k}} > 0$.

$$\frac{1-\frac{\epsilon_{\mathbf{k}st}}{E_{\mathbf{k}st}}}{1-\frac{\epsilon_{\mathbf{k}f}}{E_{\mathbf{k}f}}}\left(\frac{1}{2}+\frac{\epsilon_{\mathbf{k}i}\epsilon_{\mathbf{k}f}+\Delta_{\mathbf{k}st}\Delta_{\mathbf{k}i}}{2E_{\mathbf{k}st}E_{\mathbf{k}i}}\right)\approx\frac{1-\frac{1}{1+1/2\Delta^2_{\mathbf{k}st}/\epsilon^2_{\mathbf{k}f}}}{1-\frac{1}{1+1/2\Delta^2_{\mathbf{k}f}/\epsilon^2_{\mathbf{k}f}}}\cdot$$
$$\cdot\left(\frac{1}{2}+\frac{\epsilon_{\mathbf{k}i}\epsilon_{\mathbf{k}f}+\Delta_{\mathbf{k}st}\Delta_{\mathbf{k}i}}{2\epsilon_{\mathbf{k}st}(1+1/2\Delta^2_{\mathbf{k}st}/\epsilon^2_{\mathbf{k}st})\epsilon_{\mathbf{k}i}(1+1/2\Delta^2_{\mathbf{k}i}/\epsilon^2_{\mathbf{k}i})}\right)$$
$$\approx\frac{1-\frac{1}{1+1/2\Delta^2_{\mathbf{k}st}/\epsilon^2_{\mathbf{k}f}}}{1-\frac{1}{1+1/2\Delta^2_{\mathbf{k}f}/\epsilon^2_{\mathbf{k}f}}}$$
$$\approx\frac{\Delta^2_{st}}{\Delta^2_f}. \tag{B.50}$$

We end up with an approximation of the spectral weight for each peak that is identical to the form in [16] in the case of quenches in the interaction strength. In the case of a quench in the spin-orbit coupling the non-equilibrium case is modified somewhat as we take into account that $\xi_{\mathbf{k}\lambda i}\neq\xi_{\mathbf{k}\lambda f}$. We also note that the $\mathbf{k}$-dependence of the gaps in the case where $\Delta_{\mathbf{k}}=\Delta\gamma_{\mathbf{k}}$ where $\gamma_{\mathbf{k}}=\exp(-i\phi)$ is a phase-factor disappears from taking the absolute value in the calculation above. While the spectral function is in general complex, the spectral functions dealing with correlation functions of Hermitian adjoint operators are real, and in our case we are dealing with correlators on the form $\langle c^\dagger_{\mathbf{k}\lambda}c_{\mathbf{k}\lambda}\rangle$ which are Hermitian adjoint.

B.2 Linear gap response after a sudden quench in the SoC

In this section we perform a linear response calculation for a sudden quench in the spin-orbit interaction.

B.2.1 Definitions and preliminaries

We start with the time dependent effective mean-field Hamiltonian

$$\mathcal{H}(t)=\sum_{\mathbf{k}\lambda}\xi_{\mathbf{k}\lambda}(t)\tilde{c}^\dagger_{\mathbf{k}\lambda}\tilde{c}_{\mathbf{k}\lambda}-\frac{1}{2}\sum_{\mathbf{k}\lambda}(\Delta_{\mathbf{k}\lambda}\tilde{c}^\dagger_{\mathbf{k}\lambda}\tilde{c}^\dagger_{-\mathbf{k}\lambda}+\Delta^\dagger_{\mathbf{k}\lambda}\tilde{c}_{-\mathbf{k}\lambda}\tilde{c}_{\mathbf{k}\lambda}), \tag{B.51}$$

where $\xi_{\mathbf{k}}(t)$ has a sudden quench in the SOC strength $\alpha=\alpha(t)$.

We want to calculate the linear response of $\Delta_\lambda(t)$ after a sudden quench in the interaction, where we define

$$\tilde{\Delta}_\lambda(\mathbf{k},t) = \sum_{\mathbf{k}'\mu=\pm} \tilde{V}_{\lambda\mu}(\mathbf{k},\mathbf{k}')\langle \tilde{c}_{-\mathbf{k}'\mu}(t)\tilde{c}_{\mathbf{k}'\mu}(t)\rangle. \tag{B.52}$$

where

$$iF^<_{\mathbf{k}\lambda}(t,t) = -i\langle \tilde{c}_{-\mathbf{k}\lambda}(t)\tilde{c}_{\mathbf{k}\lambda}(t)\rangle. \tag{B.53}$$

To avoid having to compute this on the contour we want to use Langreth's theorem, specifically the identity that if [1]

$$C = \int_{contour} AB, \tag{B.54}$$

then

$$C^< = \int_t [A^r B^< + A^< B^a], \tag{B.55}$$

where a and r stands for the advanced and retarded functions respectively.

B.2.2 Calculation

We see that what we want to start with in this case is to compute the linear response of the anomalous Green's functions in the strength of the quench. The change in the Hamiltonian is given by

$$\begin{aligned}\delta\mathcal{H} &= \delta\alpha E_z \sum_{\mathbf{k}\lambda} \lambda\sqrt{\sin^2(k_x)+\sin^2(k_y)}\tilde{c}^\dagger_{\mathbf{k}\lambda}\tilde{c}_{\mathbf{k}\lambda} \\ &\equiv \sum_{\mathbf{k}\lambda} \delta\alpha_{\mathbf{k}\lambda}\tilde{c}^\dagger_{\mathbf{k}\lambda}\tilde{c}_{\mathbf{k}\lambda}.\end{aligned} \tag{B.56}$$

To first order in linear response for each band, this gives us

$$\delta F_{\mathbf{k}\lambda}(t,t') = \sum_{\mathbf{p}\sigma} \delta\alpha_{\mathbf{k}\sigma} \int_{\mathcal{K}} dt_1 \langle T_{\mathcal{K}} \tilde{c}_{-\mathbf{k}\lambda}(t)\tilde{c}_{\mathbf{k}\lambda}(t')\tilde{c}^\dagger_{\mathbf{p}\sigma}(t_1)\tilde{c}_{\mathbf{p}\sigma}(t_1)\rangle, \tag{B.57}$$

where $\mathcal{K}$ indicates the Keldysh contour. Using Wick's theorem and noting that the expectation values of two operators in different bands vanish we can rewrite it as,

[1] See additional appendix

$$\begin{aligned}\delta F_{\mathbf{k}\lambda}(t,t') &= \sum_{\mathbf{p}\sigma}\delta\alpha_{\mathbf{p}\sigma}\int_{\mathcal{K}} dt_1(-1)\langle T_{\mathcal{K}}\tilde{c}_{-\mathbf{k}\lambda}(t)\tilde{c}_{\mathbf{p}\sigma}(t_1)\rangle\langle T_{\mathcal{K}}\tilde{c}^{\dagger}_{\mathbf{p}\sigma}(t_1)\tilde{c}_{\mathbf{k}\lambda}(t')\rangle\delta_{\mathbf{k},\mathbf{p}}\delta_{\sigma,\lambda}+\\ &+\sum_{\mathbf{p}\sigma}\delta\alpha_{\mathbf{p}\sigma}\int_{\mathcal{K}} dt_1\langle T_{\mathcal{K}}\tilde{c}_{-\mathbf{k}\lambda}(t)\tilde{c}^{\dagger}_{\mathbf{p}\sigma}(t_1)\rangle\langle T_{\mathcal{K}}\tilde{c}_{\mathbf{p}\sigma}(t_1)\tilde{c}_{\mathbf{k}\lambda}(t')\rangle\delta_{\mathbf{k},-\mathbf{p}}\delta_{\sigma,\lambda}\\ &=\delta\alpha_{\mathbf{k}\lambda}\int_{\mathcal{K}} dt_1 F_{\mathbf{k}\lambda}(t_1-t)G_{\mathbf{k}\lambda}(t'-t_1)-\alpha_{-\mathbf{k}\lambda}\int_{\mathcal{K}} dt_1\mathcal{G}_{\mathbf{k}\lambda}(t_1-t)F_{\mathbf{k}\lambda}(t'-t_1).\end{aligned} \tag{B.58}$$

By applying Langreth's theorem to (B.58) and looking at correlactions at equal times we obtain

$$\begin{aligned}\delta F_{\mathbf{k}\lambda}(t) &= \delta\alpha_{\mathbf{k}\lambda}\int dt_1 F^R_{\mathbf{k}\lambda}(t_1-t)G^<_{\mathbf{k}\lambda}(t-t_1)+F^<_{\mathbf{k}\lambda}(t_1-t)G^A_{\mathbf{k}\lambda}(t-t_1)+\\ &-\delta\alpha_{-\mathbf{k}\lambda}\int dt_1\mathcal{G}^R_{\mathbf{k}\lambda}(t_1-t)F^<_{\mathbf{k}\lambda}(t-t_1)+\mathcal{G}^<_{\mathbf{k}\lambda}(t_1-t)F^A_{\mathbf{k}\lambda}(t-t_1),\end{aligned} \tag{B.59}$$

to obtain the integration limits we use the step-functions obtained from the advanced and retarded Green's functions and note that the quench $\delta\alpha$ is non-zero only for times after the quench ($t=0$)

$$\begin{aligned}\delta F_{\mathbf{k}\lambda}(t) &= \delta\alpha_{\mathbf{k}\lambda}\int_t^0 dt_1 F^R_{\mathbf{k}\lambda}(t_1-t)G^<_{\mathbf{k}\lambda}(t-t_1)+F^<_{\mathbf{k}\lambda}(t_1-t)G^A_{\mathbf{k}\lambda}(t-t_1)+\\ &-\delta\alpha_{\mathbf{k}\lambda}\int_t^0 dt_1\mathcal{G}^R_{\mathbf{k}\lambda}(t_1-t)F^<_{\mathbf{k}\lambda}(t-t_1)+\mathcal{G}^<_{\mathbf{k}\lambda}(t_1-t)F^A_{\mathbf{k}\lambda}(t-t_1),\end{aligned} \tag{B.60}$$

which can all be evaluated

$$
\begin{aligned}
\frac{\delta F_{\mathbf{k}\lambda}(t)}{\delta\alpha_{\mathbf{k}\lambda}} &= \int_t^0 dt_1(-i)u_{\mathbf{k}\lambda}v_{\mathbf{k}\lambda}(\mathrm{e}^{iE_{\mathbf{k}\lambda}(t_1-t)} - \mathrm{e}^{-iE_{\mathbf{k}\lambda}(t_1-t)})iv_{\mathbf{k}\lambda}^2\mathrm{e}^{iE_{\mathbf{k}\lambda}(t-t_1)}+ \\
&+ \int_t^0 dt_1 iu_{\mathbf{k}\lambda}v_{\mathbf{k}\lambda}\mathrm{e}^{iE_{\mathbf{k}\lambda}(t_1-t)}i(u_{\mathbf{k}\lambda}^2\mathrm{e}^{-iE_{\mathbf{k}\lambda}(t-t_1)} + v_{\mathbf{k}\lambda}^2\mathrm{e}^{iE_{\mathbf{k}\lambda}(t-t_1)})+ \\
&- \int_t^0 dt_1(-i)(u_{\mathbf{k}\lambda}^2\mathrm{e}^{iE_{\mathbf{k}\lambda}(t_1-t)} + v_{\mathbf{k}\lambda}^2\mathrm{e}^{-iE_{\mathbf{k}\lambda}(t_1-t)})iu_{\mathbf{k}\lambda}v_{\mathbf{k}\lambda}\mathrm{e}^{iE_{\mathbf{k}\lambda}(t-t_1)}+ \\
&- \int_t^0 dt_1 iu_{\mathbf{k}\lambda}v_{\mathbf{k}\lambda}(\mathrm{e}^{iE_{\mathbf{k}\lambda}((t-t_1)} - \mathrm{e}^{-iE_{\mathbf{k}\lambda}((t-t_1)})iu_{\mathbf{k}\lambda}^2\mathrm{e}^{iE_{\mathbf{k}\lambda}(t_1-t)} \\
&= u_{\mathbf{k}\lambda}v_{\mathbf{k}\lambda}^3\int_t^0 dt_1(1-\mathrm{e}^{2iE_{\mathbf{k}\lambda}(t-t_1)})+ \\
&- u_{\mathbf{k}\lambda}v_{\mathbf{k}\lambda}\int_t^0 dt_1(u_{\mathbf{k}\lambda}^2\mathrm{e}^{2iE_{\mathbf{k}\lambda}(t_1-t)} + v_{\mathbf{k}\lambda}^2)+ \\
&- u_{\mathbf{k}\lambda}v_{\mathbf{k}\lambda}\int_t^0 dt_1(u_{\mathbf{k}\lambda}^2 + v_{\mathbf{k}\lambda}^2\mathrm{e}^{-2iE_{\mathbf{k}\lambda}(t_1-t)})+ \\
&+ u_{\mathbf{k}\lambda}^3v_{\mathbf{k}\lambda}\int_t^0 dt_1(1-\mathrm{e}^{-2iE_{\mathbf{k}\lambda}(t-t_1)}) \\
&= u_{\mathbf{k}\lambda}v_{\mathbf{k}\lambda}^3\mathrm{e}^{2iE_{\mathbf{k}\lambda}t}\int_0^t dt_1\mathrm{e}^{-2iE_{\mathbf{k}\lambda}t_1} + u_{\mathbf{k}\lambda}^3v_{\mathbf{k}\lambda}\mathrm{e}^{-2iE_{\mathbf{k}\lambda}t}\int_0^t dt_1\mathrm{e}^{2iE_{\mathbf{k}\lambda}t_1}+ \\
&+ u_{\mathbf{k}\lambda}v_{\mathbf{k}\lambda}^3\mathrm{e}^{2iE_{\mathbf{k}\lambda}t}\int_0^t dt_1\mathrm{e}^{-2iE_{\mathbf{k}\lambda}t_1} + u_{\mathbf{k}\lambda}^3v_{\mathbf{k}\lambda}\mathrm{e}^{-2iE_{\mathbf{k}\lambda}t}\int_0^t dt_1\mathrm{e}^{2iE_{\mathbf{k}\lambda}t_1} \\
&= 2u_{\mathbf{k}\lambda}v_{\mathbf{k}\lambda}^3\mathrm{e}^{2iE_{\mathbf{k}\lambda}t}\left(\frac{\mathrm{e}^{-2iE_{\mathbf{k}\lambda}t}-1}{-2iE_{\mathbf{k}\lambda}}\right) + 2u_{\mathbf{k}\lambda}^3v_{\mathbf{k}\lambda}\mathrm{e}^{-2iE_{\mathbf{k}\lambda}t}\left(\frac{\mathrm{e}^{2iE_{\mathbf{k}\lambda}t}-1}{2iE_{\mathbf{k}\lambda}}\right) \\
&= \frac{iu_{\mathbf{k}\lambda}v_{\mathbf{k}\lambda}}{E_{\mathbf{k}\lambda}}\left(v_{\mathbf{k}\lambda}^2 - v_{\mathbf{k}\lambda}^2\mathrm{e}^{2iE_{\mathbf{k}\lambda}t} - u_{\mathbf{k}\lambda}^2 + u_{\mathbf{k}\lambda}^2\mathrm{e}^{-2iE_{\mathbf{k}\lambda}t}\right). \qquad \text{(B.61)}
\end{aligned}
$$

From here we insert $u_{\mathbf{k},\lambda}$ and $v_{\mathbf{k},\lambda}$

$$
\begin{aligned}
\frac{\delta F_{\mathbf{k}\lambda}(t)}{\delta\alpha_{\mathbf{k}\lambda}} &= \frac{i|\Delta_{\mathbf{k}\lambda}|}{2E_{\mathbf{k}\lambda}^2}\left(\frac{-\xi_{\mathbf{k}\lambda}}{E_{\mathbf{k}\lambda}} - \frac{1}{2}\left(1-\frac{\xi_{\mathbf{k}\lambda}}{E_{\mathbf{k}\lambda}}\right)\mathrm{e}^{2iE_{\mathbf{k}\lambda}t} + \frac{1}{2}\left(1+\frac{\xi_{\mathbf{k}\lambda}}{E_{\mathbf{k}\lambda}}\right)\mathrm{e}^{-2iE_{\mathbf{k}\lambda}t}\right) \\
&= \frac{i|\Delta_{\mathbf{k}\lambda}|}{2E_{\mathbf{k}\lambda}^2}\left(\frac{-\xi_{\mathbf{k}\lambda}}{E_{\mathbf{k}\lambda}} + i\sin(2E_{\mathbf{k}\lambda}t) + \frac{\xi_{\mathbf{k}\lambda}}{E_{\mathbf{k}\lambda}}\cos(2E_{\mathbf{k}\lambda}t)\right) \\
&= \frac{i|\Delta_{\mathbf{k}\lambda}|\xi_{\mathbf{k}\lambda}}{2E_{\mathbf{k}\lambda}^3}\left(\cos(2E_{\mathbf{k}\lambda}t)-1\right) - \frac{|\Delta_{\mathbf{k}\lambda}|}{2E_{\mathbf{k}\lambda}^2}\sin(2E_{\mathbf{k}\lambda}t), \qquad \text{(B.62)}
\end{aligned}
$$

and finally write the correction to the gaps using equation (B.52) and (B.53)

$$\delta\Delta_{\lambda\mathbf{k}}(t) = -i\sum_{\lambda'\mathbf{k}'} V_{\lambda\lambda'}(\mathbf{k}\mathbf{k}')\delta F_{\mathbf{k}'\lambda'}(t) \tag{B.63}$$

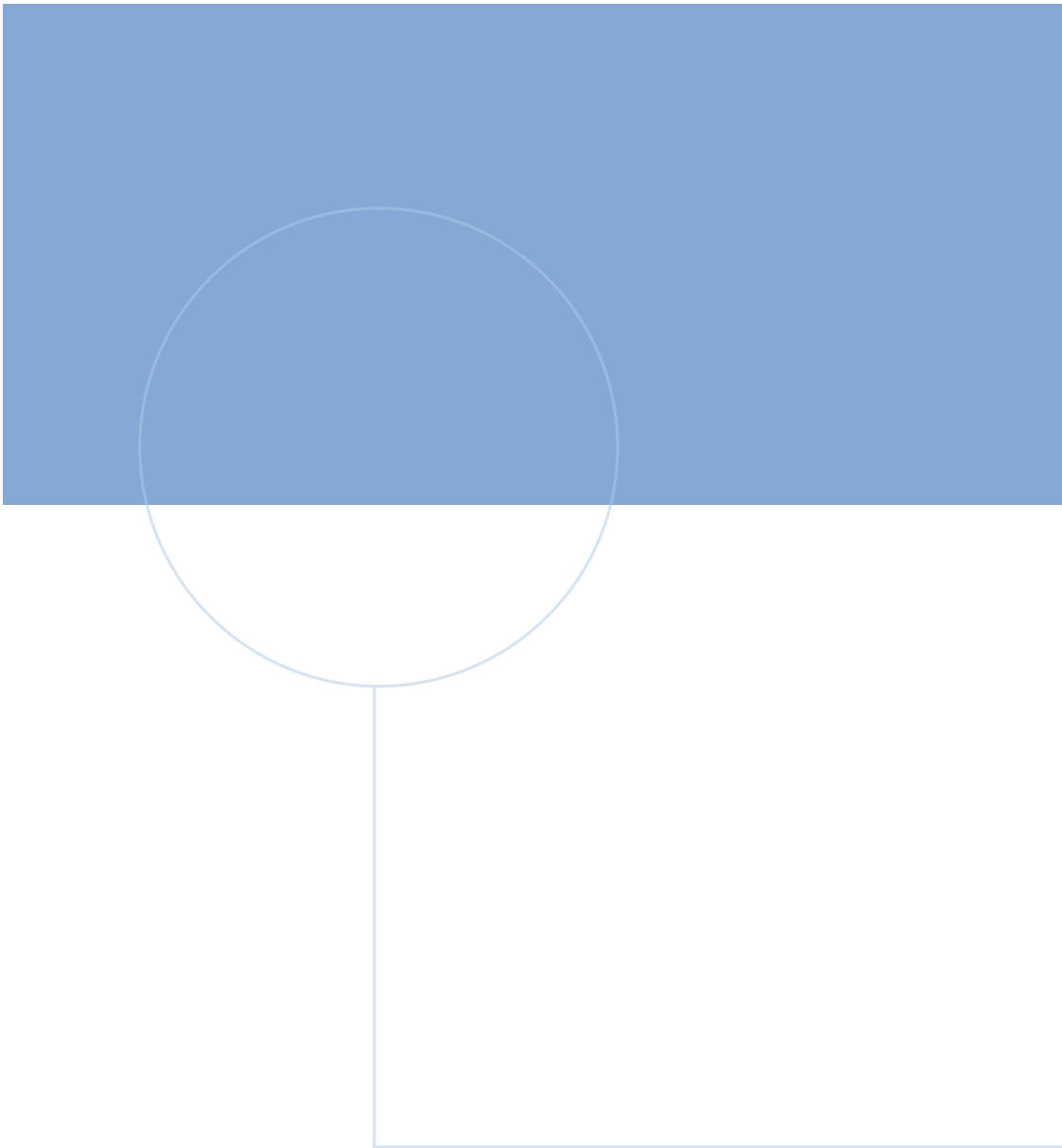

NTNU

Norwegian University of
Science and Technology